Microwave Imaging of Dielectric Objects by Stochastic Inversion

by

Youming Qin

A dissertation
presented to the University of Manitoba
in partial fulfillment of the
requirements for the degree of
Doctor of Philosophy
in
Electrical and Computer Engineering

Winnipeg, Manitoba, 1996

ISBN 0-612-16236-2

Canada

Name YOUMING QIN

Dissertation Abstracts International and *Masters Abstracts International* are arranged by broad, general subject categories. Please select the one subject which most nearly describes the content of your dissertation or thesis. Enter the corresponding four-digit code in the spaces provided.

SUBJECT TERM

~~YOUMING QIN~~, ELECTRONICS AND ELECTRICAL

SUBJECT CODE 0544

UMI

Subject Categories

THE HUMANITIES AND SOCIAL SCIENCES

COMMUNICATIONS AND THE ARTS
Architecture 0729
Art History 0377
Cinema 0900
Dance 0378
Design and Decorative Arts 0389
Fine Arts 0357
Information Science 0723
Journalism 0391
Landscape Architecture 0390
Library Science 0399
Mass Communications 0708
Music 0413
Speech Communication 0459
Theater 0465

EDUCATION
General 0515
Administration 0514
Adult and Continuing 0516
Agricultural 0517
Art 0273
Bilingual and Multicultural 0282
Business 0688
Community College 0275
Curriculum and Instruction 0727
Early Childhood 0518
Elementary 0524
Educational Psychology 0525
Finance 0277
Guidance and Counseling 0519
Health 0680
Higher 0745
History of 0520
Home Economics 0278
Industrial 0521
Language and Literature 0279
Mathematics 0280
Music 0522
Philosophy of 0998
Physical 0523
Reading 0535
Religious 0527
Sciences 0714
Secondary 0533
Social Sciences 0534
Sociology of 0340
Special 0529
Teacher Training 0530
Technology 0710
Tests and Measurements 0288
Vocational 0747

LANGUAGE, LITERATURE AND LINGUISTICS
Language
- General 0679
- Ancient 0289
- Linguistics 0290
- Modern 0291
- Rhetoric and Composition 0681

Literature
- General 0401
- Classical 0294
- Comparative 0295
- Medieval 0297
- Modern 0298
- African 0316
- American 0591
- Asian 0305
- Canadian (English) 0352
- Canadian (French) 0355
- Caribbean 0360
- English 0593
- Germanic 0311
- Latin American 0312
- Middle Eastern 0315
- Romance 0313
- Slavic and East European 0314

PHILOSOPHY, RELIGION AND THEOLOGY
Philosophy 0422
Religion
- General 0318
- Biblical Studies 0321
- Clergy 0319
- History of 0320
- Philosophy of 0322

Theology 0469

SOCIAL SCIENCES
American Studies 0323
Anthropology
- Archaeology 0324
- Cultural 0326
- Physical 0327

Business Administration
- General 0310
- Accounting 0272
- Banking 0770
- Management 0454
- Marketing 0338

Canadian Studies 0385
Economics
- General 0501
- Agricultural 0503
- Commerce-Business 0505
- Finance 0508
- History 0509
- Labor 0510
- Theory 0511

Folklore 0358
Geography 0366
Gerontology 0351
History
- General 0578
- Ancient 0579
- Medieval 0581
- Modern 0582
- Church 0330
- Black 0328
- African 0331
- Asia, Australia and Oceania 0332
- Canadian 0334
- European 0335
- Latin American 0336
- Middle Eastern 0333
- United States 0337

History of Science 0585
Law 0398
Political Science
- General 0615
- International Law and Relations 0616
- Public Administration 0617

Recreation 0814
Social Work 0452
Sociology
- General 0626
- Criminology and Penology 0627
- Demography 0938
- Ethnic and Racial Studies 0631
- Individual and Family Studies 0628
- Industrial and Labor Relations 0629
- Public and Social Welfare 0630
- Social Structure and Development 0700
- Theory and Methods 0344

Transportation 0709
Urban and Regional Planning 0999
Women's Studies 0453

THE SCIENCES AND ENGINEERING

BIOLOGICAL SCIENCES
Agriculture
- General 0473
- Agronomy 0285
- Animal Culture and Nutrition 0475
- Animal Pathology 0476
- Fisheries and Aquaculture 0792
- Food Science and Technology 0359
- Forestry and Wildlife 0478
- Plant Culture 0479
- Plant Pathology 0480
- Range Management 0777
- Soil Science 0481
- Wood Technology 0746

Biology
- General 0306
- Anatomy 0287
- Animal Physiology 0433
- Biostatistics 0308
- Botany 0309
- Cell 0379
- Ecology 0329
- Entomology 0353
- Genetics 0369
- Limnology 0793
- Microbiology 0410
- Molecular 0307
- Neuroscience 0317
- Oceanography 0416
- Plant Physiology 0817
- Veterinary Science 0778
- Zoology 0472

Biophysics
- General 0786
- Medical 0760

EARTH SCIENCES
Biogeochemistry 0425
Geochemistry 0996
Geodesy 0370
Geology 0372
Geophysics 0373
Hydrology 0388
Mineralogy 0411
Paleobotany 0345
Paleoecology 0426
Paleontology 0418
Paleozoology 0985
Palynology 0427
Physical Geography 0368
Physical Oceanography 0415

HEALTH AND ENVIRONMENTAL SCIENCES
Environmental Sciences 0768
Health Sciences
- General 0566
- Audiology 0300
- Dentistry 0567
- Education 0350
- Administration, Health Care 0769
- Human Development 0758
- Immunology 0982
- Medicine and Surgery 0564
- Mental Health 0347
- Nursing 0569
- Nutrition 0570
- Obstetrics and Gynecology 0380
- Occupational Health and Safety 0354
- Oncology 0992
- Ophthalmology 0381
- Pathology 0571
- Pharmacology 0419
- Pharmacy 0572
- Public Health 0573
- Radiology 0574
- Recreation 0575
- Rehabilitaion and Therapy 0382
- Speech Pathology 0460
- Toxicology 0383

Home Economics 0386

PHYSICAL SCIENCES
Pure Sciences
Chemistry
- General 0485
- Agricultural 0749
- Analytical 0486
- Biochemistry 0487
- Inorganic 0488
- Nuclear 0738
- Organic 0490
- Pharmaceutical 0491
- Physical 0494
- Polymer 0495
- Radiation 0754

Mathematics 0405
Physics
- General 0605
- Acoustics 0986
- Astronomy and Astrophysics 0606
- Atmospheric Science 0608
- Atomic 0748
- Condensed Matter 0611
- Electricity and Magnetism 0607
- Elementary Particles and High Energy 0798
- Fluid and Plasma 0759
- Molecular 0609
- Nuclear 0610
- Optics 0752
- Radiation 0756

Statistics 0463

Applied Sciences
Applied Mechanics 0346
Computer Science 0984
Engineering
- General 0537
- Aerospace 0538
- Agricultural 0539
- Automotive 0540
- Biomedical 0541
- Chemical 0542
- Civil 0543
- Electronics and Electrical 0544
- Environmental 0775
- Industrial 0546
- Marine and Ocean 0547
- Materials Science 0794
- Mechanical 0548
- Metallurgy 0743
- Mining 0551
- Nuclear 0552
- Packaging 0549
- Petroleum 0765
- Sanitary and Municipal 0554
- System Science 0790

Geotechnology 0428
Operations Research 0796
Plastics Technology 0795
Textile Technology 0994

PSYCHOLOGY
General 0621
Behavioral 0384
Clinical 0622
Cognitive 0633
Developmental 0620
Experimental 0623
Industrial 0624
Personality 0625
Physiological 0989
Psychobiology 0349
Psychometrics 0632
Social 0451

THE UNIVERSITY OF MANITOBA

FACULTY OF GRADUATE STUDIES

COPYRIGHT PERMISSION

MICROWAVE IMAGING OF DIELECTRIC OBJECTS BY STOCHASTIC INVERSION

BY

YOUMING QIN

A Thesis/Practicum submitted to the Faculty of Graduate Studies of the University of Manitoba in partial fulfillment of the requirements for the degree of

DOCTOR OF PHILOSOPHY

The University of Manitoba requires the signatures of all persons using or photocopying this dissertation. Please sign below, and give address and date.

ABSTRACT

This dissertation is devoted to exploring the possibility of using the stochastic inverse scheme to reconstruct high contrast dielectric objects in the spatial domain. In the first part of the dissertation we present the principle of microwave imaging, the basic problems associated with reconstructions, such as the ill–posedness and the regularization, and investigates the relation between two important techniques, the Tikhonov regularization and the stochastic inversion. This forms the theoretical basis for the entire thesis. Then, the stochastic inversion algorithm combined with the Tikhonov regularization is employed in the reconstruction process to solve the ill–conditioned systems of algebraic equations associated with microwave imaging problems. The performance of the proposed reconstruction processes is demonstrated in terms of computer simulations.

The problem of microwave imaging can be mathematically formulated in terms of two coupled electric field integral equations. These integral equations can be decoupled by introducing the equivalent current density yielding a linear integral equation (equivalent current formulation). The general procedure for microwave imaging in the spatial domain consists of discretizing the integral equations by applying the moment method. The associated ill–conditioned systems of equations are solved by implementing a regularization technique which enables to obtain the dielectric permittivity distribution inside bodies.

In this dissertation, the stochastic inverse scheme is employed to regularize the ill–conditioned system of equations in the process of reconstructing high contrast dielectric objects. The initial values necessary in the reconstruction algorithm are supplied by the application of the Tikhonov regularization. As a consequence, the number of iterations in the proposed algorithm is considerably reduced. Example tests show that this algorithm provides an efficient means to reconstruct dielectric bodies of various contrasts with high accuracy even in the presence of a high level of noise in the scattered field data.

The application of the stochastic inverse scheme in the iterative methods of solving the

two coupled integral equations permits us to determine directly the Tikhonov regularization parameter in each iteration. Three methods for the selection of this parameter are proposed. The first method is applicable to the situation when the upper bound of the object function variance and the upper bound of the measured data noise variance are known. The second method can be used if only the upper bound of the object function variance is detectable. If this information is not available, the third method can be employed to find the regularization parameter. The efficiency of these methods is illustrated by reconstructing two–dimensional dielectric objects with measured noiseless data and also with the data containing noise.

The dissertation concludes with a summary and the outline of future work in this area.

ACKNOWLEDGEMENTS

I wish to thank Professor I. R. Ciric for his guidance, constant encouragement and constructive criticism, throughout all phases of this work. I would also like to thank Professors E. Bridges, P. N. Shivakumar and E. M. Petriu for their time and effort in reviewing this work. All of their advice, suggestions and comments are much appreciated.

This dissertation is dedicated to my mother,

whose love, encouragement and expectation made the completion

of this dissertation possible.

TABLE OF CONTENTS

LIST OF FIGURES

LIST OF TABLES

1

INTRODUCTION

1.1 Generalities

Microwave reconstruction of dielectric bodies from scattered near–field measurements has many potential applications in such areas as medical imaging, geophysical exploration, remote sensing, robotic vision, and non–destructive testing.

The interest in developing microwave–based techniques, when other powerful imaging procedures already exist, is due basically to the possibility of visualizing different physical parameters involved and to the nature of the interaction between the radiation used and the dielectric materials. In medical applications, for instance, microwave imaging has some advantages over existing techniques such as X–ray tomography, magnetic resonance, ultrasound, and others. Firstly, unlike ionizing radiation, low–power microwave radiation allows a virtually safe exploration of living tissues. Thus even continuous monitoring is possible. Secondly, unlike other means of exploration, the microwave imaging is based on the reconstruction of the complex permittivity distribution of an object. It is well known that a scattered microwave field is sensitive to the complex permittivity distribution within a dielectric body. This makes it possible to develop an active imaging of a dielectric body, since the complex permittivity of the body depends on the morphology, blood flow, and temperature of a tissue. Moreover, some of the technology involved in microwave imaging is common to that in radar and communication systems, and is well developed and inexpensive, which may

make clinical and even domestic applications feasible. Therefore, microwave imaging can at least complement the existing imaging techniques.

However, there are some problems associated with the usage of this type of radiation, namely a low resolution and a high attenuation that dielectric materials present to microwaves, which impose stringent requirements on the equipment design, as well as the difficulty in developing imaging algorithms for high dielectric contrast bodies.

The microwave imaging methods proposed so far can be divided into two main groups: spectral domain methods [1]–[10], and spatial domain methods [11]–[36] (although some other techniques, such as maximum entropy [37],[38], and annealing [39],[40] have also been attempted). In the spectral domain approach, which is generally called microwave tomography, the main technique used for the microwave imaging is the Fourier transformation. Conventional systems of this type are based on illuminating the body with a plane wave and measuring the scattered field with a linear array of probes, in a way similar to that used in acoustic diffraction tomography. With plane wave illumination and on the assumption of weakly scattering bodies, the spectrum of the scattered field contains the information about the dielectric properties of the body in the two–dimensional Fourier spectral domain. By repeating the measurement for different directions of incidence, the spectral domain can be filled and inverted to obtain a section of the body. The main advantage of the diffraction tomography method lies in its fast numerical algorithm. However, the spectral approaches have, as it is well known, some limitations and can only be applied to low dielectric contrast and weak scatterers, since the Born or the Rytov approximations are used in the algorithms.

In the spatial domain approach, the object is first divided into small cells. Then the moment method [41] is employed to transform the integral equations into a set of algebraic equation systems which relate to the scattered field and to the dielectric properties of the body. An image of the object can be obtained by solving these systems of equations. Compared to the spectral domain methods, the spatial domain methods have the advantages of not requiring specific geometries for the measurements of the scattered field and of being

also applicable to high contrast dielectric bodies or strong scatterers. Furthermore, the spatial resolution does not seem to be so strictly related to the wavelength as it is for diffraction tomography. However, the main problem of this approach is the lack of good reconstruction algorithms.

The problem of microwave imaging can be mathematically formulated in terms of two coupled nonlinear integral equations. To solve these equations in spatial domain, the moment method with pulse basis function over the domain of identical square cells is usually employed, yielding two coupled nonlinear systems of equations. Two techniques are mainly used to decouple them. One is to introduce an equivalent current density to the reconstruction process (equivalent current formulation)[16]. The other one is to use the Born approximation[11]–[14] to estimate the initial total field in the investigation region. Then, the discretized integral equations are solved iteratively. Because the problem of determining the electric properties of the objects involved is ill–conditioned, regularization techniques[42]–[45] are usually employed to stabilize the matrix decomposition that are involved in the reconstruction process. In the equivalent current formulation, the pseudo–inverse transformation has been used [16]. In the approaches based on the solution of the two coupled integral equations iteratively, the Tikhonov regularization [42] is applied in each iteration. To obtain a satisfactory solution and also a satisfactory rate of convergence of the iteration process involved, the regularization parameter must be carefully selected.

In this thesis, the stochastic inverse scheme [43] with the Tikhonov regularization is applied to the above mentioned two techniques. In the equivalent current formulation, the stochastic inverse scheme allows us to find the equivalent current in the investigated body more accurately, even for the measured data with high level of noise. On the other hand, when solving the two coupled integral equations iteratively, the stochastic inversion of matrices allows us to find the regularization parameter optimally from iteration to iteration yielding a substantially increased convergence.

The stochastic inverse scheme is developed based on statistical considerations, with the

generated reconstructions and the noise modelled in terms of stochastic or random processes. Under the assumption that both the reconstructions and the noise in the measured data are uncorrelated and isotropic, the solution is stochastically optimum in the sense that repetition in the measured data produces solutions which, on the average, are optimum according to the specified error criterion.

The thesis is organized as follows. Chapter 2 is devoted to a presentation of the principle of the microwave imaging including the analytical formulations of fields, the discretization of the integral equations, the ill–posed problems and the most commonly used regularization methods, with emphasis on the Tikhonov regularization method and the stochastic inverse scheme. The relation between them is also investigated.

In Chapter 3, we explore the possibility of using the Tikhonov regularization of different orders to reconstruct dielectric bodies, with emphasis on the performance of the regularization parameter in the process of reconstructions.

In Chapter 4, a new microwave imaging algorithm based on the stochastic inverse scheme is proposed. The performance of the algorithm is demonstrated by reconstructing two dimensional objects with noise contaminated data.

One of the difficulties in the iterative methods of solving the two coupled integral equations directly is the selection of the Tikhonov regularization parameter at each iteration step. In Chapter 5, the stochastic inverse scheme is applied to the iterative reconstruction processes. By considering both the reconstruction error and the object function as random variables, the stochastic inverse scheme allows us to choose this parameter optimally. Three methods for selecting this parameter are presented. The performance of these methods is demonstrated by numerical simulations, using two–dimensional objects with noiseless data and with the data containing noise.

A conclusion of the dissertation and recommended future work are presented in Chapter 6.

1.2 Review of Previous Work

In this section, microwave imaging methods proposed by various researchers in recent decades are briefly discussed. They are: the microwave tomography technique, the pseudoinverse method with equivalent current modelling, the Born and the distorted Born iterative methods, the Newton iterative method, the conjugate gradient method, the "unrelated" illumination method, the spectral inverse technique, the maximum entropy method, the simulated annealing approach, and the time domain method.

Microwave Tomography

A great deal of work has been done in applying this approach to two and three–dimensional imaging [4]–[10], since the seminal papers [1]–[3] were published. Conventional microwave tomography systems are based on the Fourier Diffraction Theorem for a body illuminated by a plane wave and the scattered field measured with a linear array of probes. With plane wave illuminations and the assumption of weak scattering bodies, the plane wave spectrum of the scattered field contains information about the dielectric properties of the body on a circular arc of the two–dimensional Fourier spectral domain. By repeating the measurement for different directions of incidence (or view), the spectral domain can be filled and inverted to obtain an image of a cut of the body.

The main advantages of the diffraction tomography algorithm are that it permits the use of explicit formulas for solving the imaging problem and allows us to take advantage of existing efficient numerical algorithms(Fast Fourier Transform). Therefore, it is possible to complete the imaging process on a small computer. CPU time usually drops to a few seconds or a few minutes for simple two–dimensional geometries. However, as we indicated before, this method has some limitations and can only be applied to low dielectric contrast and weak scatterers since the Born or the Rytov approximations have to be used. These approximations are fundamental to the reconstruction process and limit the range of the objects that can be examined. It has been shown that for small cross–sectional area objects and small inhomoge-

neities of dielectric bodies, it is possible to use microwave tomography. However, for large inhomogeneous objects (compared to the wavelength), the reconstructed images can only give the object geometry and not a sufficient representation of the dielectric distribution inside the object.

Pseudoinverse with Equivalent Current Modelling

The first attempt to use the pseudoinverse procedure to overcome the ill–posedness associated with the permittivity reconstruction within dielectric bodies was made by Ney et al [16]. This method has been further applied by Caorsi et al [17]– [20]. In the pseudoinverse method, the moment method is first applied to the integral equation of electromagnetic inverse scattering, expressed in terms of the equivalent current density, to obtain a linear system of equation. Then the complex permittivity distribution is derived from a three–step procedure, *e.g.* (a) determining the equivalent current distribution from the measured scattered field with a pseudoinverse procedure implemented to overcome the ill–posedness in the matrix inversion process; (b) calculating the total field in the object; and (c) deriving the complex permittivities with the help of the obtained equivalent current and total field. The main advantage of this method is that the computation time is less than that of iterative algorithms, since there are no iterations involved in the algorithm. However, the low–pass effect inherent in the method limits the resolution of the image, especially when the noise level in the scattered field is high.

Born and the Distorted Born Iterative Methods

In [11] and [12], two iterative methods called the Born and the distorted Born iterative methods are proposed. In the Born iterative method, the background medium is assumed to be homogeneous and the Green functions are used in closed form. The total field within the investigation domain is initially set to be the incident field and the object function is solved numerically as a linear inverse problem. Then the object function is used to provide a new

estimate of the total field. The process is repeated iteratively until a convergence solution is obtained.

In the distorted Born iterative method, the background medium is not constrained to be homogeneous, and both the total field within the object and the wave number of the background medium are updated at each iteration.

It has been shown [13] that the Born iterative method converges for an $8.5\lambda_0$ (λ_0 is the wave number in free space) object with a permittivity contrast equal to 1:2. It has also been shown that the distorted Born iterative method converges faster than the Born iterative method. However the latter seems to be more robust when noise contamination is present.

The Newton Iterative Method

The Newton iterative method was proposed in [14] to construct dielectric permittivity distribution. In this method, the integral equations of electromagnetic inverse scattering are first transformed into matrix equations in terms of the moment method. Then an iterative procedure is developed as follows. Starting from an initial guess of the complex dielectric permittivity distribution in the investigation region, the total field inside the body is calculated. An estimate of the scattered field at the observation points is then obtained by a forward calculation. Comparing the calculated scattered field with its measured value, the variation of the scattered field is derived. Based on the relation between a small change in complex permittivity and the scattered electric field, we obtain the increased value in the complex dielectric permittivity which is used to update the initial guess or the value from previous iteration. The iterative procedure keeps going until a convergent solution is obtained.

Numerical results show that two–dimensional and three–dimensional inhomogeneous dielectric bodies immersed in water can be reconstructed. However a lot of computation is required.

The Conjugate Gradient Method

The Conjugate Gradient Method was applied in [16] to solve microwave image problems. The method starts with an initial guess that generates the first residual vector and the direction vector. Then the integral equation is solved iteratively. It has been shown [35] that lossy dielectric cylinders with contrast about 2.0 can be reconstructed. This method was further developed in [36], in which the discrepancy between the measured scattered amplitude and the calculated one is first defined for an estimated object function. Then the gradient of the functional was constructed by employing its Frechet derivative. The Conjugate Gradient Method is finally applied to minimize the functional to yield an estimate of the unknown dielectric permittivity distribution of the object.

Unrelated Illumination Method

As in the other spatial domain methods, the unrelated illumination method [15] begins with transforming the integral equations describing the electromagnetic inverse scattering into matrix equations in terms of the moment method. A non–singular incident wave matrix is then constructed by illuminating the object in different directions. The permittivity distribution within the object is obtained by solving the matrix equations, which involves the inversion of only the incident field matrix. Numerical tests show that accurate results can be obtained for ideal situations when the measured data have neither error nor noise. The main advantage of this method is that the number of detectors used for measuring scattered field can be reduced to one. The main difficulty in applying this method to microwave imaging problems is to construct the non–singular incident wave matrix, especially for large microwave imaging problems.

Spectral Inverse Technique

In this technique [48], [49], the integral equations of electromagnetic inverse scattering are first transformed into integral equations in the spectral domain by means of the Fourier

transformation. The moment method is then applied to transform the spectral domain integral equations into matrix equations. The dielectric permittivity distribution is finally reconstructed by the inversion of these matrix equations. Numerical results show that a slab with a dielectric permittivity contrast 1:2 can be reconstructed when a 2% error is present in the measured scattered field. However, no results are presented to indicate that this method can be applied to more complex geometries.

Maximum Entropy Method (MEM)

The MEM has been applied extensively to spectral analysis since 1967 when Burg presented his classic paper [65]. The basic idea is to extend a finite data time series so as to make the spectrum most probable, subject to the constraints defined in terms of a finite number of correlation coefficients. In microwave applications, the initial integral equation is first transformed into a matrix equation with the help of the moment method. An entropy function is then constructed based on the entropy concept. An algorithm is developed to maximize the entropy function. Numerical results [37],[38] indicate that the MEM is very promising for the qualitative microwave imaging of simple two–dimensional dielectric scatterers. However, for a quantitative microwave imaging of more complex two–dimensional and three–dimensional dielectric bodies, no published results are available.

Simulated Annealing Approach

This approach is based on stochastic techniques to search for the optimum state of a system. Usage of the simulated annealing technique can bypass the need for inverting large matrices and enables one to obtain the solution by applying an iterative procedure. Computer simulations [39],[40] show that simple two–dimensional dielectric scatterers can be reconstructed, but the computation time is considerable.

Time Domain Method

One of the methods in this category is that of marching–on–in–time [50] . Here, integral equations in time domain are first constructed, and then the solution is obtained by employing a marching–on–in–time procedure in terms of an iterative process, based on the Born approximation. Numerical simulations show that one–dimensional problems can be solved by this method.

1.3 Conclusion

In this Chapter, after discussing the general problem of microwave imaging, we have surveyed the reconstruction methods which have been proposed for microwave imaging by various research groups. It has been noted that more efficient microwave imaging algorithms are required for practical purposes. The basic requirements for the new algorithms are: (1) to be fast and easy to implement; (2) to be able to handle the noise in the measured data and to reduce its effect on the reconstructions; (3) to yield images of satisfactory resolution.

2

PRINCIPLE OF MICROWAVE IMAGING

2.1 Introduction

In principle, microwave imaging is aimed at obtaining some information about the inside of an object exposed to low power incident microwave radiation from limited external scattered field measurements. In general, consider a dielectric body with a complex permittivity $\varepsilon(\mathbf{r})$ situated in a homogeneous medium with known dielectric permittivity ε_b as shown in Fig. 2.1. If an electromagnetic incident wave crosses this body, a scattered field which is related to the electrical properties of the dielectric scatterer is produced. The relation between the scattered field and the scatterer can be mathematically expressed in terms of two coupled integral equations. By solving these two integral equations, the location, the shape and the permittivities of the object can be determined. If the main objective is to detect the location and the shape of the unknown body, it is traditionally called a qualitative imaging[46],[47]. If the objective is to determine the permittivity distribution as well, it is usually called a quantitative imaging.

The microwave imaging problem is inherently ill–posed[51]. Theoretical difficulties arising from issues of continuity and uniqueness can exist with all such kinds of problems, but in practice, these take the second place for it is only possible to make a limited number of discrete and noisy measurements of the scattered field that is otherwise a continuous function. When only a limited number of scattered field data can be measured, an infinite number

of scattered functions consistent with these data can be arbitrarily constructed. Therefore, there are fundamental difficulties in formulating a useful inversion algorithm, and more mundane optimization and signal processing techniques have to be considered in the practical implementation.

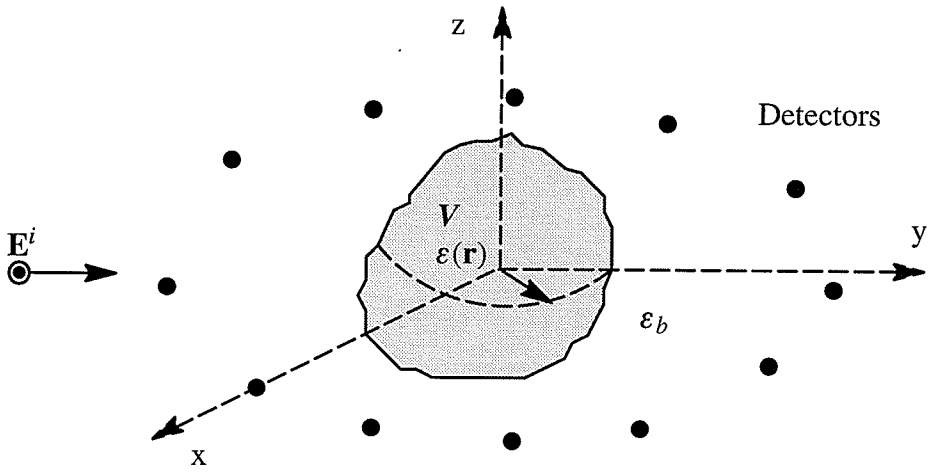

Fig. 2.1 Geometrical configuration of the microwave imaging system.

For the purpose of applying the stochastic inversion and the Tikhonov regularization method to microwave imaging problems, in this chapter, the theoretical basis of the two methods is briefly reviewed, and the inherent relation between the two methods is investigated. The statistical explanations for some of the parameters related to the methods are also given.

2.2 Integral Equations

2.2.1 Basic Integral Equations

Assume that an inhomogeneous dielectric body with arbitrary shape is immersed in a homogeneous dielectric background. The dielectric body has a complex dielectric permitivity

$$\varepsilon(\mathbf{r}) = \varepsilon'(\mathbf{r}) - j\varepsilon''(\mathbf{r}) \tag{2.1}$$

and a permeability μ_0. The background consists of a complex dielectric permittivity ε_b and a permeability μ_0. No real electric current or magnetic source current present within the body is assumed. The outline and the permittivity distribution of the body are assumed to be unknown. If incident electromagnetic fields, $\mathbf{E}^i$ and $\mathbf{H}^i$, of frequency ω, are used to illuminates the body, the incident fields satisfy the following Maxwell's equations

$$\nabla \times \mathbf{E}^i = -j\omega\mu_0\mathbf{H}^i \tag{2.2}$$

$$\nabla \times \mathbf{H}^i = j\omega\varepsilon_b\mathbf{E}^i \tag{2.3}$$

where the time dependence of $e^{j\omega t}$ has been assumed. The incident fields induce the total fields, $\mathbf{E}^t$ and $\mathbf{H}^t$, which also satisfy the following Maxwell's equations in the dielectric body

$$\nabla \times \mathbf{E}^t = -j\omega\mu_0\mathbf{H}^t \tag{2.4}$$

$$\nabla \times \mathbf{H}^t = j\omega\varepsilon(\mathbf{r})\mathbf{E}^t \tag{2.5}$$

Physically, the total electromagnetic fields, $\mathbf{E}^t$ and $\mathbf{H}^t$, can be visualized to be the sum of the incident electromagnetic fields, $\mathbf{E}^i$ and $\mathbf{H}^i$, and the scattered electromagnetic fields, $\mathbf{E}^s$ and $\mathbf{H}^s$, *i.e.*

$$\mathbf{E}^t = \mathbf{E}^i + \mathbf{E}^s \tag{2.6}$$

$$\mathbf{H}^t = \mathbf{H}^i + \mathbf{H}^s \tag{2.7}$$

From eqns. (2.2) and (2.3), a differential equation for $\mathbf{E}^i$ can be derived as

$$\nabla \times \nabla \times \mathbf{E}^i(\mathbf{r}) - k_b^2 \mathbf{E}^i(\mathbf{r}) = 0 \tag{2.8}$$

with k_b denoting the background wave number

$$k_b = \omega \sqrt{\varepsilon_b \mu_0} \tag{2.9}$$

And from eqns. (2.4) and (2.5), we have

$$\nabla \times \nabla \times \mathbf{E}^t(\mathbf{r}) - k^2(\mathbf{r})\mathbf{E}^t(\mathbf{r}) = 0 \tag{2.10}$$

where $k(\mathbf{r})$ is the wave number in the dielectric body

$$k(\mathbf{r}) = \omega \sqrt{\varepsilon(\mathbf{r})\mu_0} \tag{2.11}$$

From eqns. (2.8) and (2.10) with eqn. (2.6), we can derive the electric field equation in the body

$$\nabla \times \nabla \times \mathbf{E}^s(\mathbf{r}) - k_b^2 \mathbf{E}^s(\mathbf{r}) = [k^2(\mathbf{r}) - k_b^2] E^t(\mathbf{r}) \tag{2.12}$$

or

$$\nabla \times \nabla \times \mathbf{E}^s(\mathbf{r}) - k_b^2 \mathbf{E}^s(\mathbf{r}) = O(\mathbf{r}) E^t(\mathbf{r}) \tag{2.13}$$

where

$$O(\mathbf{r}) = [k^2(\mathbf{r}) - k_b^2] \tag{2.14}$$

is the so–called "object function" describing the electric properties of the investigated region.

Using the Green function for an unbounded space $G(\mathbf{r}, \mathbf{r}')$ [52],[53], eqn. (2.13) can be expressed in an equivalent form, as

$$\mathbf{E}^s(\mathbf{r}) = \int_{V'} G(\mathbf{r}, \mathbf{r}') O(\mathbf{r}') \mathbf{E}^t(\mathbf{r}') d\mathbf{r}' \tag{2.15}$$

The total field in (2.15) can be calculated from $\mathbf{E}^t(\mathbf{r}) = \mathbf{E}^i(\mathbf{r}) + \mathbf{E}^s(\mathbf{r})$ as

$$\mathbf{E}^t(\mathbf{r}) = \mathbf{E}^i(\mathbf{r}) + \int_{V'} G(\mathbf{r}, \mathbf{r}') O(\mathbf{r}') \mathbf{E}^t(\mathbf{r}') d\mathbf{r}' \tag{2.16}$$

The Green's function is expressed as

$$G(\mathbf{r},\mathbf{r}') = -\frac{j}{4} H_0^{(2)}(k_b|\mathbf{r}-\mathbf{r}'|) \tag{2.17}$$

for two dimensional problems with TM (Transverse Magnetic) field illumination;

$$G(\mathbf{r},\mathbf{r}') = \left(\bar{\bar{I}} + \frac{1}{k_b^2}\nabla\nabla \right) \frac{-j}{4} H_0^{(2)}(k_b|\mathbf{r}-\mathbf{r}'|) \tag{2.18}$$

for two dimensional problems with TE (Transverse Electric) field illumination; and

$$G(\mathbf{r},\mathbf{r}') = \left(\bar{\bar{I}} + \frac{1}{k_b^2}\nabla\nabla \right) \frac{\exp(-jk_b|\mathbf{r}-\mathbf{r}'|)}{4\pi\,|\mathbf{r}-\mathbf{r}'|} \tag{2.19}$$

for three dimensional problems with $\bar{\bar{I}}$ indicating unit dyad and $H_0^{(2)}$ standing for the Hankel function of the second kind and zero order.

Equations (2.15) and (2.16) are the basic integral equations for microwave imaging. Once the scattered fields are measured by detectors at observation points, the effort is made to find the object function by solving these two coupled nonlinear integral equations. The complex permittivity distributions of the unknown body can be obtained with the help of eqns. (2.14) and (2.11) if the object function has been reconstructed.

2.2.2. Integral Equations with Equivalent Current Modelling

In this formulation, an equivalent current density defined as

$$\mathbf{J}_e(\mathbf{r}) \equiv j(\omega\mu_0)^{-1} O(\mathbf{r})\mathbf{E}^t(\mathbf{r}) \tag{2.20}$$

is introduced to eqns. (2.15) and (2.16). Then they become

$$\mathbf{E}^s(\mathbf{r}) = -j\omega\mu_0 \int_{V'} G(\mathbf{r},\mathbf{r}')\mathbf{J}_e(\mathbf{r}')d\mathbf{r}' \tag{2.21}$$

and

$$\mathbf{E}^t(\mathbf{r}) = \mathbf{E}^i(\mathbf{r}) + (-j\omega\mu_0) \int_{V'} G(\mathbf{r},\mathbf{r}')\mathbf{J}_e(\mathbf{r}')d\mathbf{r}' \tag{2.22}$$

Equation (2.21) offers a clear physical picture. The scattered field $\mathbf{E}^s$ is maintained by

equivalent current density $\mathbf{J}_e(\mathbf{r})$ which occupies the dielectric body. The amplitude and the phase of the equivalent current depends on the complex permittivity $\varepsilon(\mathbf{r})$ and the total field in the body and the frequency of the incident wave. The reconstruction can also be performed by solving the linearized integral eqn. (2.21). From the scattered field measurements, the equivalent current distribution within the object can be obtained. The total field inside the body is then calculated in terms of eqn. (2.22). The object function and the permittivity distributions of the dielectric body can be determined with the help of eqns. (2.20) and (2.14).

Equivalent current modelling can also be used for qualitative electromagnetic imaging [46], [47] in which only the location and the outline of the dielectric body are concerned. By defining

$$\mathbf{J}_e(\mathbf{r}) = 0, \quad \text{inside the body}$$

$$\mathbf{J}_e(\mathbf{r}) \neq 0, \quad \text{outside the body}$$

the location and the outline of the object can be detected.

2.2.3. Integral Equation with Born Approximation

Consider the total electric field $\mathbf{E}^t(\mathbf{r})$ expressed as the sum of the incident electric field $\mathbf{E}^i(\mathbf{r})$ and the scattered electric field $\mathbf{E}^s(\mathbf{r})$. We rewrite the integral eqn. (2.15) as

$$\mathbf{E}^s(\mathbf{r}) = \int_{V'} G(\mathbf{r},\mathbf{r}')O(\mathbf{r}')\mathbf{E}^i(\mathbf{r}')d\mathbf{r}' + \int_{V'} G(\mathbf{r},\mathbf{r}')O(\mathbf{r}')\mathbf{E}^s(\mathbf{r}')d\mathbf{r}' \tag{2.23}$$

If the object is of a low contrast inhomogeneous material, *i.e.* the permittivity differences between the dielectric body and the background are very small, and the magnitude of the scattered field in the object is much smaller than that of the incident field, the second term of eqn. (2.23) may be neglected yielding

$$\mathbf{E}^s(\mathbf{r}) \approx \int_{V'} G(\mathbf{r},\mathbf{r}')O(\mathbf{r}')\mathbf{E}^i(\mathbf{r}')d\mathbf{r}' \tag{2.24}$$

This constitutes the first order Born approximation. Studies have shown that [10] for the first

order Born approximation to be valid, a necessary condition is that the change in phase between the incident field and the wave propagating through the object be less than π.

2.2.4. Integral Equation with Rytov approximation

Unlike the Born approximation formulation, the Rytov approximation is based on the fact that the change in the scattered phase over one wavelength is small. The phase of the scattered field can be expressed for the two–dimensional case as

$$\phi^s(\mathbf{r}) = \frac{1}{E^i(\mathbf{r})} \int_{S'} G(\mathbf{r}, \mathbf{r}') O(\mathbf{r}') E^i(\mathbf{r}') d\mathbf{r}' \tag{2.25}$$

It has been proven that [4] the Born approximation provides a better estimate of the scattered field for objects small in size with relatively larger contrast of the dielectric medium. On the other hand, the Rytov approximation gives a more accurate estimate of the scattered field for larger sized objects with relatively smaller contrast in permittivity.

2.3. Discretization of the Integral Equations

For the purpose of solving the general integral equations in spatial domain numerically, the integral equations discretized appropriately. Consider a cylindrical dielectric body with arbitrary shape situated in a two dimensional region S of a square area, called the investigation domain. Detectors for measuring the scattered field are situated on a loop surrounding the investigation domain, as shown in Fig. 2.2. Suppose a TM electric field is employed to illuminate the object. The scattered field at the receiving points can be expressed in terms of the two dimensional Green's function as

$$\mathbf{E}^s = \int\int_{S'} G(x, y; x', y') O(x', y') \mathbf{E}^t(x', y') dx' dy' \tag{2.26}$$

To discretize this integral equation, we divide the investigation domain S in terms of rectangular patches. For graphic simplicity, we assume that all patches have the same size. Each patch is labeled with index i, where i indicates the *i–th* patch in the investigation do-

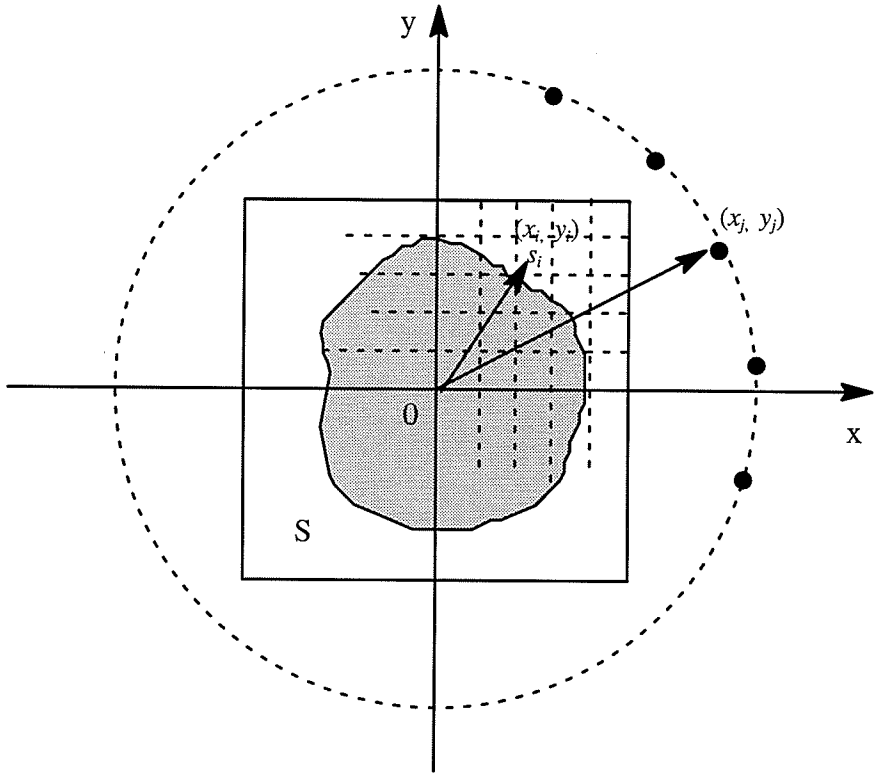

Fig. 2.2 Discretizing the investigation domain.

main. The area of the *i–th* patch is designated as s_i, and the radius vector from the original point to the central point of the *i–th* patch as $\mathbf{r}_i = (x_i, y_i)$. We then expand the object function $O(x, y)$ and the total field $E^t(x, y)$ inside the investigation region in a piecewise–constant manner as

$$O(x, y) = \sum_{i=1}^{n} O_i \, f_i(\mathbf{r}) \tag{2.27}$$

$$E^t(x, y) = \sum_{i=1}^{n} E_i^t \, f_i(\mathbf{r}) \tag{2.28}$$

where $f_i(\mathbf{r})$ is called basis function and n indicates the total number of the patches. O_i and E_i^t are coefficients. Following the classical prescription of the moment method [41], the ex-

pansion (2.27) and (2.28) are inserted into eqn. (2.26). If the puls function is selected as the basis function, *i.e.*

$$f_i(\mathbf{r}) = \begin{cases} 1, & \mathbf{r} \in s_i \\ 0, & \mathbf{r} \notin s_i \end{cases} \tag{2.29}$$

and Dirac's delta function as the test function, considering that the measured data are at the finite points around the object, we have a system of linear algebraic equations

$$E^s(x_j, y_j) = \sum_{i=1}^{n} G(i,j) E_i^t \, O_i \quad , \quad (j = 1, 2, \ldots, \mathrm{m}) \tag{2.30}$$

with m indicating the total number of detectors, and the coefficient $G(i, j)$ is

$$G(i, j) = \int\int_{S_i} G(k_b \sqrt{(x' - x_j)^2 + (y' - y_j)^2}\ ) dx' dy' \tag{2.31}$$

To evaluate the term $G(i,j)$, we adopt the technique from the work [54]. The integral region s_i in (2.30) is replaced with a circular cell of a radius $a = \sqrt{s_i/\pi}$ centered at (x_i, y_i) having the same area as s_i. With the problem considered here, the corresponding result is

$$G(i,j) = \begin{cases} -\dfrac{j\pi a}{2k_b} J_1(k_b a) H_0^{(2)}(k_b |\mathbf{r}_i - \mathbf{r}_j|) & , \quad i \neq j \\ -\dfrac{j}{2k_b^2} [\pi k_b a H_1^{(2)}(k_b a) - 2j] & , \quad i = j \end{cases} \tag{2.32}$$

where J_1, and $H_1^{(2)}$ are the first kind Bessel and the first kind Hankel functions of the second order. Now we can write eqn. (2.30) in matrix form as

$$\mathbf{E}^s = [G_2] \ [E^t] \ \mathbf{O} \tag{2.33}$$

where $\mathbf{E}^s$ is a vector of dimension m (one illumination is considered here)

$$\mathbf{E}^s = [E_1^s, E_2^s, \ldots, E_m^s]^T \tag{2.34}$$

with T representing the transpose of a vector or a matrix, and $[G_2]$ is a matrix of dimension $m \times n$ containing the Green function relating the observation points to the investigation points,

$$[G_2] = \begin{bmatrix} G_{11} & G_{12} & \cdots & G_{1n} \\ \vdots & \vdots & \vdots & \vdots \\ G_{m1} & G_{m1} & \cdots & G_{mn} \end{bmatrix} \tag{2.35}$$

$[E^t]$ is a diagonal matrix of dimension n containing the total field at each patch

$$[E^t] = \begin{bmatrix} E_1^t & & & 0 \\ & E_2^t & & \\ & & \ddots & \\ 0 & & & E_n^t \end{bmatrix} \tag{2.36}$$

and $\mathbf{O}$ is a vector of dimension n containing the object function.

$$\mathbf{O} = [O_1, O_2, \ldots, O_n]^T \tag{2.37}$$

From the relation of eqn. (2.6), we can also write the discretized integral equation (2.16) in matrix form

$$\mathbf{E}^t = \mathbf{E}^i + [G_1]\ [O]\ \mathbf{E}^t \tag{2.38}$$

where $[G_1]$ is the Green function relating the points in the investigation region, $\mathbf{E}^t$ and $\mathbf{E}^i$ are vectors of dimension n.

$$\mathbf{E}^t = [E_1^t, E_2^t, \ldots, E_n^t]^T \tag{2.39}$$

$$\mathbf{E}^i = [E_1^i, E_2^i, \ldots, E_n^i]^T \tag{2.40}$$

and $[O]$ is a diagonal matrix containing the object functions in the patches

$$[O] = \begin{bmatrix} O_1 & & & \\ & O_2 & & 0 \\ & & \ddots & \\ 0 & & & O_n \end{bmatrix} \tag{2.41}$$

In the same manner, we can write discretized integral equations for eqns. (2.22), and (2.24) in matrix forms as

$$\mathbf{E}^s = [G_2]\ \mathbf{J}_e \tag{2.42}$$

where $\mathbf{J}_e$ is a vector of dimension n containing the equivalent current density which has been factorized by $(-j\omega\mu_0)$ in order to keep a uniform expression for the Green function, and

$$\mathbf{E}^s = [G_2]\ [E^i]\ \mathbf{O} \tag{2.43}$$

where $[E^i]$ presents a diagonal matrix with its elements being the incident fields in the patches.

If the total field $[E^t]$ in the investigation region is obtained, the eqn. (2.33) can also be written as

$$\mathbf{E}^s = [D]\ \mathbf{O} \tag{2.44}$$

with [D] = $[G_2]\ [E^t]$, being an $m \times n$ dimension matrix. Equations (2.33), (2.38), (2.42) and (2.44) are the discretized integral equations employed to develop microwave imaging in spatial domain. Visually, these operators are nothing more than complex. The difficulties in the solution of these equations arise from the so–called "ill–posed problems".

2.4 Ill–posedness in Microwave Imaging

The microwave imaging problem is, in general, an ill–posed problem. First, the number of the total detectors is not necessarily equal to the number of patches used to divide the investigation domain, *i.e.* $m \neq n$ referring eqns. (2.33), (2.42) and (2.44). In the practical point of view, the selection of the number of patches depends on the requirement of the resolution to the image, the characteristics of the body to be detected, the capacity of the computer used, and so on. The number of the detectors can be limited by the physical construction of the imaging system, also the capacity of the computer. Increasing either the number of the patches or the number of detectors results in increase of expensive computation time. On the other hand, even if we carefully select the number of the detectors and the number of patches, *i.e.* $m = n$ it is hard to guarantee the operator is not singular. Secondly, the solution of the microwave imaging is not unique [56]–[58]. This nonunique solution is generated by so called "nonradiating sources" [57] inherited in the body, and also by the limited measurements mentioned before. Thirdly, there is always noise and errors accompanied with the measured data, such as the surrounding noise and measurement error. There are also numerical errors accumulated in the calculation of the inverse of the matrix, especially when the dimension of the matrix is large. The condition number of the matrix representing the Green's function can be very large. In order to solve an ill–posed problem, techniques called "regularization" usually have to be employed. The solution to a regularized problem can be well–behaved and give a reasonable approximation to the solution of the ill–posed problem allowing us to develop a satisfactory image from a practical point of view.

2.5 Regularization

2.5.1 Methods of handling ill–posed problems

Numerous methods have been proposed for treating and regularizing various types of ill–posed problems mathematically[42]–[44]. The rationale in most methods is to construct

a "solution" that is acceptable as a meaningful approximation and is sufficiently stable from the computational standpoint. The main techniques that are employed to treat an ill–posed problem are summarized as follows:

1) changing the definition of what is meant by an acceptable solution;
2) changing the space to which the acceptable solution belongs;
3) revising the problem statement;
4) introducing regularizing operators;
5) introducing probability concepts so as to obtain a stochastic extension of the original deterministic problem.

For the purpose of exploring the possibility of using the Tikhonov regularization and the stochastic inverse scheme to reconstruct high contrast dielectric objects in the spatial domain, we briefly review the fundamental principles of them.

2.5.2 Tikhonov Regularization

In its general form, this method is discussed in detail in [42]. Its objective is to produce an "estimate" of some unknown quantity $\mathbf{X}$, usually a vector or a function, with the help of data $\mathbf{Y}$. The estimate is derived as the solution of an optimization problem, in the form of

$$\min_{\mathbf{X}} \left\{ \Delta(\mathbf{X}, \mathbf{Y}) + \alpha\, \Omega(\mathbf{X}) \right\} \tag{2.45}$$

in which Δ is a measure to the solution $\mathbf{X}$, Ω is a regularization functional, and $\alpha > 0$ is called regularization or smoothing parameter.

Specifically, for an ill–posed system of linear equations

$$\mathbf{Y} = [A]\mathbf{X} + \mathbf{N} \tag{2.46}$$

where $\mathbf{Y}$ and $\mathbf{N}$ are an $m \times 1$ vectors with $\mathbf{N}$ standing for the noise and error in the data $\mathbf{Y}$, $\mathbf{X}$ an $n \times 1$ vector, $[A]$ an $m \times n$ matrix. Reasonable choices of the Δ and Ω in this case are

$$\Delta(\mathbf{X}, \mathbf{Y}) = \| [A]\mathbf{X} - \mathbf{Y} \|^2 \tag{2.47}$$

and

$$\Omega(\mathbf{X}) = \| [T]\mathbf{X} \|^2 \tag{2.48}$$

where $\| . \|$ indicates the Euclidean norm, and $[T]$ is a linear operator having to be conveniently chosen. If $[T]\mathbf{X}$ is the *i–th* derivative of $\mathbf{X}$, then it is called the *i–th* order of the Tikhonov regularization. Thus our estimate of $\mathbf{X}$ is the solution of

$$\min_{\mathbf{X}} \left\{ \| [A]\mathbf{X} - \mathbf{Y} \|^2 + \alpha \| [T]\mathbf{X} \|^2 \right\} \tag{2.49}$$

The solution of the problem posed in eqn. (2.49) is equivalent to the solution of the matrix equation

$$([A]^H[A] + \alpha [T]^H[T])\mathbf{X}_T = [A]^H\mathbf{Y} \tag{2.50}$$

and is given

$$\mathbf{X}_T = ([A]^H[A] + \alpha [T]^H[T])^{-1}[A]^H\mathbf{Y} \tag{2.51}$$

where $\mathbf{X}_T$ indicates the Tikhonov regularization solution of $\mathbf{X}$ and H denotes the conjugate transpose of a matrix.

The existence of the solution of eqn. (2.51) is obvious. However, care must be taken in choosing the regularization parameter. If it is too big, too much useful information may be lost. If it is too small, we may not obtain a stable solution.

2.5.3 Stochastic Inverse scheme

The stochastic approach [43] starts from very different assumptions, with the errors in measured data being treated as Gaussian random variables and the solution of unknown being a stochastic process. After an error criterion is specified, the solution is stochasticlly optimum in the sense that repetition in the measurements of the data produces solutions which are optimum according to the specified error criterion. Consider a general ill–posed system of linear equations

$$\mathbf{Y} = [A]\mathbf{X} + \mathbf{N} \tag{2.52}$$

in which both **N** and **X** are assumed to be stochastic processes. Without loss of generality, **X, N** and **Y** each can be considered to have zero mean value since an equation identical in form to eqn. (2.52) is obtained when the known means are subtracted from the equation. The stochastic inverse method seeks an estimate $\mathbf{X}_s$ of **X** from measured data **Y**

$$\mathbf{X}_s = L\mathbf{Y} \tag{2.53}$$

that minimizes the mean square error

$$\delta_{\mathbf{X}}^2 = E\left\{\| \mathbf{X} - \mathbf{X}_s \|^2\right\} \tag{2.54}$$

where $E\{\ .\ \}$ denotes the expected value of a random number, L is a linear operator and $\|\ .\ \|$ is the Euclidean norm . The eqn. (2.54) can also be written in terms of the trace (Tr) of the error matrix[60]

$$\delta_{\mathbf{X}}^2 = \mathrm{E}\{\ Tr[(\mathbf{X} - \mathbf{X}_s)\ (\mathbf{X} - \mathbf{X}_s)^H]\ \} = \mathrm{E}\{\ (\mathbf{X} - \mathbf{X}_s)^H\ (\mathbf{X} - \mathbf{X}_s)\ \} \tag{2.55}$$

The error matrix can be expanded for simplification as

$$(\mathbf{X} - \mathbf{X}_s)\ (\mathbf{X} - \mathbf{X}_s)^H = (\mathbf{X}\mathbf{X}^H - \mathbf{X}\mathbf{X}_s^H - \mathbf{X}_s\mathbf{X}^H + \mathbf{X}_s\mathbf{X}_s^H) \tag{2.56}$$

Since

$$\mathbf{X}_s^H = \mathbf{Y}^H L^H = (\mathbf{X}^H[A]^H + \mathbf{N}^H)L^H \tag{2.57}$$

then

$$\mathbf{X}\mathbf{X}_s^H = \mathbf{X}\mathbf{X}^H[A]^H L^H + \mathbf{X}\mathbf{N}^H L^H \tag{2.58}$$

Also

$$\mathbf{X}_s\mathbf{X}^H = L\mathbf{Y}\mathbf{X}^H = L([A]\mathbf{X} + \mathbf{N})\mathbf{X}^H \tag{2.59}$$

$$\mathbf{X}_s\mathbf{X}^H = L[A]\mathbf{X}\mathbf{X}^H + L\mathbf{N}\mathbf{X}^H \tag{2.60}$$

and

$$\mathbf{X}_s\mathbf{X}_s^H = L([A]\mathbf{X}\mathbf{X}^H[A]^H + [A]\mathbf{X}\mathbf{N}^H + \mathbf{N}\mathbf{X}^H[A]^H + \mathbf{N}\mathbf{N}^H)L^H \tag{2.61}$$

Since the trace of a sum of two matrices is equal to the sum of the two traces, the ex-

pected value and the trace operators can be interchanged. Considering the expected values of the four terms separately, we obtain

$$\mathrm{E}\{\ \mathbf{X}\mathbf{X}^H\ \} = [R_{\mathbf{X}}] \tag{2.62}$$

where $[R_{\mathbf{X}}]$ is the correlation matrix of the random vector $\mathbf{X}$.

If $\mathbf{X}$ and $\mathbf{N}$ are independent

$$\mathrm{E}\{\ \mathbf{X}\mathbf{N}^H\ \} = 0 \tag{2.63}$$

$$\mathrm{E}\{\ \mathbf{X}\mathbf{X}_s^H\ \} = [R_{\mathbf{X}}][A]^H L^H \tag{2.64}$$

and

$$\mathrm{E}\{\ \mathbf{X}_s\mathbf{X}^H\ \} = L[A][R_{\mathbf{X}}] \tag{2.65}$$

$$\mathrm{E}\{\ \mathbf{X}_s\mathbf{X}_s^H\ \} = L[A][R_{\mathbf{X}}][A]^H L^H + L[R_{\mathbf{N}}]L^H \tag{2.66}$$

where

$$[R_{\mathbf{N}}] = \mathrm{E}\ \{\ \mathbf{N}\mathbf{N}^H\ \} \tag{2.67}$$

Now the mean square error can be expressed as

$$\delta_{\mathbf{X}}^2 = Tr([R_{\mathbf{X}}] - [R_{\mathbf{X}}][A]^H L^H - L[A][R_{\mathbf{X}}] + L[A][R_{\mathbf{X}}][A]^H L^H + L[R_{\mathbf{N}}]L^H) \tag{2.68}$$

Since the correlation matrix is symmetric and the trace of the transpose of a matrix is equal to the trace of the matrix, the error expression may be simplified further to

$$\delta_{\mathbf{X}}^2 = Tr([R_{\mathbf{X}}] - 2[R_{\mathbf{X}}][A]^H L^H + L[A][R_{\mathbf{X}}][A]^H L^H + L[R_{\mathbf{N}}]L^H) \tag{2.69}$$

The desired linear transform L can now be determined by

$$\frac{\partial \delta_{\mathbf{X}}^2}{\partial L} = -2[R_{\mathbf{X}}][A]^H + 2L[A][R_{\mathbf{X}}][A]^H + 2L[R_{\mathbf{N}}] \tag{2.70}$$

Let this equation to zero, we obtain the optimum L_o which minimizes $\delta_{\mathbf{X}}^2$

$$L_o = [R_{\mathbf{X}}][A]^H([A][R_{\mathbf{X}}][A]^H + [R_{\mathbf{N}}])^{-1} \tag{2.71}$$

Hence, the optimum estimate $\mathbf{X}_s$ is

$$\mathbf{X}_s = [R_{\mathbf{X}}][A]^H([A][R_{\mathbf{X}}][A]^H + [R_{\mathbf{N}}])^{-1}\ \mathbf{Y} \tag{2.72}$$

which is the equation we desired. Equation (2.72) can also be written as

$$\mathbf{X}_s = ([A]^H[R_\mathbf{N}]^{-1}[A] + [R_\mathbf{X}]^{-1})^{-1}[A]^H[R_\mathbf{N}]^{-1}\mathbf{Y} \tag{2.73}$$

Equations (2.72) and (2.73) are algebraically identical. Computationally, they are quite different, however, because eqn. (2.72) involves the inverse of an $m \times m$ symmetric matrix, and eqn. (2.73) an $n \times n$ symmetric matrix. Thus, if the number of data is less than the number of unknowns, eqn. (2.72) is more economical and *vice versa.*

2.5.4 Relations between Stochastic Inversion and Tikhonov Regularization

In eqn. (2.73), If we further assume that both the random vectors $\mathbf{N}$ and $\mathbf{X}_s$ are uncorrelated and also isotropic, we have

$$[R_\mathbf{N}] = \sigma_\mathbf{N}^2[I] \tag{2.74}$$

$$[R_\mathbf{X}] = \sigma_\mathbf{X}^2[I] \tag{2.75}$$

with $\sigma_\mathbf{N}^2$ and $\sigma_\mathbf{X}^2$ denoting the variances of the random vectors $\mathbf{N}$ and $\mathbf{X}_s$. Thus, eqn. (2.73) becomes

$$\mathbf{X}_s = ([A]^H[A] + \sigma_\mathbf{N}^2/\sigma_\mathbf{X}^2[I])^{-1}[A]^H\mathbf{Y} \tag{2.76}$$

which is equivalent to the zero–order Tikhonov regularization with the regularization parameter taking the form of

$$\alpha = \sigma_\mathbf{N}^2/\sigma_\mathbf{X}^2 \tag{2.77}$$

It also can be shown that equivalence between eqn. (2.51) and eqn. (2.73) also holds when[61]

$$[R_\mathbf{X}] = ([T]^H[T])^{-1} \tag{2.78}$$

At this point, the Tikhonov regularization can be statistically interpreted in terms of the noise variance and the reconstruction variance. Besides this, eqn. (2.78) also shows us a possible

way to estimate the regularization parameter.

2.5.5 Maximum Likelihood Estimate of the Noise Variance

Consider matrix equation[62]

$$\mathbf{Y} = [A]\ \mathbf{X} + \mathbf{N} \tag{2.79}$$

where $\mathbf{Y}$ is a vector of dimension m, $[A]$ is matrix of dimension of $m \times n$, $\mathbf{X}$ is a vector of dimension n and $\mathbf{N}$ is a vector of dimension m, presenting the random error in the measured data $\mathbf{Y}$. We assume $\mathbf{N}$ follows normal distribution with its expected value being zero, *i.e.* $\mathrm{E}\{\mathbf{N}\} = 0$ and its variance being $\sigma_{\mathbf{N}}^2$. The vector $\mathbf{Y}$ follows a mutilate normal distribution with the mean vector $[A]\mathbf{X}$ and variance matrix $\sigma_{\mathbf{N}}^2\,[I]$, *i.e.*

$$Y : ([A]\mathbf{X},\ \sigma_{\mathbf{N}}^2[I]) \tag{2.80}$$

Thus the likelihood functional can be expressed as[62]

$$H = H(\mathbf{X}, \sigma_{\mathbf{N}}^2/\mathbf{Y}) = f(\mathbf{Y}/\mathbf{X}, \sigma_{\mathbf{N}}^2) = f(\mathbf{Y}_1, \mathbf{Y}_2, \ \ldots\ , \mathbf{Y}_m/\mathbf{X}, \sigma_{\mathbf{N}}^2)$$

$$= \frac{1}{(2\pi)^{m/2}(\sigma_{\mathbf{N}}^2)^{m/2}} \exp[-\frac{1}{2\sigma_{\mathbf{N}}^2}(\mathbf{Y} - [A]\mathbf{X})^H(\mathbf{Y} - [A]\mathbf{X})] \tag{2.81}$$

and the log of the functional is

$$\log(H) = \log(\mathbf{X}, \sigma_{\mathbf{N}}^2/\mathbf{Y})$$

$$= -\frac{m}{2}\log(2\pi\sigma_{\mathbf{N}}^2) - \frac{1}{2\sigma_{\mathbf{N}}^2}(\mathbf{Y} - [A]\mathbf{X})^H(\mathbf{Y} - [A]\mathbf{X}) \tag{2.82}$$

Let

$$\frac{\partial}{\partial \mathbf{X}} \log(H) = 0$$

we obtain

$$\hat{\mathbf{X}} = ([A]^H[A])^{-1}[A]^H\ \mathbf{Y} \tag{2.83}$$

where $\hat{\mathbf{X}}$ denotes the maximum likelihood estimate of $\mathbf{X}$.

Let

$$\frac{\partial}{\partial \sigma_{\mathbf{N}}^2} \log(H) = 0$$

we get

$$\hat{\sigma}_{\mathbf{N}}^2 = \frac{1}{m}(\mathbf{Y} - [A]\hat{\mathbf{X}})^H \ (\mathbf{Y} - [A]\hat{\mathbf{X}}) \tag{2.84}$$

with $\hat{\sigma}_{\mathbf{N}}^2$ presenting the maximum likelihood estimate of variance $\sigma_{\mathbf{N}}^2$.

2.5.6 An estimate of the Object Function Correlation Matrix by the Tikhonov Regularization

Considering the maximum likelihood solution (2.83), we can rewrite the Tikhonov regularization solution eqn. (2.51) as

$$\begin{aligned}\mathbf{X}_T &= ([A]^H[A] + \alpha[T]^H[T])^{-1}[A]^H\mathbf{Y} \\ &= ([A]^H[A] + \alpha[T]^H[T])^{-1}([A]^H[A])\,\hat{\mathbf{X}} \\ &= [Z_T]\ \hat{\mathbf{X}}\end{aligned} \tag{2.85}$$

where $[Z_T] = ([A]^H[A] + \alpha[T]^H[T])^{-1}([A]^H[A])$

The expected value of $\mathbf{X}_T$ is

$$E\{\mathbf{X}_T\} = E\left\{[Z_T]\ \hat{\mathbf{X}}\right\} = [Z_T]\ E(\hat{\mathbf{X}}) \tag{2.86}$$

The expected value of the maximum likelihood $\hat{\mathbf{X}}$ is

$$\begin{aligned}E\{\ \hat{\mathbf{X}}\ \} &= E\left\{([A]^H[A])^{-1}[A]^H\mathbf{Y}\right\} \\ &= E\left\{([A]^H[A])^{-1}[A]^H([A]\mathbf{X} + \mathbf{N})\right\} \\ &= E\left\{([A]^H[A])^{-1}[A]^H[A]\mathbf{X} + ([A]^H[A])^{-1}[A]^H\mathbf{N})\right\}\end{aligned}$$

Since $E\{\mathbf{N}\} = 0$, and $([A]^H[A])^{-1}[A]^H[A] = [I]$, we obtain

$$E\left\{ \hat{\mathbf{X}} \right\} = \mathbf{X} \tag{2.87}$$

and

$$E\left\{ \mathbf{X}_T \right\} = [Z_T]\ \mathbf{X} \tag{2.88}$$

The correlation matrix of $\mathbf{X}_T$ can be expressed as

$$[R_{\mathbf{X}}] = E\left\{[\mathbf{X}_T - E\{\mathbf{X}_T\}][\mathbf{X}_T - E\{\mathbf{X}_T\}]^H\right\}$$

Since

$$\mathbf{X}_T - E\{\mathbf{X}_T\} = \mathbf{X}_T - Z_T\ \mathbf{X}$$

$$= ([A]^H[A] + \alpha[T]^H[T])^{-1}[A]^H\mathbf{Y} - ([A]^H[A] + \alpha[T]^H[T])^{-1}([A]^H[A])\ \mathbf{X}$$

$$= ([A]^H[A] + \alpha[T]^H[T])^{-1}[A]^H\mathbf{N}$$

and $E\left\{ \mathbf{N}\mathbf{N}^H \right\} = \sigma_{\mathbf{N}}^2\,[I]$. The correlation matrix of $\mathbf{X}_T$ is given by

$$[R_{\mathbf{X}}] = E\left\{([A]^H[A] + \alpha[T]^H[T])^{-1}[A]^H\mathbf{N}\mathbf{N}^H[A]([A]^H[A] + \alpha[T]^H[T])^{-1}\right\}$$

$$= ([A]^H[A] + \alpha[T]^H[T])^{-1}[A]^H E\{\mathbf{N}\mathbf{N}^H\}[A]([A]^H[A] + \alpha[T]^H[T])^{-1}$$

$$= ([A]^H[A] + \alpha[T]^H[T])^{-1}[A]^H\sigma_{\mathbf{N}}^2[I][A]([A]^H[A] + \alpha[T]^H[T])^{-1}$$

$$= \sigma_{\mathbf{N}}^2([A]^H[A] + \alpha[T]^H[T])^{-1}[A]^H[A]([A]^H[A] + \alpha[T]^H[T])^{-1} \tag{2.89}$$

It is worth noting that when the regularization parameter goes to zero, the correlation matrix goes to

$$[R_{\mathbf{X}}] \approx \sigma_{\mathbf{N}}^2([A]^H[A])^{-1}\,. \tag{2.90}$$

This result is used in chapter 5 for obtaining initial Tikhonov regularization parameter.

2.5.7 Total variance

The total variance of $\mathbf{X}_T$ is defined as[64]

$$Tr\left([R_{\mathbf{X}}]\right) = \sigma_{\mathbf{N}}^2 \; Tr\left[([A]^H[A]+\alpha[I])^{-1}[A]^H[A]([A]^H[A]+\alpha[I])^{-1}\right]$$

$$= \sigma_{\mathbf{N}}^2 \sum_{i=1}^{s} \frac{\lambda_i}{(\lambda_i+\alpha)^2} \tag{2.91}$$

for the 0–*th* order Tikhonov regularization, where $\lambda_1, \lambda_2, \ldots, \lambda_s$ are the non–zero eigenvalues of $([A]^H[A])$. From the form above, we notice that the Tikhonov regularization parameter α can improve the total variance of $\mathbf{X}_T$, especially when one or more of the eigenvalues are very small.

2.6 Conclusion

In this chapter, after reviewing the equations used in microwave imaging, we discussed some of the related problems such as the ill–posed problem and the regularization. Two regularization methods, the Tikhonov regularization method and the stochastic inversion method, were presented. It has been shown that for the Gaussian distribution random noise, the Tikhonov regularization parameter can be interpreted statistically in terms of the noise variance and the reconstruction variance. The maximum likelihood estimate of the noise variance and statistic properties of the Tikhonov regularization were also given.

3

MICROWAVE IMAGING OF DIELECTRIC BODIES WITH EQUIVALENT CURRENT MODELLING AND TIKHONOV REGULARIZATION

3.1 Introduction

As mentioned before, the microwave imaging methods proposed so far fall into two main categories, namely the spectral domain methods and the spatial domain methods. As for the spectral domain methods, they are fast and seem not to be sensitive to the random noise in the measured field, but they are only valid for low contrast dielectric bodies and week scatterers, since the Born or the Rytov approximations have to be employed in the reconstruction algorithms. On the other hand, the spatial domain methods have the advantage that no strict limitations are imposed relative to the size and dielectric nature of the scatterers, but, until now, there are at least three obvious difficulties: a long duration in the reconstruction process, a low tolerance of noise and errors in the scattered data, and an image that is not of a satisfactory resolution. For practical applications, more efficient algorithms are required. In this chapter, we explore the possibility of using the Tikhonov regularization of different orders to reconstruct dielectric bodies and report on an experimental study of the performance of this method, with emphasis on the optimum selection of the regularization parameter as it relates to the noise level [30]–[32]. The reconstruction process has three steps: first, the equivalent current density distribution within the scatterer is obtained by inverting eqn. (2.21) with the Tikhonov regularization of different orders; second, the total

field within the body is calculated in terms of eqn. (2.22); finally, the permittivity distribution inside the object is computed by means of eqn. (2.20). It is shown that in the presence of noise in the scattered field data, the application of the Tikhonov regularization for the treatment of the equivalent current density integral yields an efficient solution for these types of inverse problems.

3.2 Tikhonov Regularization

Consider the noise in the measured scattered field, we may rewrite eqn. (2.42) as

$$\mathbf{E}^s = [G_2]\mathbf{J}_e + \mathbf{N} \tag{3.1}$$

where $\mathbf{N}$ is a $m \times 1$ vector representing the noise in the measured data $\mathbf{E}^s$, which may include environment noise, instrument noise, detector position error, and measuring error. As indicated earlier, the solution of (3.1) is in general not unique. For if $[G_2]$ is singular, there may exist a family of solution $\mathbf{J}_e^0$ of the homogeneous equation $[G]\mathbf{J}_e^0 = 0$, corresponding (3.1). The component $\mathbf{J}_e^0$ represents the "nonradiating sources", which produce no electric field at the observation points. On the other hand, the number of the measurements is usually less than the unknowns and the unknowns may not all be independent of each other. This limits the least–squares to apply our problems. Applying the Tikhonov regularization to (3.1), our problem is simply stated to find a solution which minimizes the functional

$$\min_{\mathbf{J}_e} \left\{ \| [G_2]\mathbf{J}_e - \mathbf{E}^s \|^2 + \alpha \| [T]\mathbf{J}_e \|^2 \right\} \tag{3.2}$$

which is equivalent to solving the following linear system of equations

$$\mathbf{J}_e^T = ([G_2]^H[G_2] + \alpha[T]^H[T])^{-1}[G_2]^H\mathbf{E}^s \tag{3.3}$$

where $\mathbf{J}_e^T$ indicates the Tikhonov regularization solution of (3.1). $[T]$ is defined in eqn. (2.48) and α the regularization parameter. For the zero–order Tikhonov regularization, $[T]^H[T]$ is a $n \times n$ identity matrix denoted as $[I]$. For the first and the second order Tikho-

nov regularization, the corresponding $[T]^H[T]$ matrices are

$$[T]^H[T] = \begin{bmatrix} 1 & -1 & & & & \\ -1 & 2 & -1 & & & \\ & -1 & 2 & -1 & & \\ & & \ddots & \ddots & \ddots & \\ & & & -1 & 2 & -1 \\ & & & & 1 & -1 \end{bmatrix} \tag{3.4}$$

and

$$[T]^H[T] = \begin{bmatrix} 1 & -2 & 1 & & & & \\ -2 & 5 & -4 & 1 & & & \\ 1 & -4 & 6 & -4 & 1 & & \\ & 1 & -4 & 6 & -4 & 1 & \\ & & \ddots & \ddots & \ddots & \ddots & \ddots \\ & & & 1 & -4 & 6 & -4 & 1 \\ & & & & 1 & -4 & 5 & -2 \\ & & & & & 1 & -2 & 1 \end{bmatrix} \tag{3.5}$$

respectively.

It is worth noting that the matrix $([G_2]^H[G_2] + \alpha[T]^H[T])$ is always invertable if the Tikhonov regularization is carefully chosen. Using the following relation

$$([G_2]^H[G_2] + \alpha[T]^H[T])^{-1}[G_2]^H = [G_2]^H([G_2][G_2]^H + \alpha[T][T]^H)^{-1} \tag{3.6}$$

we may also write (3.3) as

$$\mathbf{J}_e^T = [G_2]^H([G_2][G_2]^H + \alpha[T][T]^H)^{-1}\mathbf{E}^s \tag{3.7}$$

Mathematically, eqn. (3.3) and eqn. (3.7) are the same. Numerically, they are quite different. Equation (3.3) deals with the inversion of a matrix of dimension $n \times n$, and eqn. (3.7) is associated with an $m \times m$ matrix inversion. Therefore, if the number of unknown variables is less than the number of equations, computationally, eqn. (3.3) is more economical. If the number of the unknowns is larger than the number equations, eqn. (3.7) is more efficient.

After the equivalent current is obtained, the total field inside the investigation region can be determined by a forward calculation

$$\mathbf{E}^t = [G_1]\mathbf{J}_e^T + \mathbf{E}^i \tag{3.8}$$

The object function is then calculated in terms of the eqn. (2.20) with matrix form

$$\mathbf{J}_e^T = [E^t]\mathbf{O} \tag{3.9}$$

with $[E^t]$ being defined eqn. (2.36).

The problem of the choice of the regularization parameter α has been the object of many studies. Theoretical works can be found in [42], [45]. However, to the best of my knowledge, there is no general rule available so far for selecting this parameter for microwave imaging problems. In this chapter, the selection of this parameter is based on the numerical simulations for the purpose of showing the application of the Tikhonov regularization to the solution of the microwave imaging problems. The reconstruction process can be summarized in the following three steps

(1) solving eqn. (3.3) or (3.7) for a given regularization parameter;

(2) calculating the total electric field in the investigation region using eqn. (3.8);

(3) finding the object function using eqn. (3.9).

3.3 Numerical Results

A thin inhomogeneous dielectric slab of finite width, assumed to be infinitely long, is illuminated by a plane electromagnetic wave with an electric field intensity of unit amplitude, polarized in the z–axis direction, as shown in Fig. 3.1 (λ_0 is the wavelength in free space). The slab is divided into 25 cells of the same size and the relative permittivity is considered to be 4 for the cells 1 to 4 and 22 to 25, 8 for the cells 5 to 9 and 17 to 21, and 12 for the cells 10 to 16. 25 detectors are used. The electric field values measured by the detectors are provided by direct scattering computation[54] and the presence of the noise is simulated by adding a random Gaussian noise of zero mean value. The signal–to–noise ratio is defined

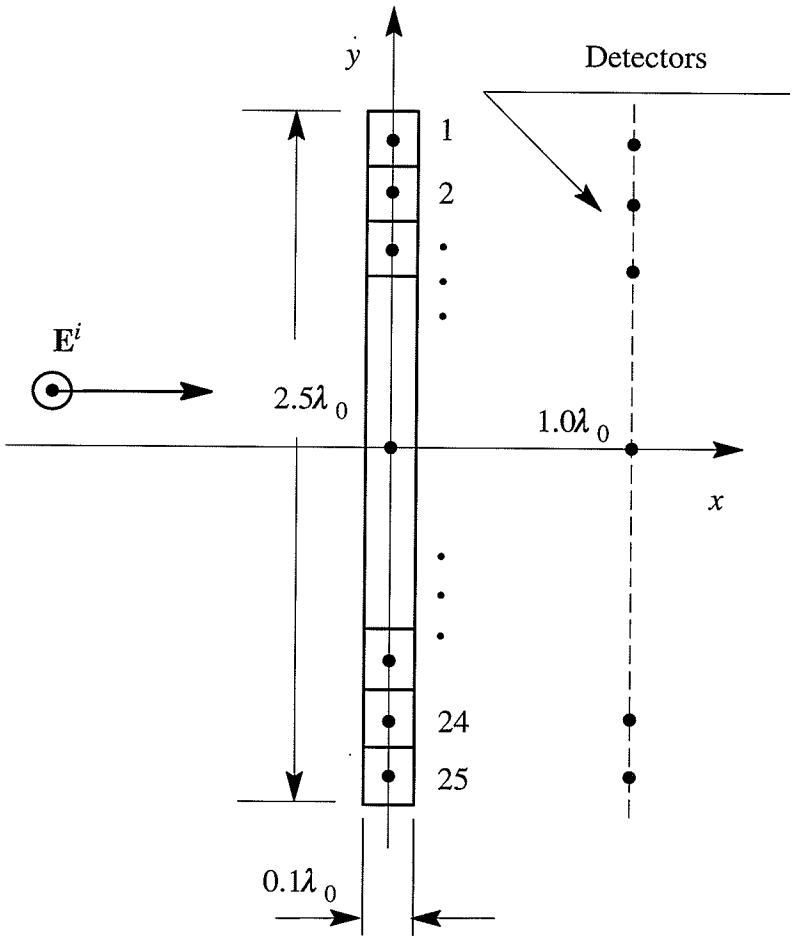

Fig. 3.1 Cross section of a dielectric slab.

as

$$S/N = 10 \log \frac{\| \mathbf{E}^s \|^2}{\| \mathbf{N} \|^2} \tag{3.10}$$

In order to compare the overall accuracy of the reconstructed equivalent current densities inside the object, we define the relative error as

$$\delta_{\mathbf{J}}(\alpha) = \frac{\| \mathbf{J}_e - \tilde{\mathbf{J}}_e \|}{\| \mathbf{J}_e \|} \tag{3.11}$$

with $\mathbf{J}_e$ and $\tilde{\mathbf{J}}_e$ being, respectively, the original and reconstructed equivalent current densities.

Figs. 3.2, 3.3 and 3.4 show the behavior of the relative error $\delta_{\mathbf{J}}(\alpha)$ versus the regularization parameter α under the signal–to–noise levels of 20dB, 40dB, and 60dB, for different regularization orders. It is shown that for each case, an optimum regularization parameter α which minimizes the relative errors exists. In the cases of signal–to–noise levels of 20dB and 40dB, the relative errors obtained by the 2nd–order regularization are slightly less than those by the 0th–order and the 1st–order regularizations at the optimum regularization parameters. But, in the case of the signal–to–noise level of 60dB, it seems that only the 0th–order regularization is reasonable.

Fig. 3.5 shows the original and the reconstructed equivalent current densities. The reconstructed one is obtained under the signal–to–noise level of 20dB by selecting the second order regularization and the optimum regularization parameter α.

Figs. 3.6, 3.7, and 3.8 present the reconstructed permittivities under a signal–to–noise of 20dB, 40dB, and 60dB, respectively. In each case, the optimum order of regularization and the optimum regularization parameter are used.

Now, we test the method by using only 13 detectors assuming that the investigation domain has the same shape as that in Fig. 3.1. Figs. 3.9, 3.10, and 3.11 give the reconstructed permittivities under signal–to–noise levels of 20dB, 40dB, and 60dB, where the optimum orders of the Tikhonov regularization and the optimum regularization parameters are employed.

Next, we consider an homogeneous cylinder of square cross section occupying the black cell in Fig. 3.12. The side of its cross section is taken to be equal to $\lambda_0/4$, where λ_0 is the wavelength of the incident plane wave in free space, and the permittivity of the scatterer is $\epsilon_r = 3$. A square grid of 4×4 cells for investigation and 16 measurement points around the cylinder are considered, as indicated in Fig. 3.12. The electric field values measured by

detectors are provided by a direct scattering computation[54], and the presence of the noise is simulated by adding a generated random Gaussian noise of zero mean value.

Fig. 3.13 presents the reconstructed permittivity under a high level of noise in the scattered field data. The optimum order of regularization (*i.e.* the zero order here) and the optimum regularization parameter are used. The latter has been determined by minimizing the error $\| \mathbf{J}_e - \tilde{\mathbf{J}}_e \| / \| \mathbf{J}_e \|$, with $\mathbf{J}_e$ and $\tilde{\mathbf{J}}_e$ being, respectively, the original current and the reconstructed current. The computed results for the reconstructed permittivity are in good agreement with the corresponding exact value, especially taking into account the high level of noise considered and the fact that no iteration was used.

As shown in Fig. 3.14, the identification of the dielectric body in the presence of noise becomes practically impossible if regularization is not applied. Fig. 3.15 shows the object image when the investigation domain is the same as in Fig. 3.12, but with only 12 detectors which are located symmetrically on a concentric circular loop of a diameter of $2\lambda_0$. The result is obtained under the signal–to–noise level (S/N) of 20dB. Both the position and outline of the unknown body can be clearly identified.

4.4 Conclusion

Computer simulation shows that the equivalent current modelling combined with the Tikhonov regularization technique is an efficient procedure for locating and reconstructing dielectric bodies. By selecting the regularization parameter properly, it is possible to obtain a picture of satisfactory resolution, even for measured data with a relatively high level of noise (with up to 10% uncertainties in the measured scattered field values). Computer simulations have shown that the regularization parameter plays an important role in the procedure of the reconstruction. In order to get a good results, this parameter must be carefully selected.

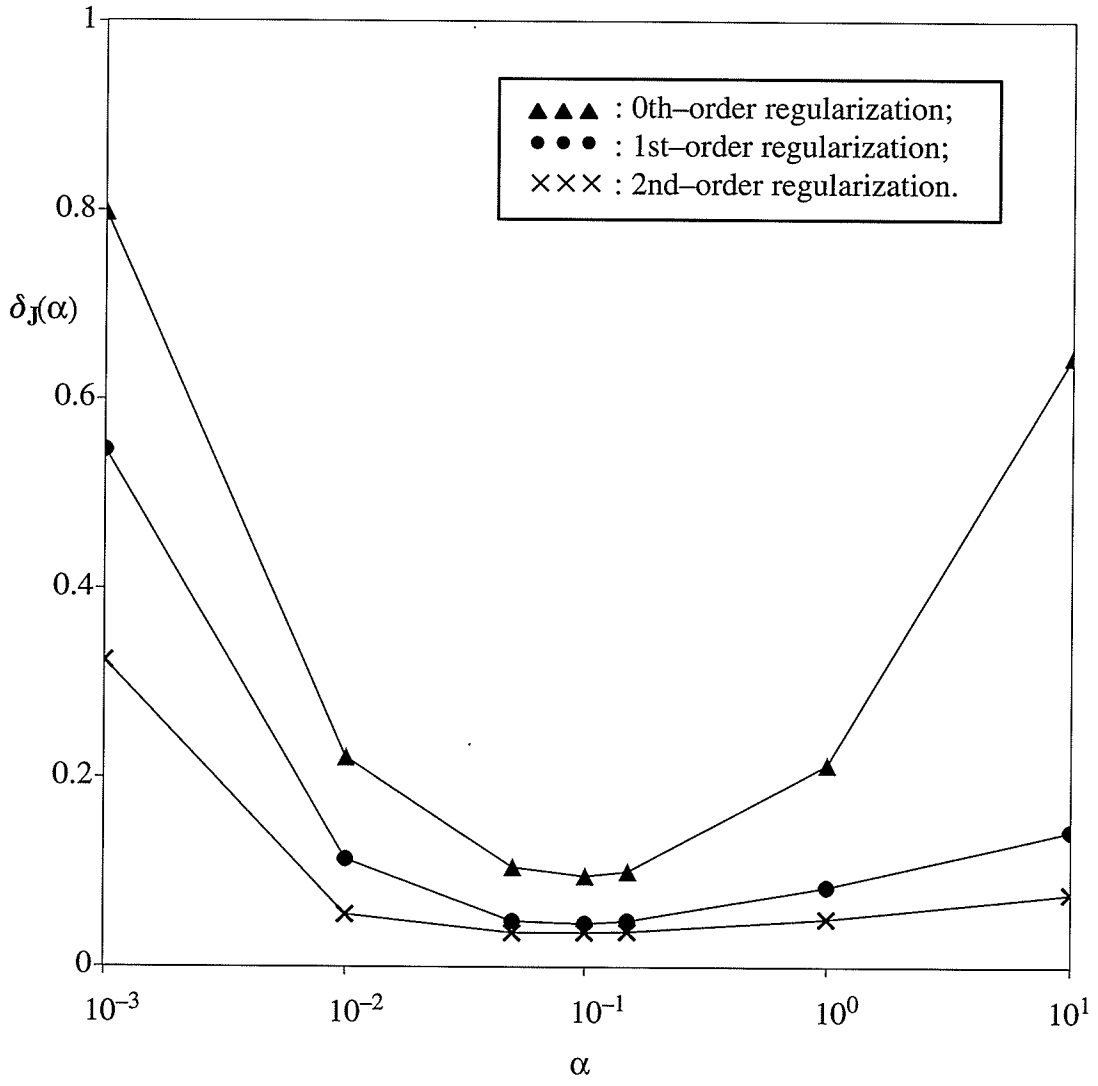

Fig. 3.2 Mean square error versus the regularization parameter under the signal–to–noise level of 20 dB.

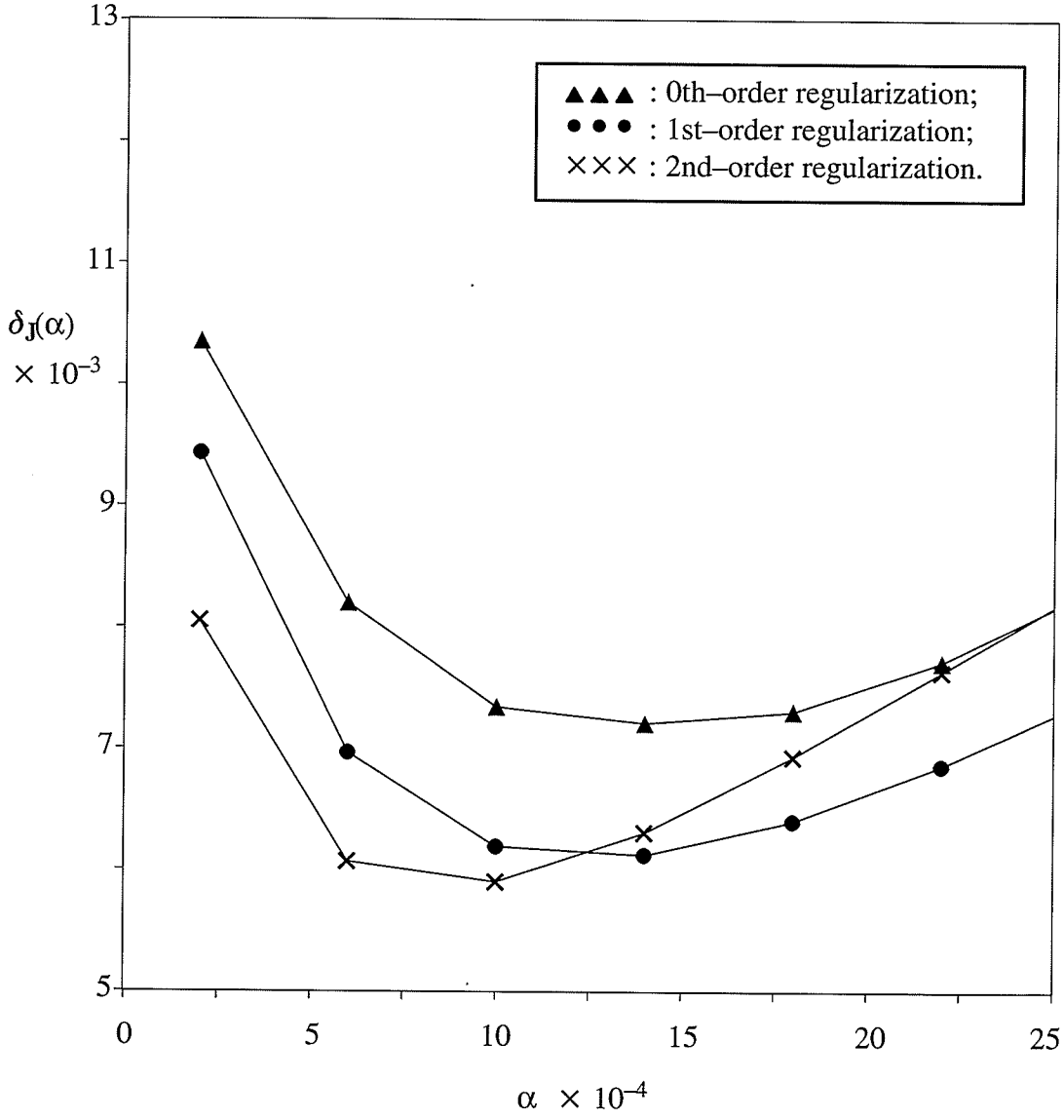

Fig. 3.3 Mean square error versus the regularization parameter under the signal–to–noise level of 40 dB.

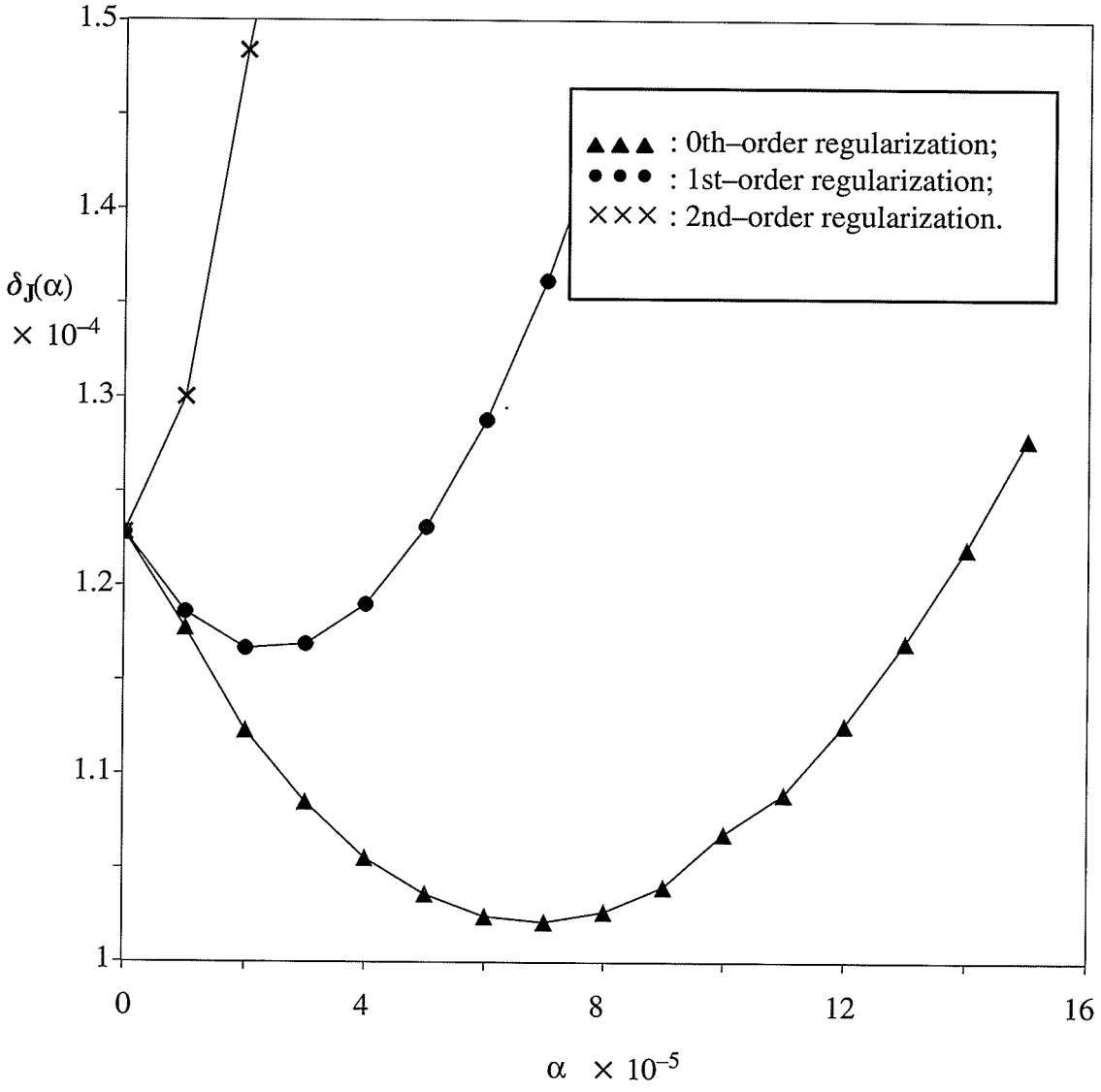

Fig. 3.4 Mean square error versus the regularization parameter under the signal–to–noise level of 60 dB.

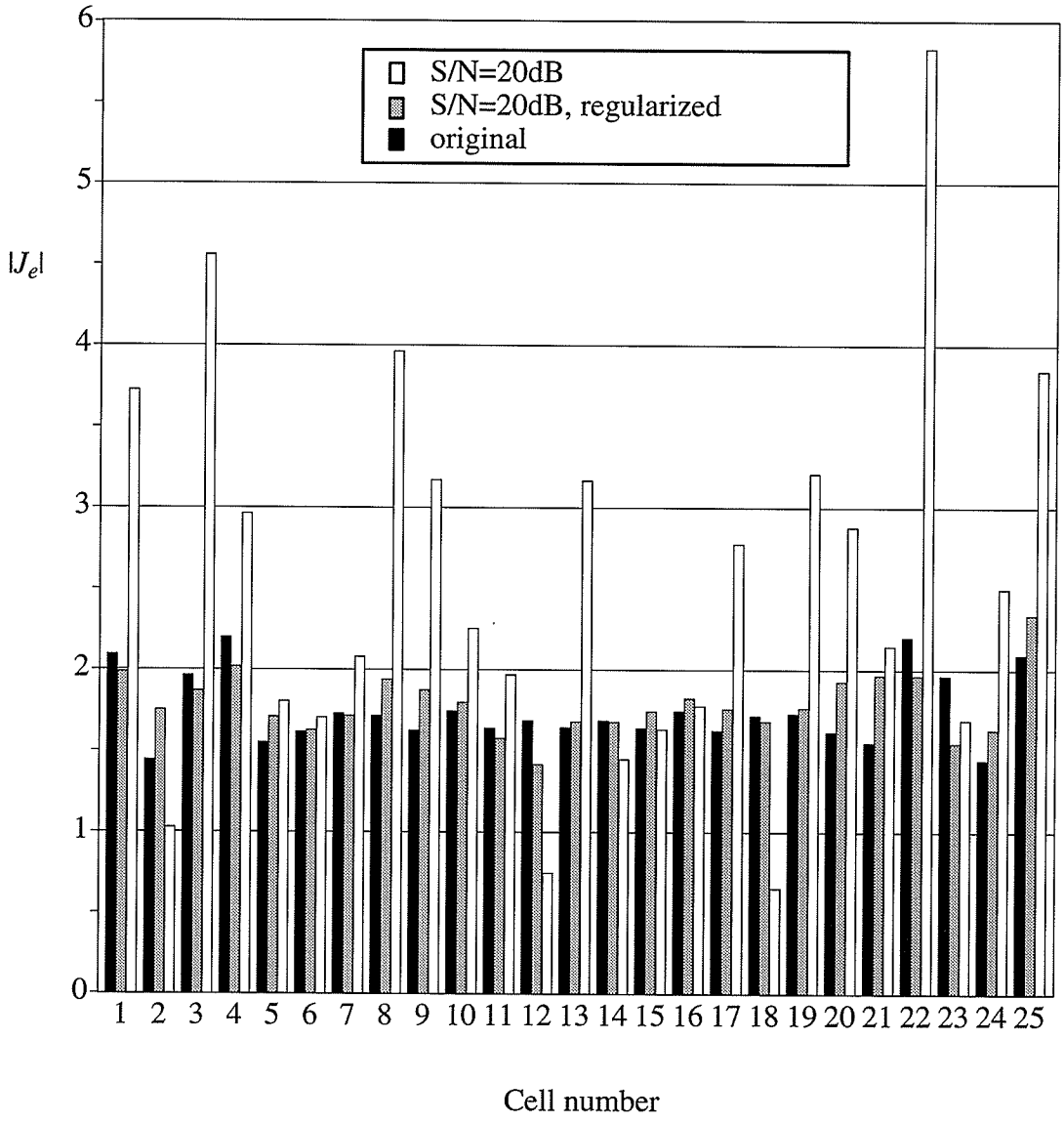

Fig. 3.5 Equivalent current density distributions in a dielectric slab reconstructed under the signal–to–noise level of 20 dB.

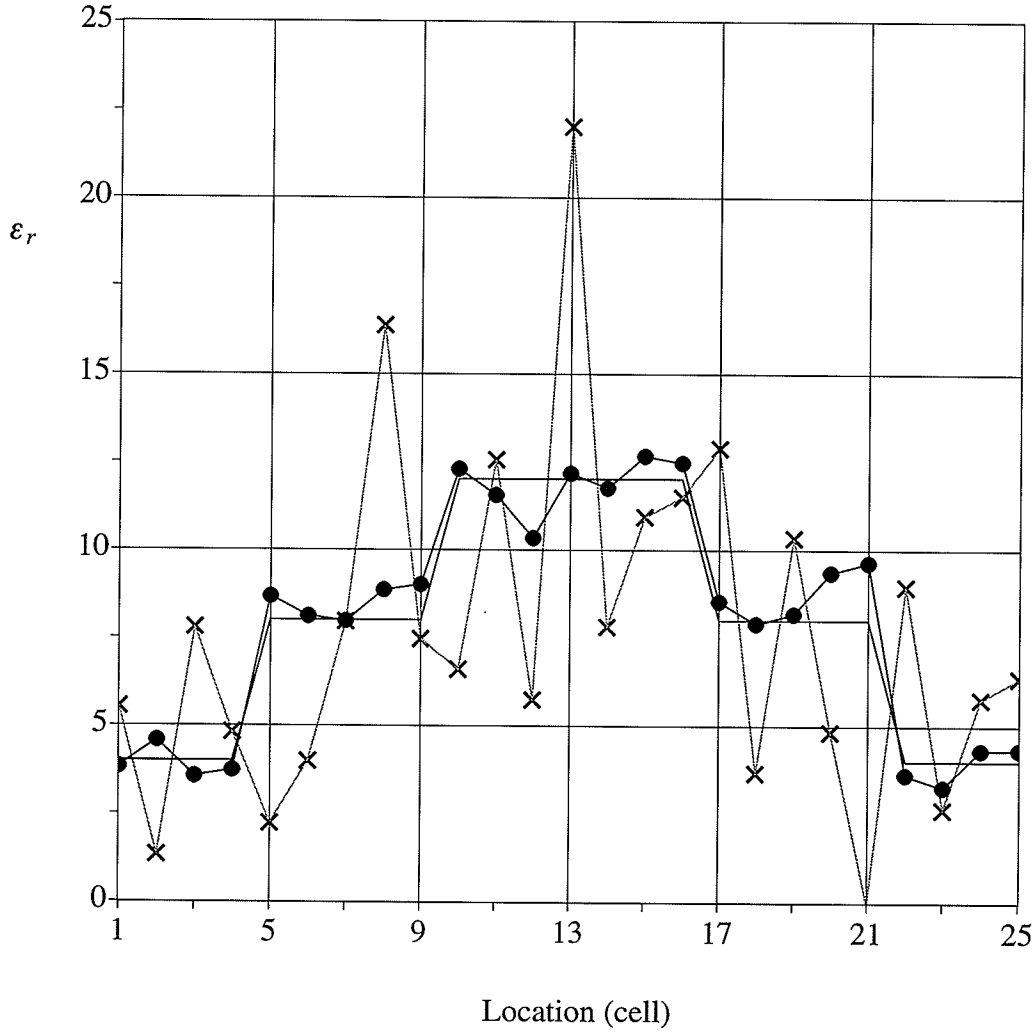

Fig. 3.6 Reconstructed permittivity with 25 detectors, S/N=20dB.

××× No regularization;

••• 2nd–order regularization, $\alpha = 0.1$.

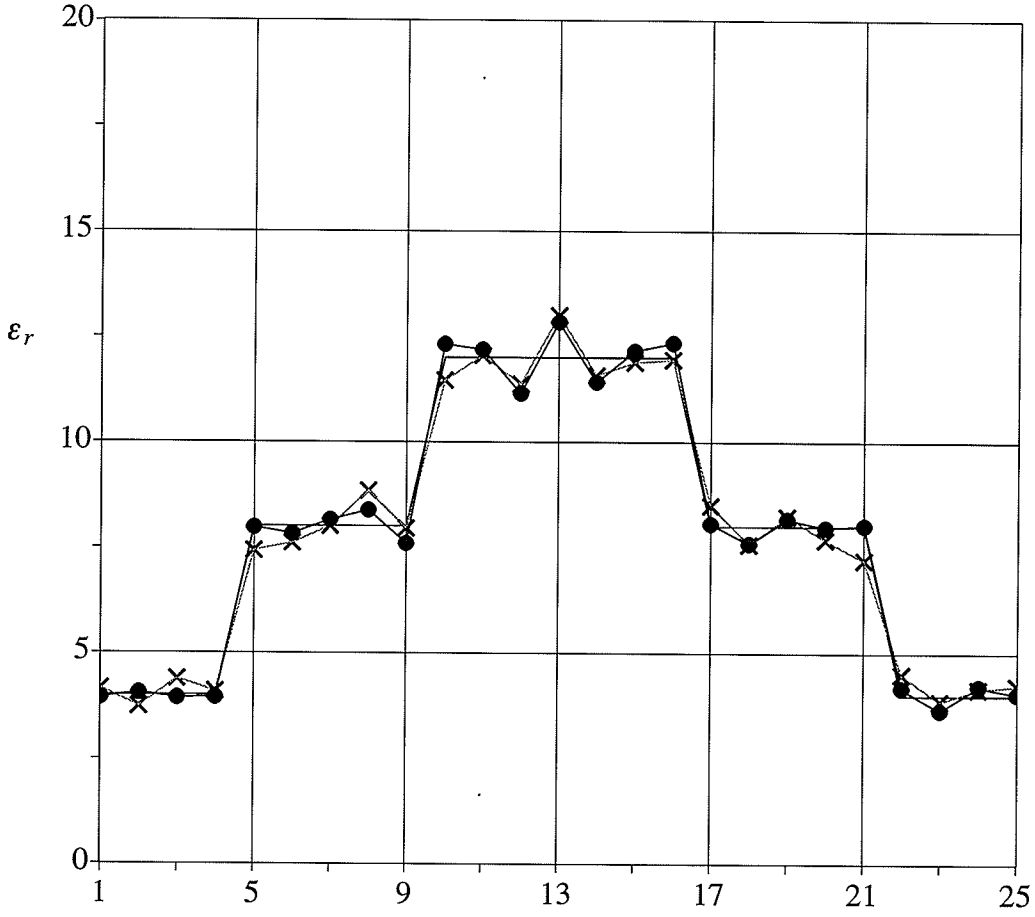

Fig. 3.7 Reconstructed permittivity with 25 detectors, S/N=40dB.

××× No regularization;

• • • 1st–order regularization, $\alpha = 1.4 \times 10^{-3}$.

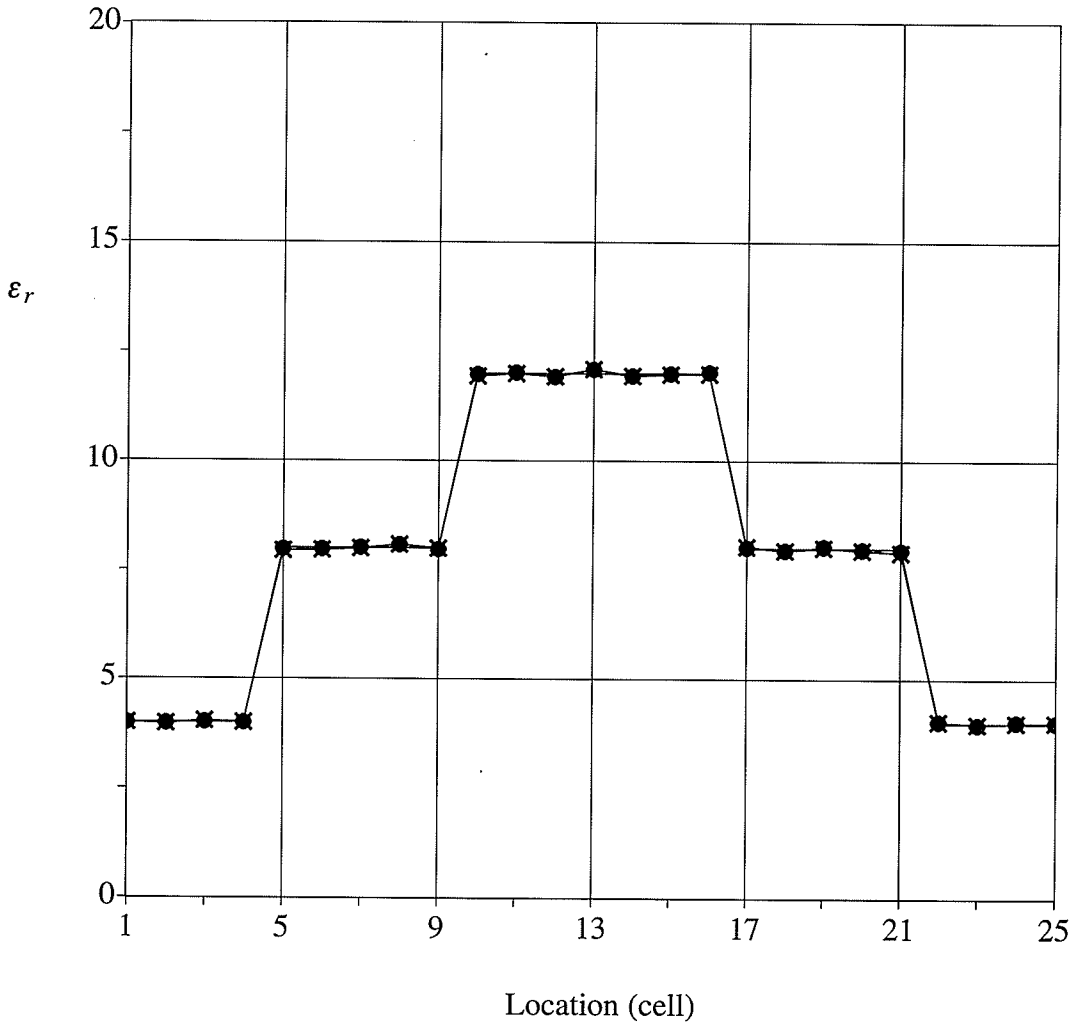

Fig. 3.8 Reconstructed permittivity with 25 detectors, S/N=60dB.
××× No regularization;
• • • 0th–order regularization, $\alpha = 7.0 \times 10^{-5}$.

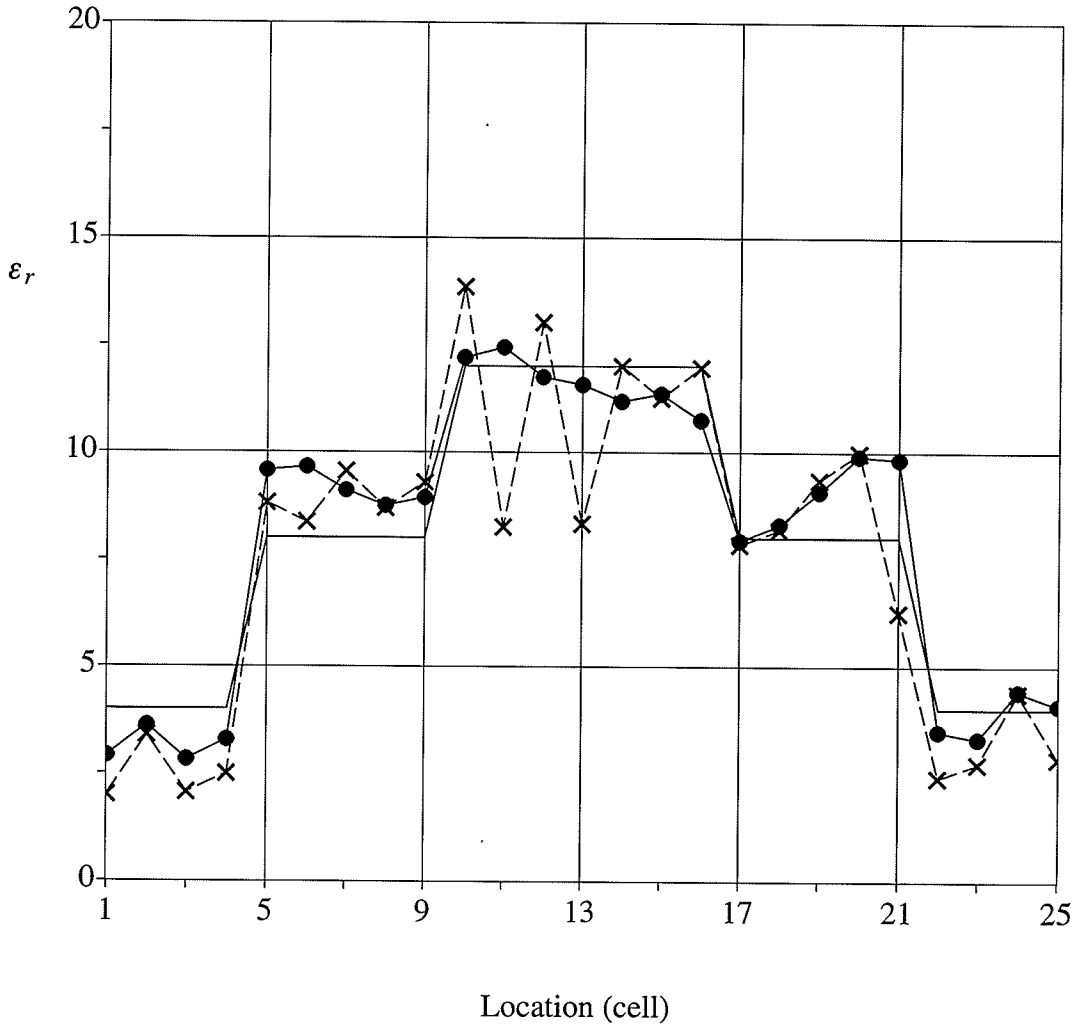

Fig. 3.9 Reconstructed permittivity with 13 detectors, S/N=20dB.
××× 0th–order regularization, $\alpha = 0.1$;
• • • 2nd–order regularization, $\alpha = 1.2$.

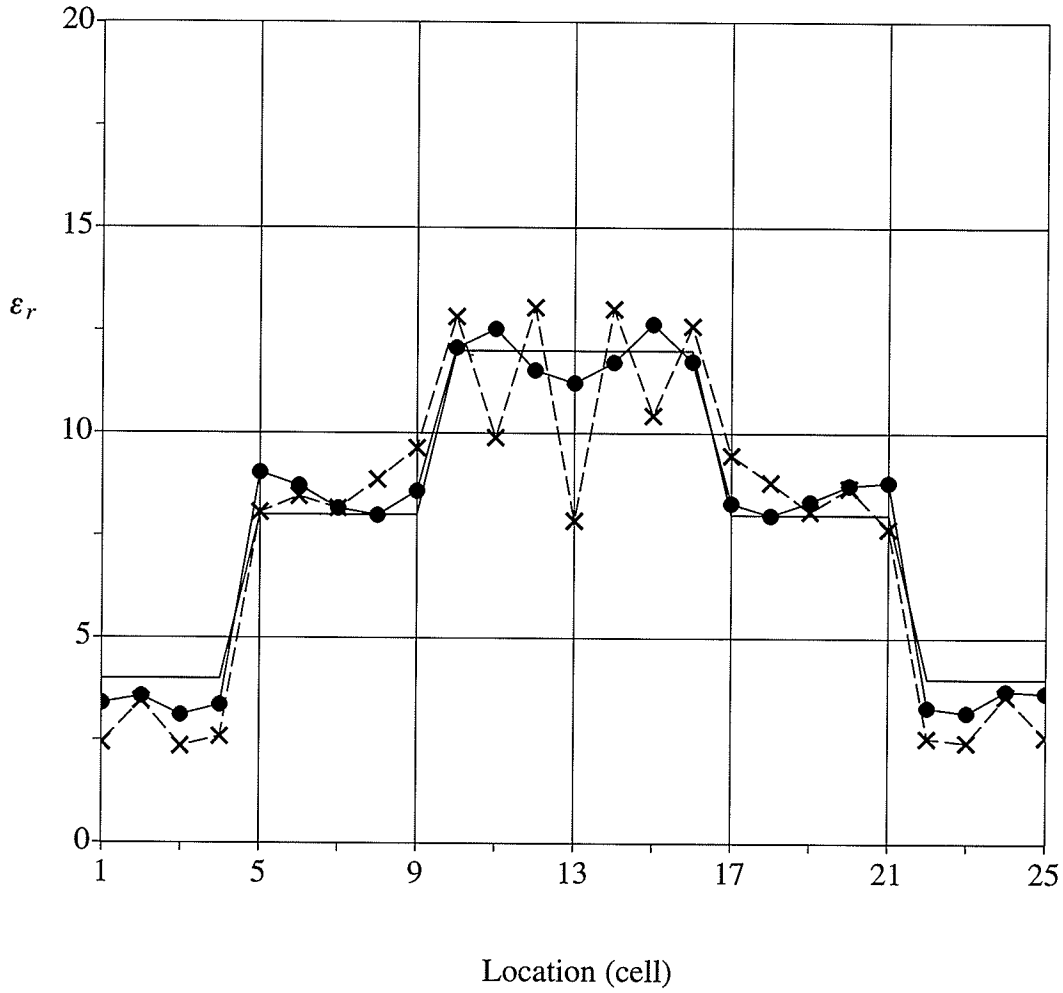

Fig. 3.10 Reconstructed permittivity with 13 detectors, S/N=40dB.
××× 0th–order regularization, $\alpha = 1.0 \times 10^{-2}$;
• • • 2nd–order regularization, $\alpha = 1.0 \times 10^{-4}$.

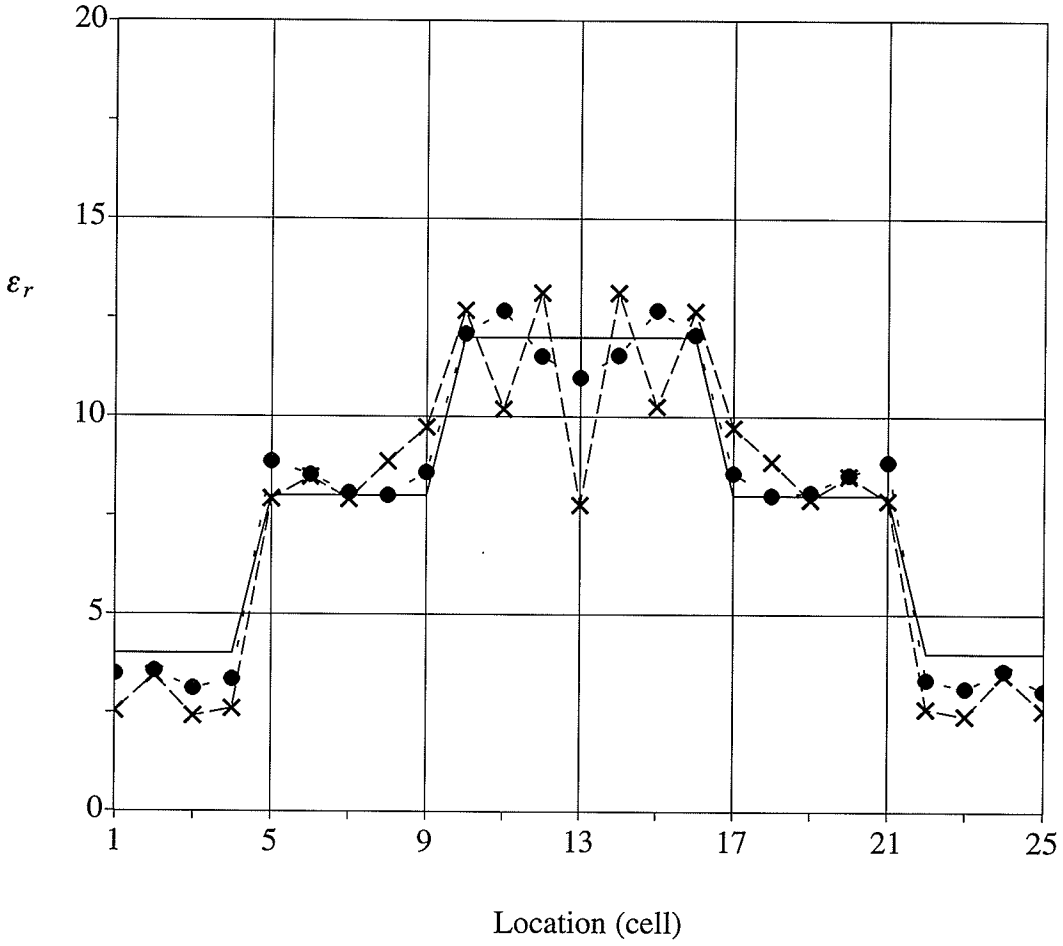

Fig. 3.11 Reconstructed permittivity with 13 detectors, S/N=60dB.
××× 0th–order regularization, $\alpha = 1.0 \times 10^{-3}$;
• • • 2nd–order regularization, $\alpha = 1.0 \times 10^{-5}$.

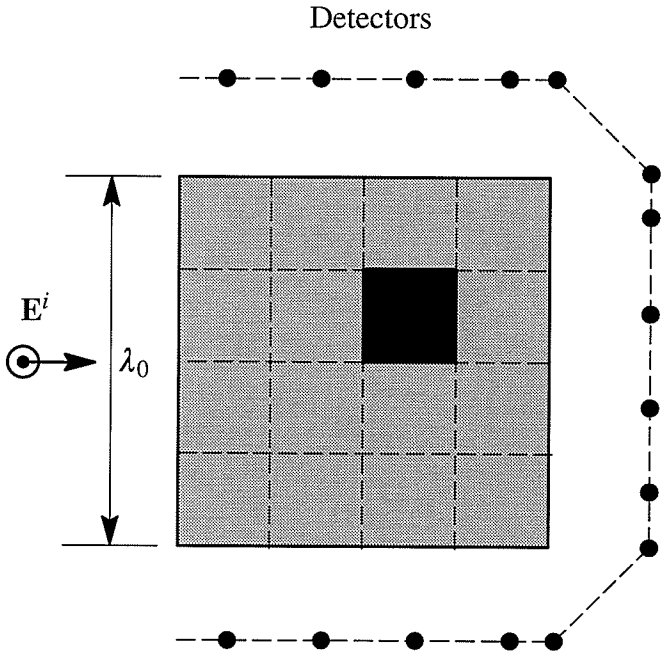

Fig. 3.12 Cross section of two–dimensional dielectric structure.

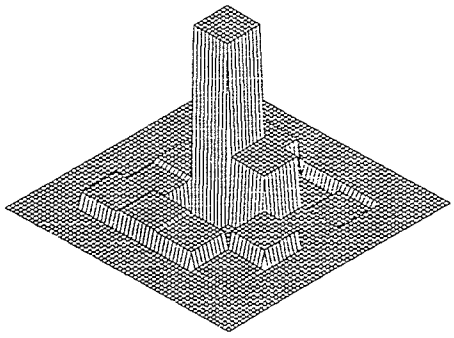

Fig. 3.13 Dielectric cylinder reconstruction:
S/N=20 dB, α=0.001, $\varepsilon_r = 2.59$.

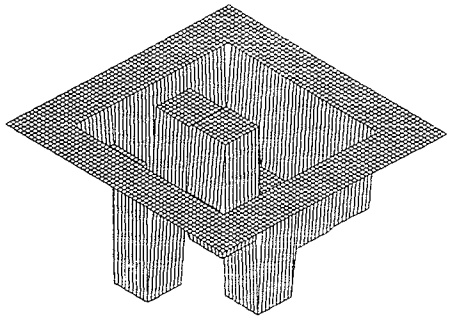

Fig. 3.14 Results computed with no regularization:
S/N=20dB, no regularization.

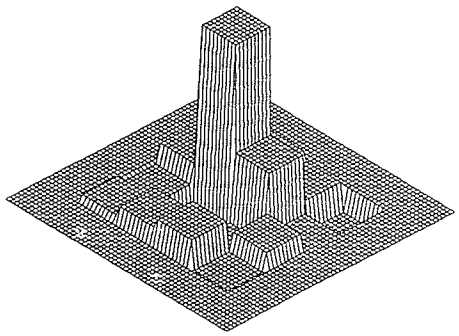

Fig. 3.15 Dielectric cylinder reconstruction with 12 detectors on a circular loop: S/N=20dB, α=0.05, $\varepsilon_r = 2.58$.

4

MICROWAVE IMAGING OF DIELECTRIC BODIES IN THE PRESENCE OF NOISE BY STOCHASTIC INVERSION

4.1 Introduction

In Chapter 3, the equivalent current modelling and the Tikhonov regularization technique are combined to reconstruct two–dimensional dielectric bodies. This procedure can be efficiently employed to locate dielectric objects in the presence of noise in the measured scattered field, but the optimum regularization parameter needed in the reconstruction process has to be selected for best results.

In this chapter, a new method for reconstructing dielectric bodies based upon a stochastic inversion transformation is presented. The stochastic treatment of ill–posed problems [43] has been successfully used in image processing and recognition techniques [60], seismology studies [67], and synthetic aperture radar imaging [68]. Here, we apply the stochastic inversion of matrices to the area of microwave imaging of dielectric bodies and illustrate the efficiency of this new approach. A difficulty in this case is that appropriate initial data necessary in the associated iterative process are practically impossible to be made and inappropriate guesses can cause the algorithm to be slowly convergent or even divergent. We obtain the required prior knowledge by applying the Tikhonov regularization procedure, which we have found to give very good first approximations. The proposed algorithm consists of three main steps. The nonlinear integral equation used for the reconstruction of the dielectric body is first linearized by introducing an equivalent current density. Secondly, Tikhonov regular-

ization [42] is employed to obtain the best approximation of the *a priori* data required in the algorithm. Finally, the stochastic inverse is applied to compute the equivalent current density distribution within the body. From the reconstructed equivalent current density distribution, one can simply derive the permittivity distribution. The object images can be developed by using the distribution of either the permittivity or the equivalent current density. An important feature of this algorithm is its high efficiency in the presence of noise. Numerical experiments show that sufficiently accurate results can be obtained even in an environment with a relatively high level of noise. This enables us to develop high resolution images.

4.2 Stochastic Inverse

As indicated earlier, if we consider the noise in the measured scattered field $\mathbf{E}^s$, we may rewrite eqn. (2.42) as

$$\mathbf{E}^s = [G_2]\mathbf{J}_e + \mathbf{N} \tag{4.1}$$

with $\mathbf{N}$ indicating the noise in the measured data. Applying the stochastic inversion scheme, *i.e.*, eqn. (2.72), to eqn. (4.1), we obtain

$$\mathbf{J}_e^r = [R_\mathbf{J}][G_2]^H([G_2][R_\mathbf{J}][G_2]^H + [R_\mathbf{N}])^{-1}\mathbf{E}^s \tag{4.2}$$

where $[R_\mathbf{J}]$ is the correlation matrix of $\mathbf{J}_e$, $[R_\mathbf{N}]$ is the correlation matrix of $\mathbf{N}$, $\mathbf{J}_e^r$ indicates the stochastic estimate of the equivalent current, and H denotes the conjugate transpose of a matrix. In this dissertation, the additive noise is assumed to have a normal distribution and the random noise vectors are uncorrelated and isotropic, and thus $[R_N]$ is a diagonal matrix

$$[R_\mathbf{N}] = \sigma_\mathbf{N}^2[I] \tag{4.3}$$

where $\sigma_\mathbf{N}^2$ is the noise variance, which is assumed to be available from prior knowledge, and $[I]$ is a unit matrix. Since $\mathbf{J}_e$ is assumed to be an uncorrelated random vector, its correlation matrix $[R_\mathbf{J}]$ is approximated as consisting of the elements [68]

$$R_{J_{ij}} = |J_{e_i}^r|^2 \delta_{ij}\,, \tag{4.4}$$

with δ_{ij} denoting the Kronecker delta symbol. For the problems analyzed so far by using this technique, the initial estimate is provided by available *a priori* knowledge of the system investigated. Since in the case of our problem the unknown $\mathbf{J}_e$ is the equivalent current density, with no initial information about its distribution in most cases, in this paper we propose the usage of the Tikhonov regularization technique in order to obtain a first approximation of $\mathbf{J}_e$ in the form

$$\mathbf{J}_e^r = [G_2]^H([G_2][G_2]^H + \alpha[I])^{-1}\mathbf{E}^s \tag{4.5}$$

which corresponds to letting the equivalent current correlation matrix in eqn. (2.76) be a unit matrix and $\sigma_{\mathbf{N}}^2$ therefore be the regularization parameter α. Although this is not the best selection of α, it allows us to obtain a good first estimate in a very simple way. In addition, we have found that the proposed algorithm is practically sensitive only to the order of magnitude of α. Thus, we only use a regularization parameter equal to the order of magnitude of $\sigma_{\mathbf{N}}^2$. With the classical definition of the signal–to–noise ratio, $\mathrm{S/N} = 20\log(\| E^s \| / \| N \|)$, we set $\alpha = 10^{-2}$ when S/N = 20dB, $\alpha = 10^{-4}$ when S/N = 40dB, and so on, for an $\| \mathbf{E}^s \|$ of the order of magnitude of unity. This simplifies the implementation of the algorithm since in practical cases the signal–to–noise ratio is readily available.

In the next section, the following iterative algorithm is used for numerical computations based upon the discussion above. An initial estimate of $\mathbf{J}_e^r$ is obtained by applying the Tikhonov regularization technique, with the regularization parameter in (4.5) chosen to be equal to the order of magnitude of the elements in the correlation matrix of the noise. The diagonal matrix $[R_{\mathbf{J}}]$ in (4.4) is then calculated from this $\mathbf{J}_e^r$. Subsequent estimates of $\mathbf{J}_e^r$ are obtained from (4.2), with $[R_{\mathbf{N}}]$ from (4.3) and with the latest evaluation of $[R_{\mathbf{J}}]$. The iteration process continues until a stable solution is obtained.

Once the equivalent current is obtained, the total field $\mathbf{E}^t$ in the investigation region is calculated by means of eqn. (2.22) with its matrix form

$$\mathbf{E}^t = [G_1]\mathbf{J}_e^r + \mathbf{E}^i \tag{4.6}$$

where $\mathbf{E}^t$ and $\mathbf{E}^i$ are n–dimensional vectors containing the arrays of the values of the total electric field and incident electric field inside the investigation region, $[G_1]$ is $n \times n$ Green function matrix for the scattering region. The object function is then calculated in terms of

$$\mathbf{J}_e^r = [O]\mathbf{E}^t \tag{4.7}$$

with $[O]$ being a $n \times n$ diagonal matrix containing object function inside the region, and the dielectric permittivity distributions can be obtained from eqns. (2.11) and (2.14). Please note that the equivalent current density vector in eqn. (4.7) has been factorized by $(-j\omega\mu_0)$.

4.3 Numerical Results

4.3.1 Lossless Objects

In order to compare our quantitative results with those available in [17], we first consider an investigation domain of a square cross section of $5/3\lambda_0$ to each side, where λ_0 is the wavelength of the incident plane wave. 25 cells are used to discretize the domain and 25 equally spaced detectors are located on three straight line segments as indicated in Fig. 4.1. The electric field values measured by the detectors are provided by direct scattering computation [54], and the presence of noise in the scattered field is simulated by adding to the real and imaginary parts of the field values two independent sequences of Gaussian random variables of zero mean value.

Table 4.1 shows the reconstructed results when a homogeneous scatterer of a relative dielectric permittivity $\varepsilon_r = 3$ occupies the 17th cell. For comparison purposes, the second column shows the results computed by applying the pseudoinverse[17] in the absence of the noise. Accurate results are obtained by using only three iterations in our method. The same

level of accuracy was obtained by considering a more practical situation where 25 equally spaced detectors were located on a concentric circular loop of diameter $3\lambda_0$. It is clear that the results obtained by the proposed method even in the presence of a high level of noise are much more accurate than the results obtained by the pseudoinverse in the absence of noise.

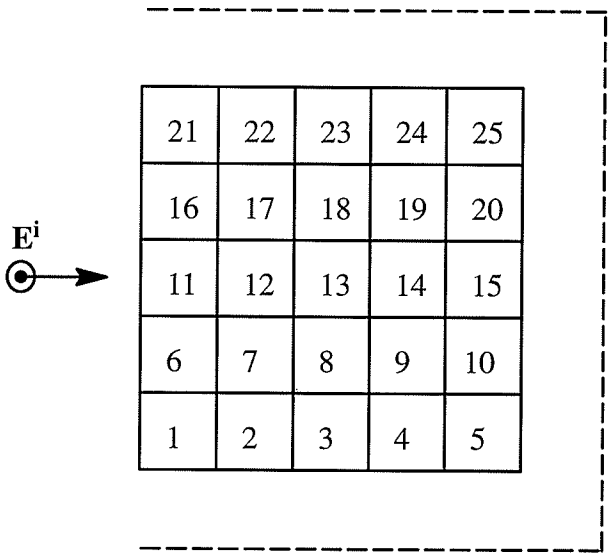

Fig. 4.1 Cross section of a two–dimensional region with detectors along the broken line.

Table 4.2 indicates the results of a situation when a scatterer of permittivity $\varepsilon_r = 3$ occupies two cells in the investigation domain, with the first column showing the adopted configuration according to Fig. 4.2. The second column indicates the results given in [17] in the absence of the noise. Again the reconstructed permittivities by the proposed method, with only three iterations, are very accurate even with a 10% level of uncertainty (*i.e.* *S/N*=20 dB)

in the measured scattered data. As before, the same high accuracy is obtained after three iterations with the detectors located symmetrically on the circular loop.

Fig. 4.3 shows the results of reconstructed permittivity versus signal–to–noise ratio when the scatterer of relative permittivity $\varepsilon_r = 3$ is located in the 17th cell of the investigation domain. The results obtained by the stochastic inverse are much more accurate than the results obtained by the pseudoinverse especially for high levels of noise.

In order to compare the overall accuracy of the reconstructed permittivities, one defines the relative mean square error(MSE) as

$$\delta_\varepsilon = \frac{\left[\sum_{i=1}^{n}(\varepsilon_{r_i} - \tilde{\varepsilon}_{r_i})^2\right]^{1/2}}{\left[\sum_{i=1}^{n}(\varepsilon_{r_i})^2\right]^{1/2}} \tag{4.8}$$

where ε_{r_i} and $\tilde{\varepsilon}_{r_i}$ stand for the values of the original relative permittivity and of the reconstructed relative permittivity in the i–th cell, respectively. Fig. 4.4 shows the relative MSE of the reconstructed permittivities for all the cells in Fig. 4.1 as a function of the signal–to–noise ratio, when the scatterer with a relative permittivity of $\varepsilon_r = 3$ is located in the 17th cell of the investigation domain.

Next, we consider a homogeneous dielectric cylinder of a relative permittivity $\varepsilon_r = 3$ that occupies four cells in the investigation domain, as shown in Fig. 4.5(a), with 25 equally spaced detectors located on a concentric circular loop of diameter $3\lambda_0$. Table 4.3 shows the numerical values of the relative permittivites reconstructed by the proposed method, with three iterations, for noise levels of 40dB and of 20 dB. Compared to the original ones, the reconstructed values are accurate enough to develop images with high resolution. Fig. 4.5(b) shows the original image, while Figs. 4.5(c) and 4.5(d) show the images for *S/N*=40dB and *S/N*=20dB, respectively. The relative MSE of the reconstructed permittivity distribution as a function of the number of iterations for two levels of noise is plotted in Fig. 4.6. Both lines

drop close to a constant just after the second iteration. In the 20dB case the MSE stays at 3.8% after three iterations, while in the 40dB case it drops to 0.4% after the same number of iterations. Fig. 4.7 shows the relationship between the initial guess of the equivalent current density (considered for illustration to be the same for all cells) and the convergence of the proposed algorithm. It indicates that an inappropriate initial guess of the equivalent current can cause a very slow convergence of the iterative process, or even its divergence. On the other hand, by applying the Tikhonov regularization, the algorithm will converge in only two or three iterations.

The method was also tested by using less detectors than cells. Consider a case in which the investigation domain has the same shape as that in Fig. 4.1 but with only 16 detectors symmetrically located on a concentric circular loop of diameter $3\lambda_0$. The dielectric scatterer with a relative permittivity $\varepsilon_r = 3$ occupies four cells as shown in Fig. 4.5(a). Table 4.4 presents the numerical values of the reconstructed permittivities. When the signal–to–noise ratio in the measured field is 40dB, only three iterations are required to make the MSE reach a constant value. For *S/N*=20dB, five iterations are needed.

4.3.2 Lossy Objects

As a first illustrative example of lossy object, we consider an investigation domain of a square cross section of $5/3\lambda_0$ a side, where λ_0 is the wavelength of the illuminating incident wave taken to be a plane wave propagating normally to the left hand side of the domain. 25 cells are used to discretize the investigation region and 16 equally spaced detectors are located on a concentric circular loop of a diameter of $3\lambda_0$. The electric field values measured by the detectors are provided by a direct scattering computation using the moment method for the scatterer shown in Fig. 4.8 and the presence of the noise in the scattered field is simulated by adding to the real and imaginary parts of the field values two independent sequences of Gaussian random variables of zero mean value. Fig. 4.9 shows the results after four itera-

tions for the reconstructed average permittivity versus signal–to–noise ratio for a relative permittivity $\varepsilon_r = 5.5 - j1.2$ of the scatterer. The relative mean square error defined in eqn. (4.6) is used to compare the overall accuracy of the reconstructed permittivities. Fig. 4.10 shows the errors of reconstruction after four iterations as a function of the signal–to–noise ratio. Similar quantitative results are obtained for any location and orientation within the investigation region of the lossy object considered. The error in the permittivity reconstruction as a function of the number of iterations for two levels of noise is represented in Fig. 4.11. In both cases a stable value is reached after the fourth iteration. In the 20dB case this value is approximately 16.0% , while in the 40dB case it drops to 1.6%. It should be noted that even for a level of noise of 10 dB, a practically constant value of α is obtained in only six iterations. Fig. 4.12 shows the relationship between the initial guess of the equivalent current density (considered for illustration to be the same for all the cells) and the convergence of the proposed algorithm for S/N = 20 dB. It indicates that an inappropriate initial guess of the equivalent current can cause a slow convergence of the iterative process or even its divergence. On the other hand, by applying the Tikhonov regularization, the algorithm will converge in only four iterations.

The second example of a lossy scatterer of complex permittivity $\varepsilon_r = 5.5 - j1.2$ is presented in a cross section in Fig. 4.13. In this case we use 25 detectors for the same illumination as in the first example. The reconstructed average permittivities of the scatterer are $\varepsilon_r = 5.49 - j1.20$ with $\alpha = 0.02$ for S/N = 40dB, after 5 iterations, and $\varepsilon_r = 5.11 - j1.61$ with $\alpha = 0.22$ for S/N = 20dB, after 6 iterations.

4.3.3 Very High Contrast Dielectric Bodies

One of the features of the proposed method is its capability to reconstruct very high contrast permittivity objects even with high noise contaminated data. For the purpose of demonstration, we consider a region of $\lambda_0 \times \lambda_0$ in size. The region is divided into 144 square sub-

cells and 16 receivers uniformly located on a concentric loop of diameter 1.5 λ_0 are used to detect the scattered field. This results in an algebraic system of 16 equations and 144 unknowns in accordance with eqn. (4.1). The dielectric cylinder with complex permittivity occupies one cell in the region as shown in Fig. 4.14. The background is assumed to be a free space in the following examples. One TM incident wave is used to illuminate the region. Fig. 4.15 shows the 3D image of the reconstructed object with the signal–to–noise ratio of 40 dB after 8 iterations. The original value of dielectric permittivity is $(46 - j12)$ and the reconstructed value is $(46.09 - j11.76)$. The relative reconstruction error of real part is 0.2%, and the relative error of imaginary part is 2%. Fig. 4.16 shows the reconstructed results when 20 dB signal–to–noise ratio is used after 8 iterations. The reconstructed value is $(44.7 - j11.18)$ with relative reconstruction errors of 2.7% for real part and 6.8% for imaginary part. It is worth noting that not only the dielectric permittivity is well reconstructed, the background is also well reconstructed. No low–pass filtering effect [16] is exhibited. This allows us to develop images with very high resolution.

Fig. 4.17(a) and Fig. 4.17(b) present the reconstructed dielectric permittivity versus the original dielectric permittivity regarding the location of the dielectric object in Fig. 4.14 for different signal–to–noise levels. In Fig. 4.17(a), all results are obtained after 8 terations. The imaginary part of the dielectric permittivity of the object is assumed to be zero, and the real part varies from 10 to 250. When the signal–to–noise ratios 100dB and 40 dB are used, the dielectric permittivities of the object can be reconstructed almost completely. When 20 dB signal–to–noise ratio is used, relative reconstruction errors are 0.03% for the contrast of 10, 6.24% for the contrast of 100 and 11.7% for the contrast of 200. In Fig. 4.17(b), the real part of the dielectric permittivity of the object is assumed to be unity, and the imaginary part varies from 10 to 1000. The reconstruction accuracies similar to Fig. 4.17(a) are obtained.

4.3.4 Multiview Illuminations

Numerical results have shown that dielectric permittivities of relatively simple two–dimensional objects can be reconstructed with satisfactory accuracy even with one wave illumination. For more complex objects, multiview techniques can be employed to improve the quality of the images. The multiview techniques which can be utilized are[46]:

1) changing the incident wave direction and keeping a constant wavelength and a steady object;
2) changing the wavelength and keeping a steady incident wave direction and object;
3) changing the object orientation and keeping a constant wavelength and a steady incident wave direction.

In this thesis, we simply use the first technique to demonstrate the efficiency of the stochastic method by reconstructing two–dimensional objects. In the process of the imaging, each illumination gives different values of the object function due to the the noise in the measured data and to the reconstruction errors. The imaging is performed by using the average value of the object function, that is

$$\mathbf{O} = \frac{1}{v}\sum_{k=1}^{v} \mathbf{O}_k \tag{4.9}$$

where v is the number of illuminations and $\mathbf{O}_k$ is the object function vector yielded from the k–th view.

As the first multiview reconstruction, we consider an investigation domain of $\lambda_0 \times \lambda_0$, divided into 144 cells with 16 detectors uniformly located on a concentric loop of a diameter $1.5\lambda_0$. A dielectric cylinder of a cross–sectional dimension of $\lambda_0/2$, with a relative permittivity of $\varepsilon_r = 3$, occupies 24 cells, as shown in Fig. 4.18(a). The noise and error in the measured data are introduced by adding Gaussian random variables to the real and imaginary parts of the scattered field. The signal–to–noise ratio (S/N) used is defined by

$S/N = 10\log(\| \mathbf{E}^s \|^2 / \| \mathbf{N} \|^2)$. Figure 4.18(b) shows the image obtained after three iterations with one incident wave illumination with a signal–to–noise level of 40dB in the measured data. In Fig. 4.18(c), the image is obtained by using four incident waves to illuminate the object successively. Figure 4.18(d) presents the reconstruction in a highly noisy environment, where 17.8% Gaussian noise (S/N=15dB) was added to the measured data and four incident waves were employed. Please note that the blurt technique has been used to smooth the edge of the images.

In the second computer simulation, the reconstruction system is the same to the first one but a circular dielectric cylinder of two layers with complex dielectric permittivity is considered. The outer layer of the cylinder has a dimension of diameter $\lambda_0/2$ with a relative dielectric permittivity of $\varepsilon_r = 2.75 - j0.01$. The inner layer has a dimension of diameter $\lambda_0/6$ with a relative dielectric permittvity of $\varepsilon_r = 3.5 - j0.15$. 16 detectors are used on a concentric loop of a diameter of $1.5\lambda_0$ to detect the scattered fields. The cylinder is modeled by 24 square cells in the test region, with 4 cells for the inner layer and 20 cells for the outer layer. The real part of the original dielectric permittivity distributions of the modeled cylinder is shown in Fig. 4.19(a). Figure 4.19(b) shows the real part of the dielectric permittivities reconstructed by the single–view technique after three iterations for S/N=40dB with the incident wave coming from the left side of the region. Figure 4.19(c) and Figure 4.19(d) show the real parts of the dielectric permittivities obtained by the muliview technique (where four views from each side of the test region are used) from three iterations for S/N=40 dB and for S/N=15 dB respectively. The results with similar accuracy have been obtained for the imaginary parts of the dielectric permittivities.

4.4 Conclusion

An iterative method for reconstructing complex dielectric permittivity distribution of an inhomogeneous cylindrical scatterer has been presented. The method is developed based

on the stochastic inversion algorithm which seeks an optimal solution in the stochastic sense that minimizes the expected value of the reconstruction error.

The performance of the proposed reconstruction method is demonstrated in terms of reconstructing two dimensional objects. Although the development of a good image depends on many factors such as the configuration of the image system, the number of the detectors, the number of waves used and the organization of the object, it has been shown that, by the proposed method, the dielectric object with very high dielectric contrast can be reconstructed with high accuracy even for measured data containing a high level of noise. The low–pass filtering effect which have been noticed in other reconstruction algorithms is not presented in the proposed method. Compared with other iterative methods presented so far for dielectric body microwave imaging problems, the stochastic technique requires less computation time since the number of iterations can be reduced by utilizing *a priori* information which has been supplied by the application of the Tikhonov regularization in the proposed examples. Moreover, for each iteration, only one matrix inversion is needed, while other iterative techniques require two matrix inversion operations per iteration. These features recommend the method presented for some special applications when a high resolution is required in the presence of noise such as in defect detection, material characterization and remote sensing.

TABLE 4.1

Reconstructed permittivities when the scatterer with $\varepsilon_r = 3$ occupies the 17th cell.

Cell Number	ε_r Pseudoinverse Noise–Free	ε_r Proposed Method	
		S/N=40dB	S/N=20dB
1	0.98	1.00	1.00
2	1.03	1.00	1.00
3	1.00	1.00	1.00
4	1.01	1.00	1.00
5	0.99	1.00	1.00
6	1.03	1.00	1.00
7	0.99	1.00	1.00
8	0.88	1.00	1.00
9	1.03	1.00	1.00
10	0.99	1.00	1.00
11	1.08	1.00	1.00
12	1.25	1.00	1.00
13	0.97	1.00	1.00
14	1.20	1.00	1.00
15	1.00	1.00	1.00
16	1.01	1.00	1.00
17	2.63	3.00	3.02
18	0.89	1.00	1.00
19	1.03	1.00	1.00
20	0.99	1.00	1.00
21	0.99	1.00	1.00
22	1.01	1.00	1.00
23	0.99	1.00	1.00
24	1.00	1.00	1.00
25	0.98	1.00	1.00

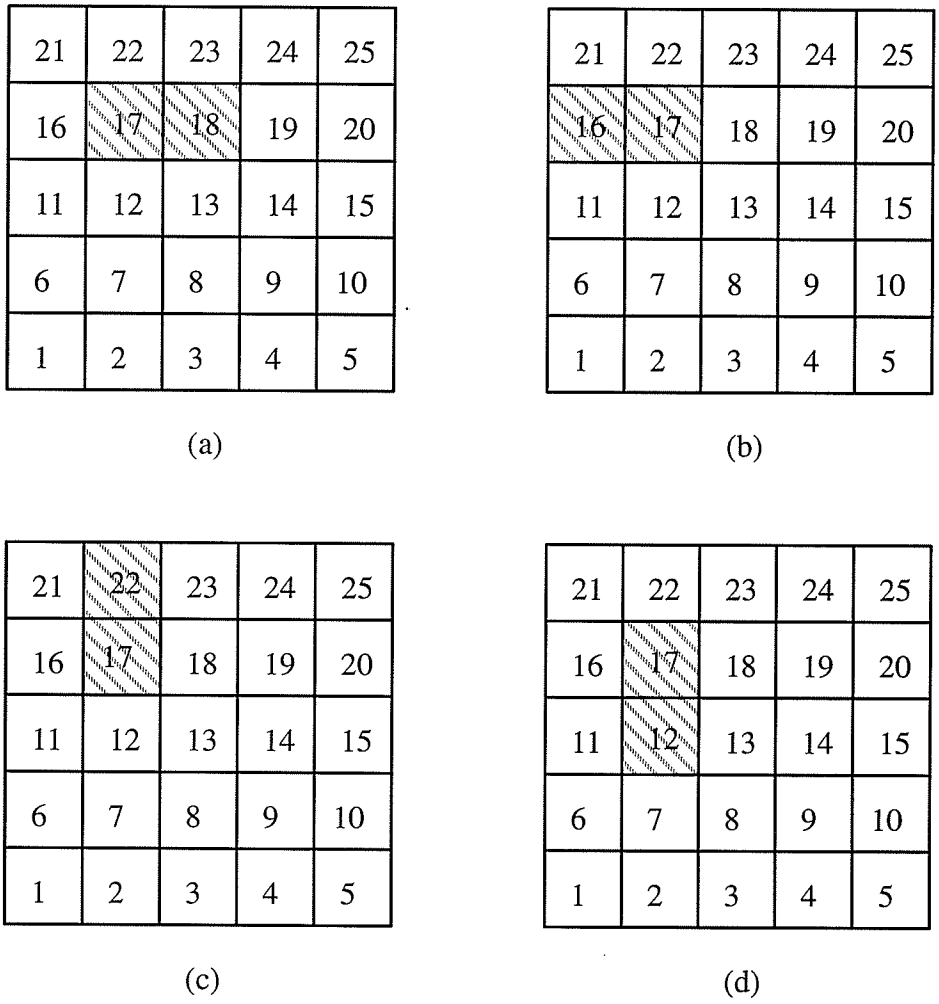

Fig. 4.2 Configurations for a scatterer occupying two cells in the investigation domains.

TABLE 4.2

Permittivity reconstruction for the scatterer configurations in Fig. 4.2, with the same locations of the detectors as in Fig. 4.1.

Configuration	ε_r Pseudoinverse Noise–Free	ε_r Proposed Method	
		S/N=40dB	S/N=20dB
(a)	$\varepsilon_{r17} = 2.01$ $\varepsilon_{r18} = 3.87$	$\varepsilon_{r17} = 3.00$ $\varepsilon_{r18} = 3.01$	$\varepsilon_{r17} = 3.09$ $\varepsilon_{r18} = 3.11$
(b)	$\varepsilon_{r16} = 2.45$ $\varepsilon_{r17} = 2.24$	$\varepsilon_{r16} = 3.01$ $\varepsilon_{r17} = 3.00$	$\varepsilon_{r16} = 3.10$ $\varepsilon_{r17} = 3.00$
(c)	$\varepsilon_{r17} = 2.51$ $\varepsilon_{r22} = 2.75$	$\varepsilon_{r17} = 3.00$ $\varepsilon_{r22} = 3.00$	$\varepsilon_{r17} = 2.92$ $\varepsilon_{r22} = 2.95$
(d)	$\varepsilon_{r12} = 1.87$ $\varepsilon_{r17} = 2.24$	$\varepsilon_{r12} = 3.00$ $\varepsilon_{r17} = 3.01$	$\varepsilon_{r12} = 2.97$ $\varepsilon_{r17} = 3.04$

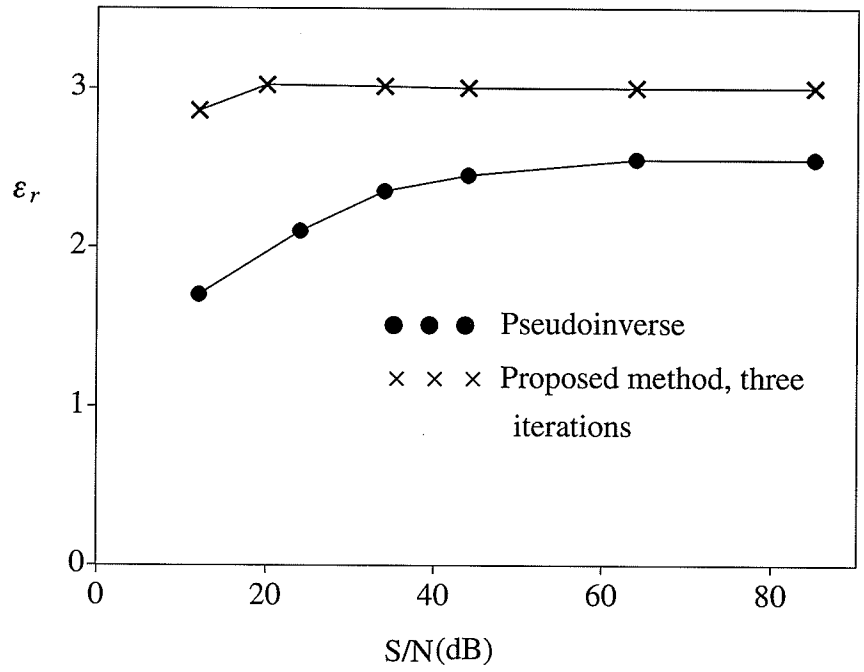

Fig. 4.3 Plots of the reconstructed permittivity versus *S/N* ratio for the scatterer with $\varepsilon_r = 3$ occupying the 17th cell in Fig. 4.1.

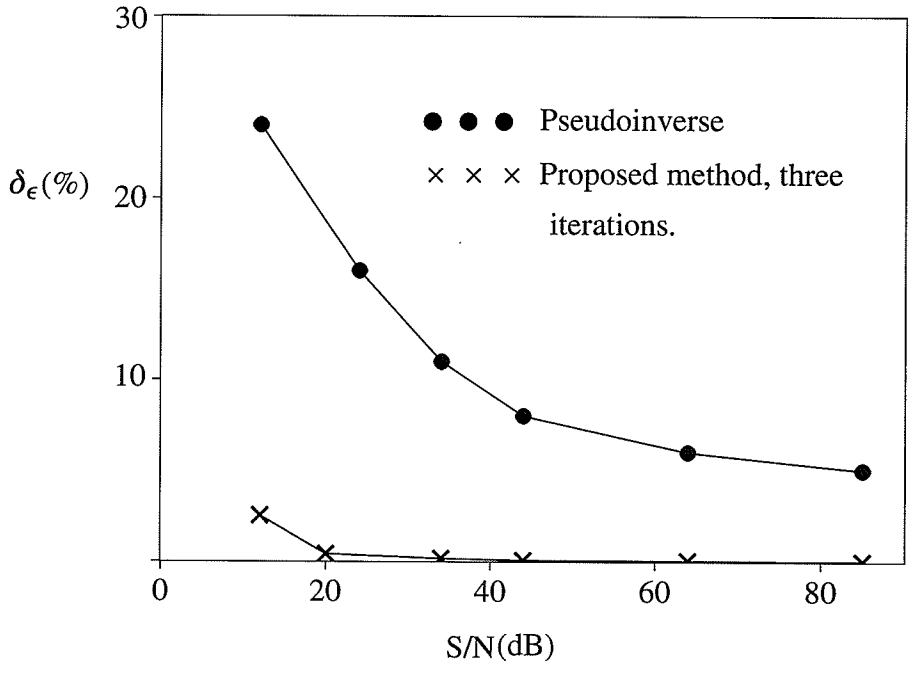

Fig. 4.4 Relative mean square errors of the reconstructed permittivities versus *S/N* ratio.

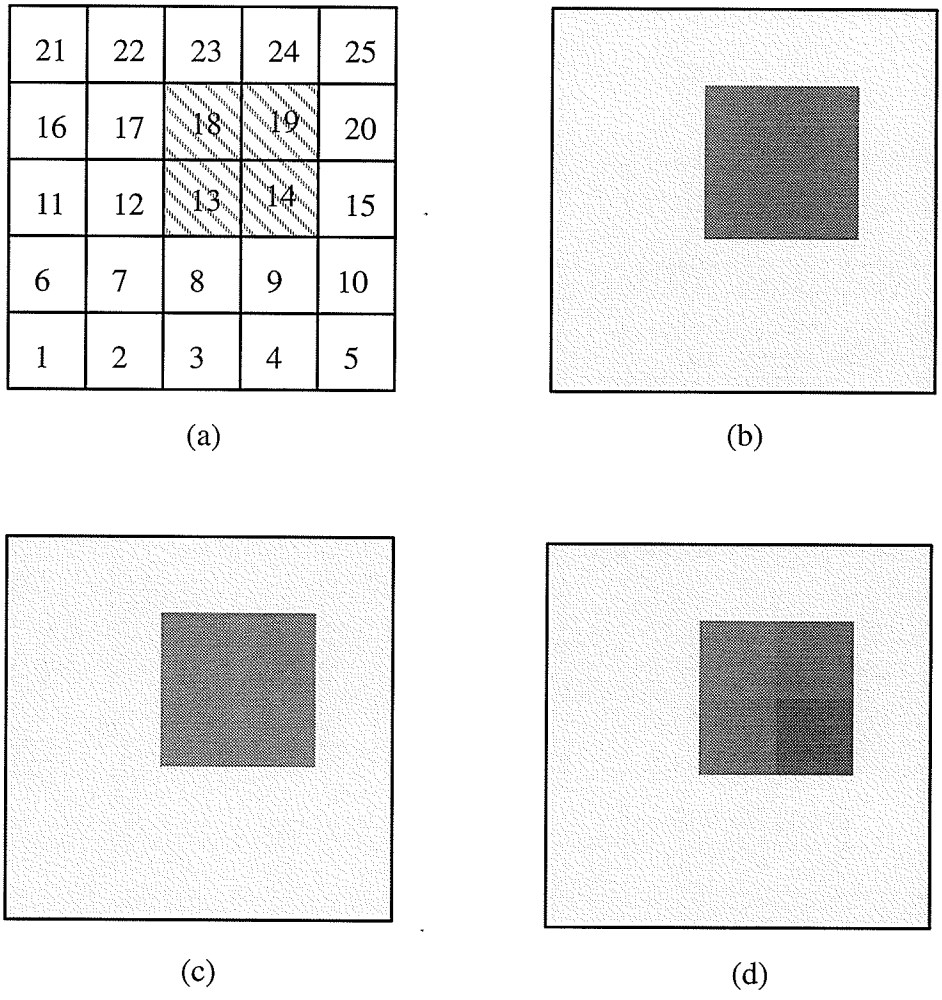

Fig. 4.5 Configuration and images for the scatterer occupying four cells in the investigation domain, corresponding to Table 4.3.

TABLE 4.3

Reconstructed permittivities in all the cells for the scatterer with $\varepsilon_r = 3$ shown in Fig. 4.5.

Cell Number	ε_r	
	S/N=40dB	S/N=20dB
1	1.00	1.00
2	1.00	1.00
3	1.00	1.00
4	1.00	1.00
5	1.00	1.00
6	1.00	1.00
7	1.00	1.00
8	1.00	1.00
9	1.00	1.00
10	1.00	1.00
11	1.00	1.00
12	1.00	1.00
13	3.00	3.03
14	3.03	3.26
15	1.00	1.00
16	1.00	1.00
17	1.00	1.00
18	2.99	2.87
19	3.02	3.09
20	1.01	1.02
21	1.00	1.00
22	1.00	1.00
23	1.00	1.00
24	1.00	1.00
25	1.00	1.00

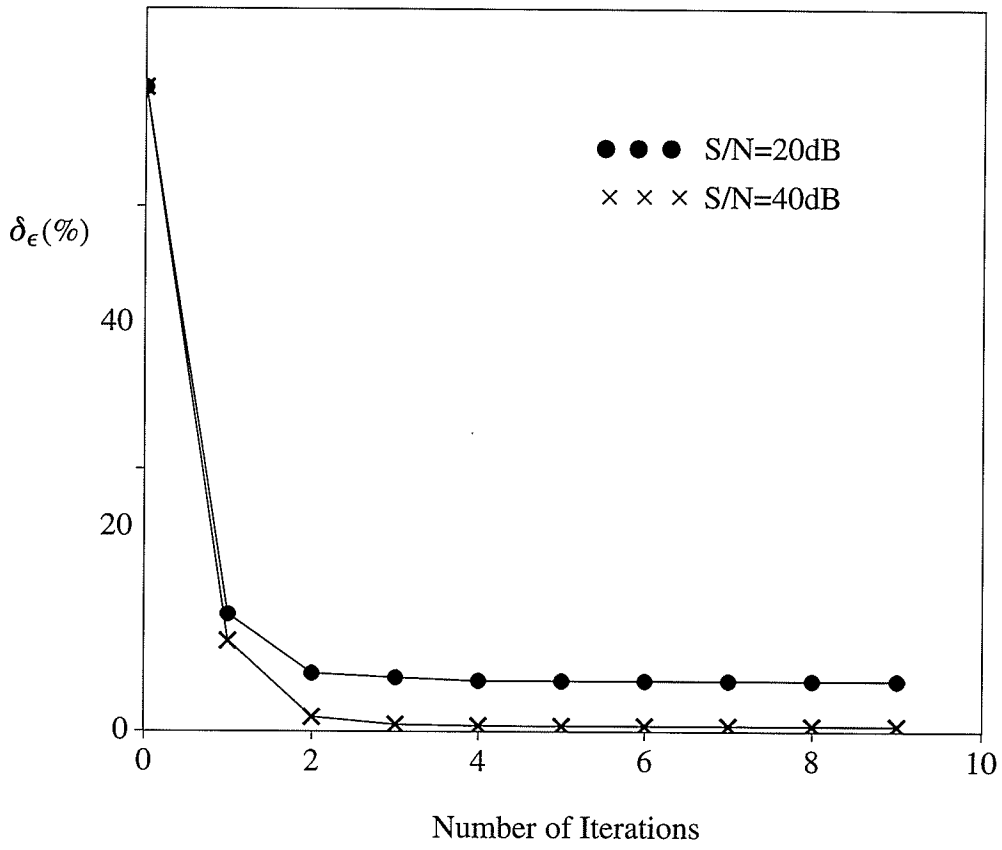

Fig. 4.6 Relative mean square error of the reconstructed permittivities versus the number of iterations for the scatterer in Fig. 4.5.

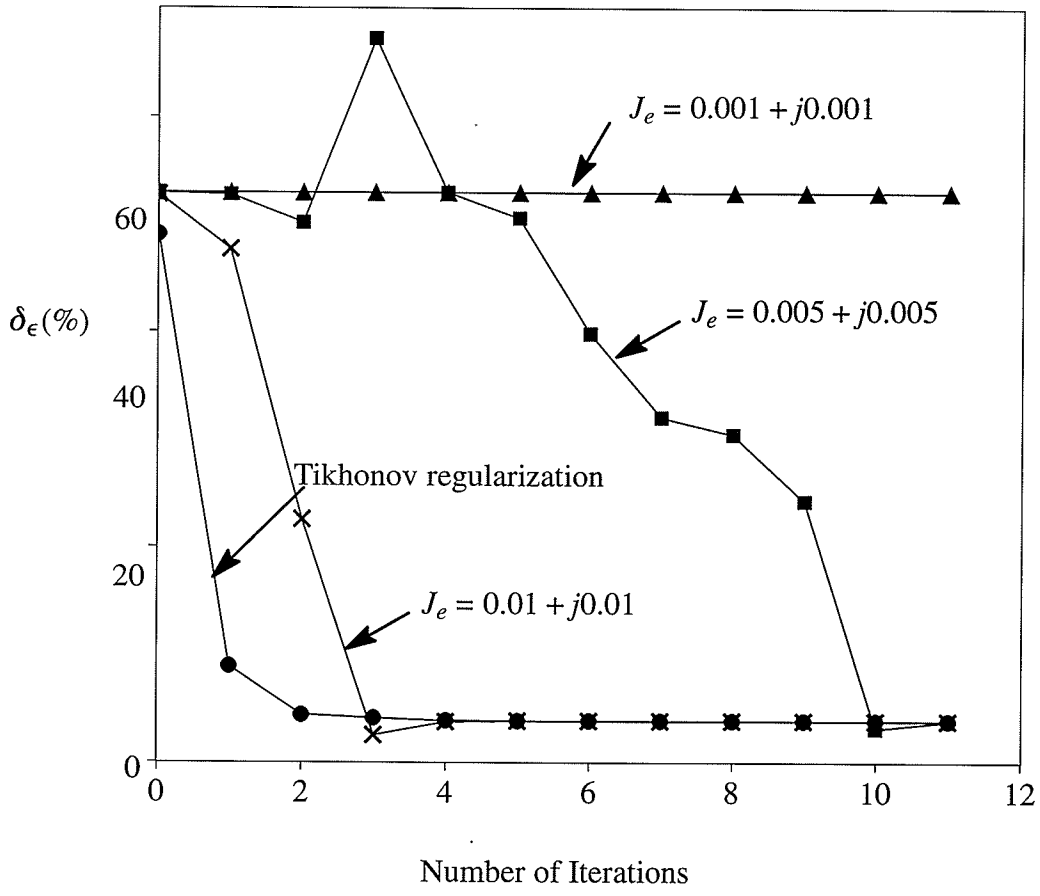

Fig. 4.7 Influence of the initial guess for the current density upon the number of iterations, for the structure in Fig. 4.5(a) and *S/N*=20dB.

TABLE 4.4

reconstructed permittivities for the scatterer shown in Fig. 4.5(a) with only 16 detectors.

Cell Number	ε_r *S/N*=40dB Three iterations	ε_r *S/N*=20dB Five iterations
1	1.00	1.00
2	1.00	1.00
3	1.00	1.00
4	1.00	1.00
5	1.00	1.00
6	1.00	1.00
7	1.00	1.00
8	1.00	1.00
9	1.00	1.00
10	1.00	1.00
11	1.00	1.00
12	1.00	1.00
13	3.03	3.08
14	2.99	2.77
15	1.00	1.00
16	1.00	0.99
17	1.00	1.00
18	3.00	3.06
19	2.96	2.32
20	1.01	1.00
21	1.00	1.00
22	1.00	1.00
23	1.00	1.00
24	1.00	1.00
25	1.00	1.00

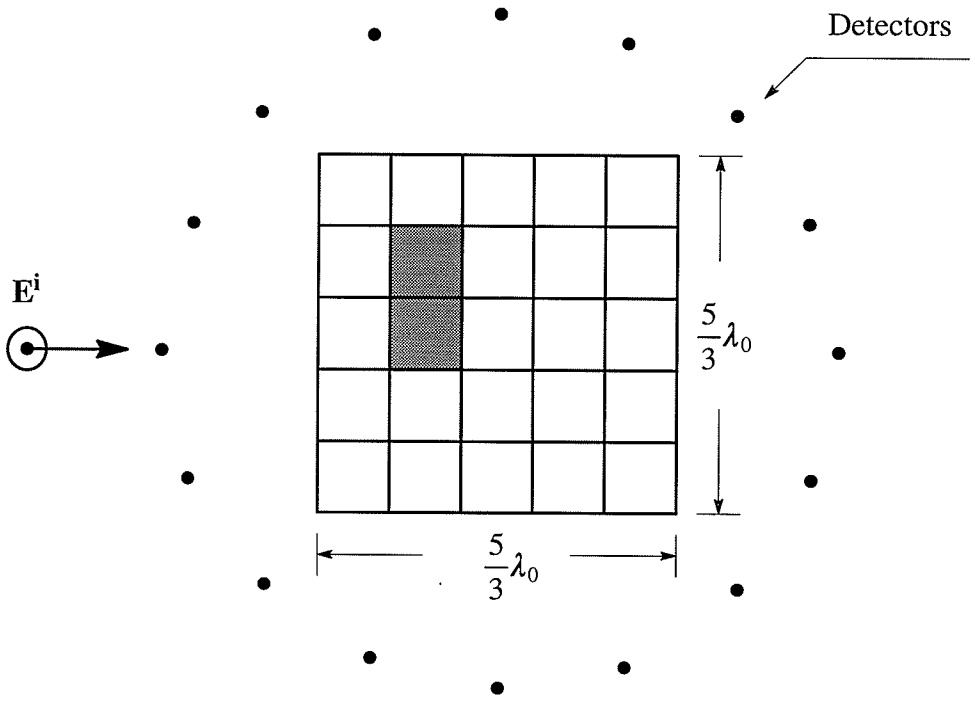

Fig. 4.8 Discretization of the investigation region.

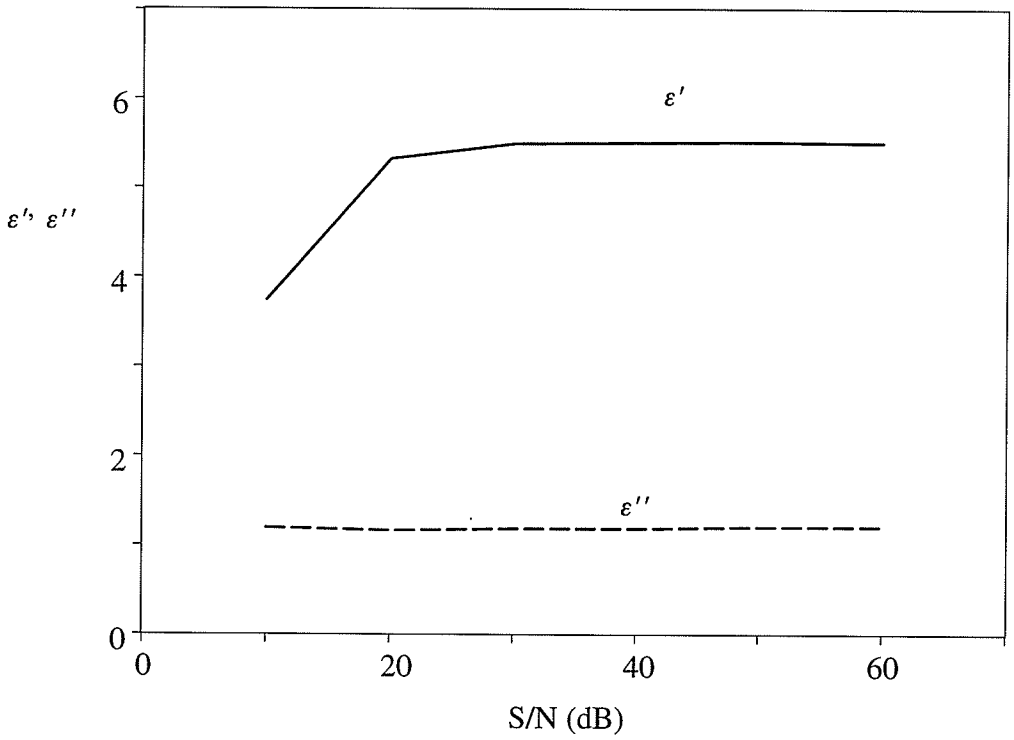

Fig. 4.9 Reconstructed permittivity versus the signal–to–noise ratio.

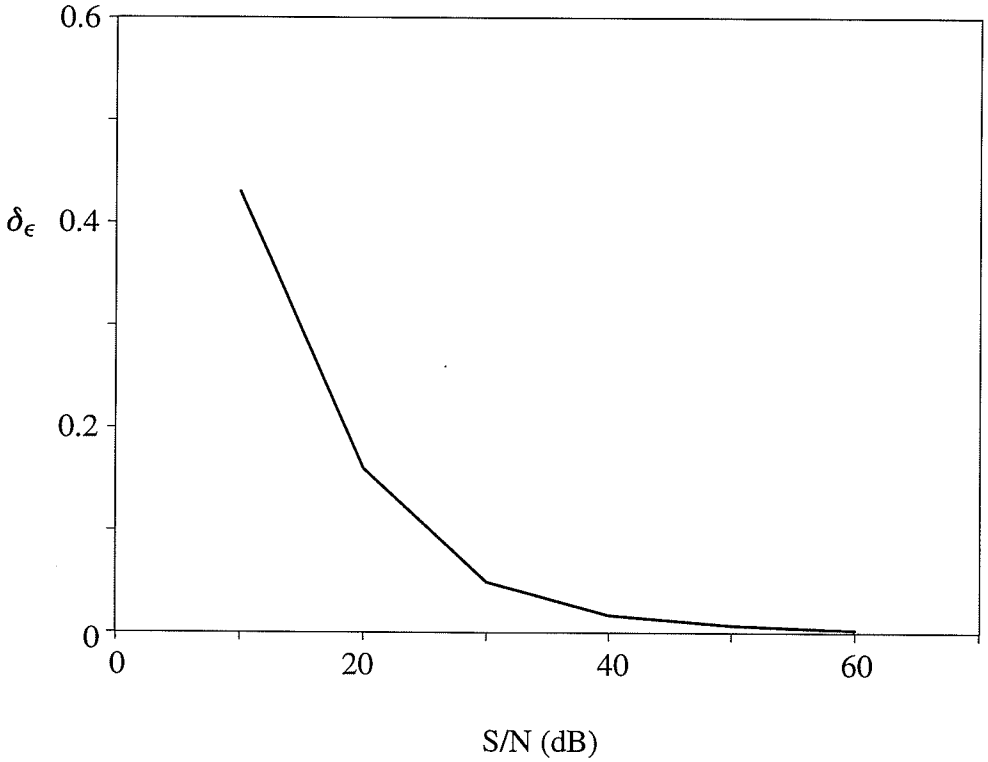

Fig. 4.10 Error of reconstruction versus the signal–to–noise ratio.

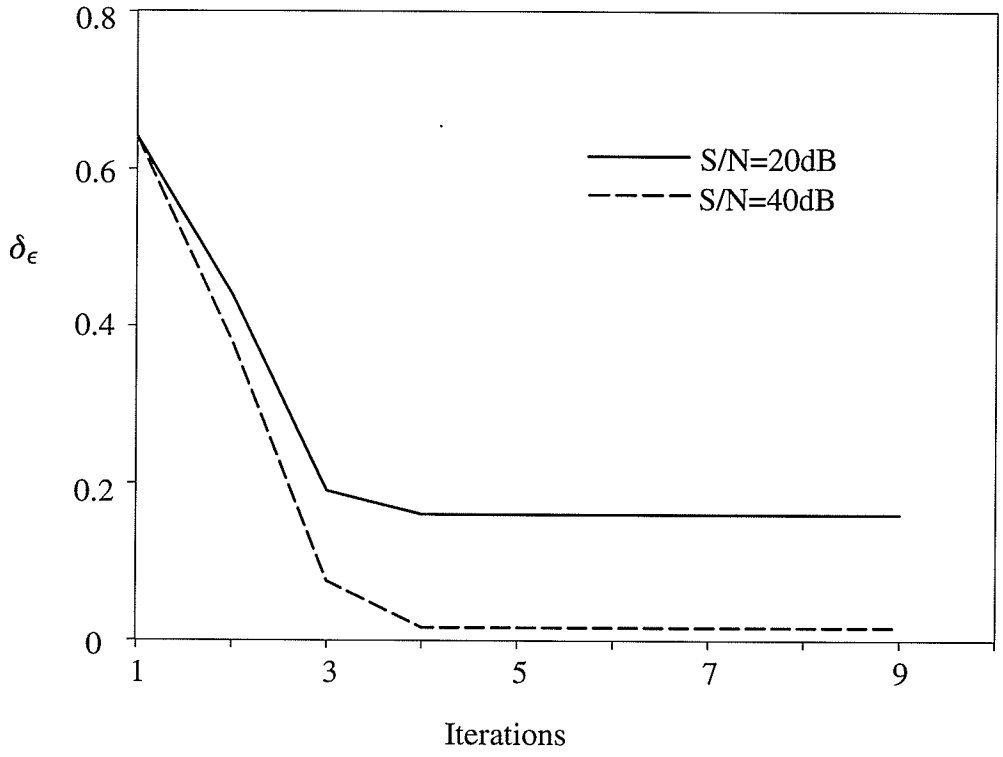

Fig. 4.11 Error of reconstruction versus the number of iterations.

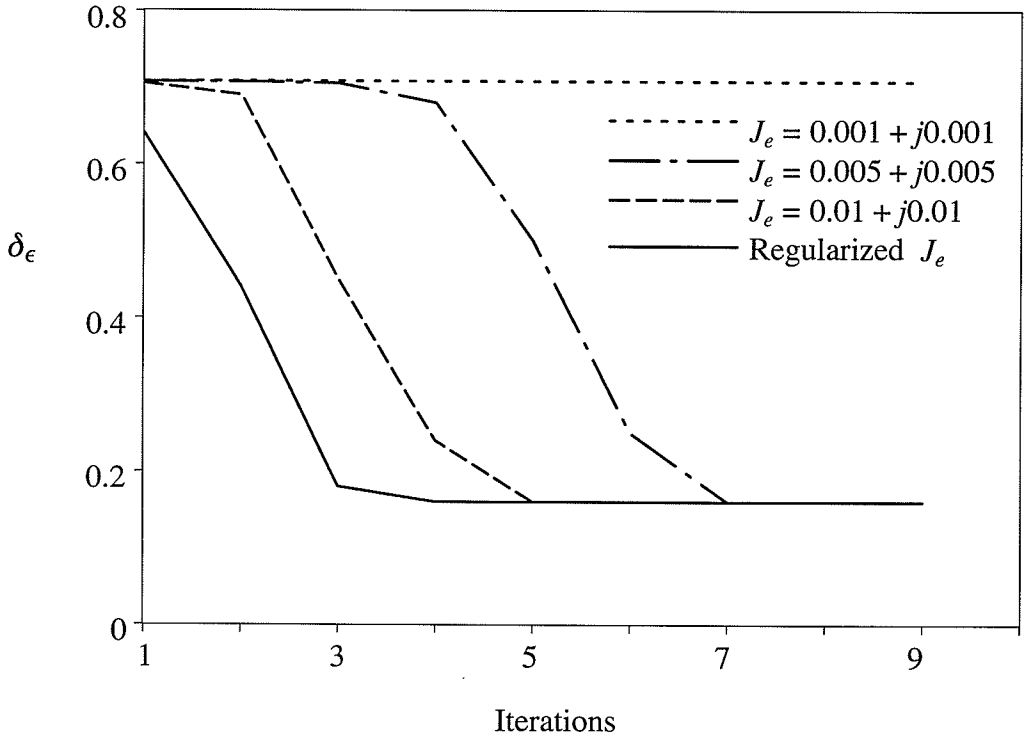

Fig. 4.12 Influence of the initial guess for the current density upon convergence when S/N = 20 dB.

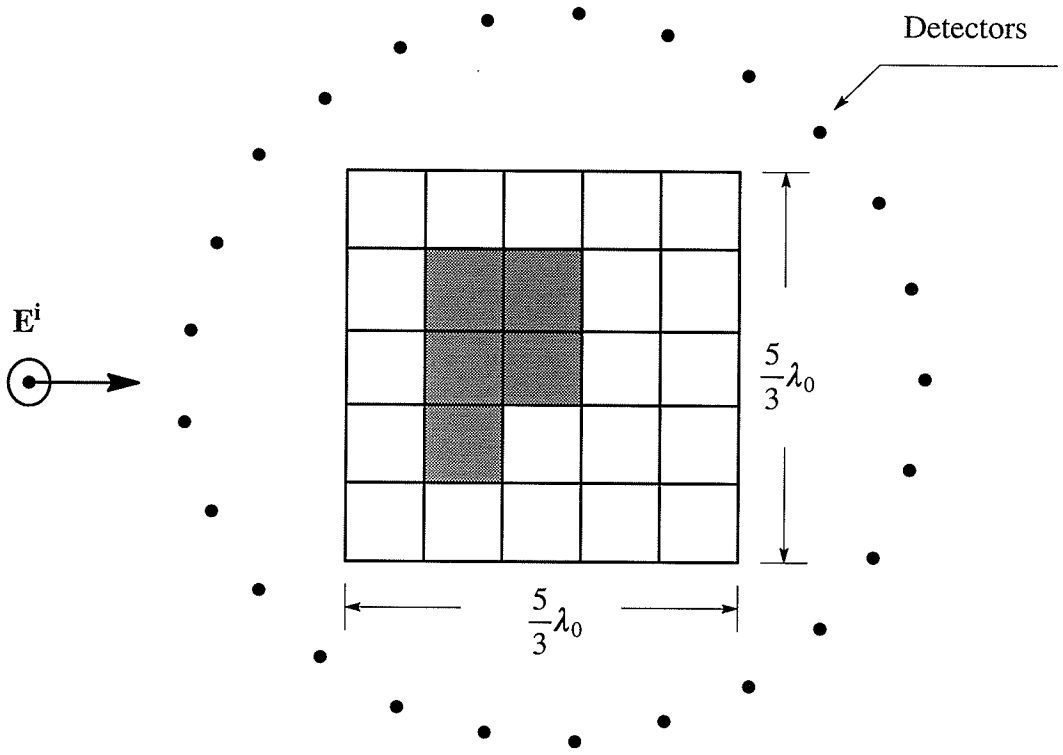

Fig. 4.13 Discretization grid for a scatterer occupying 20% of the investigation region.

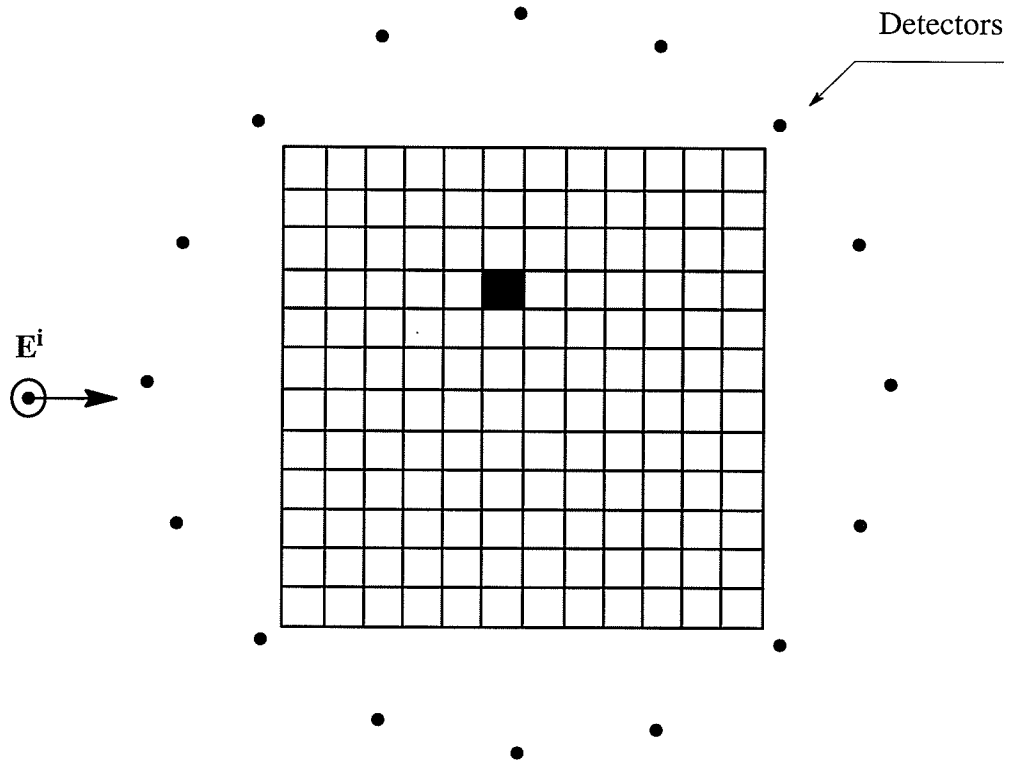

Fig. 4.14 Discretization grid for a scatterer occupying one cell.

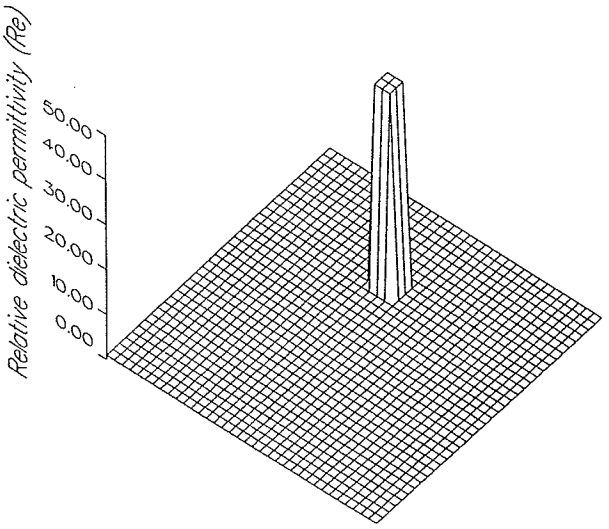

(a)

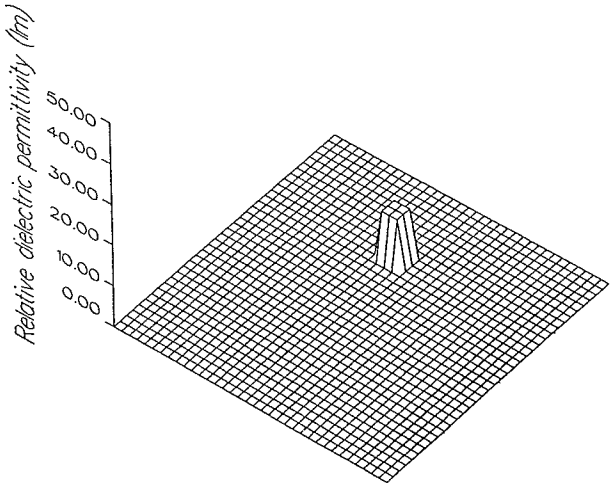

(b)

Fig. 4.15 Pictorial presentation of the reconstructed permittivity, S/N=40dB.

(a) Real part; (b) Imaginary part.

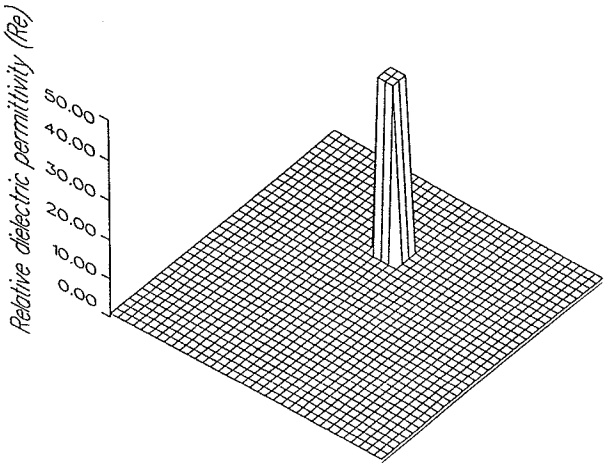

(a)

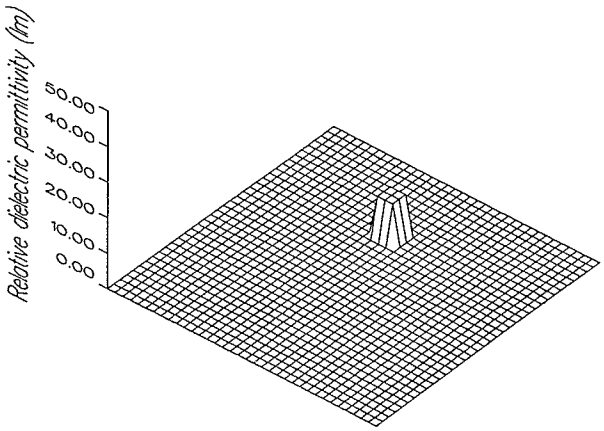

(b)

Fig. 4.16 Pictorial presentation of the reconstructed permittivity, S/N=20dB.

(a) Real part; (b) Imaginary part.

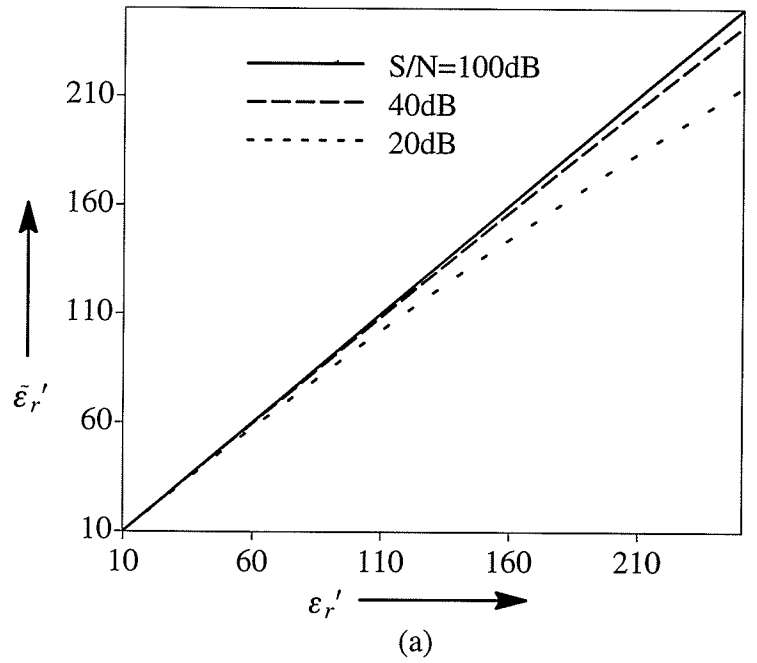

(a)

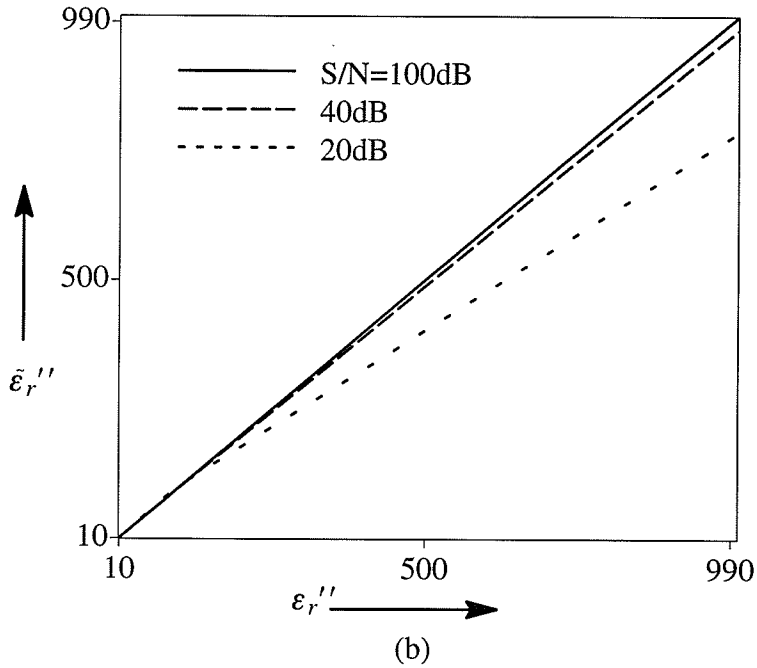

(b)

Fig. 4.17 Reconstructed permittivities versus original permittivities:

(a) Real part;
(b) Imaginary part.

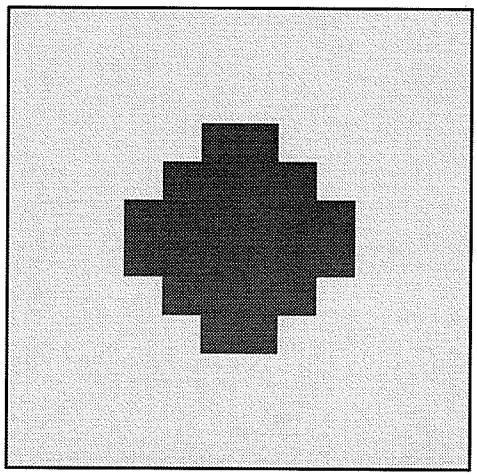

(a) Investigation region and object model.

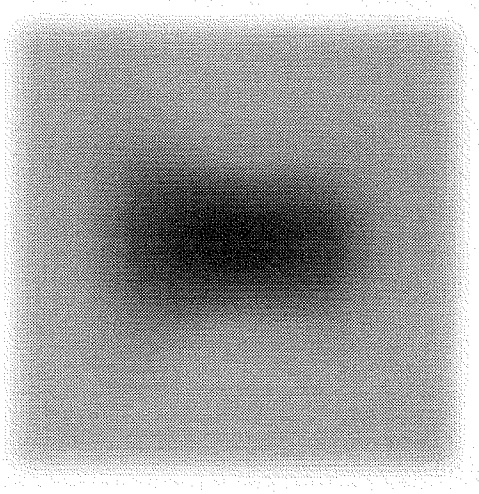

(b) one incident wave with S/N=40dB.

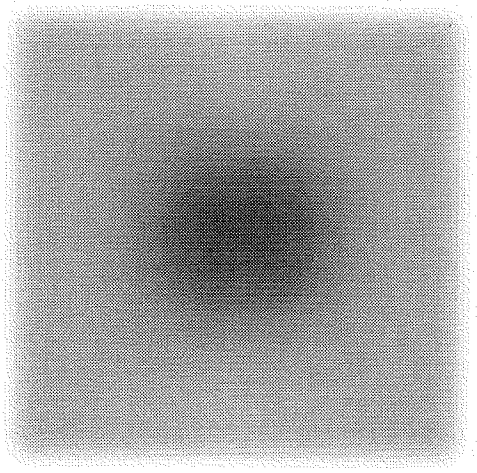

(c) four incident waves with S/N=40dB.

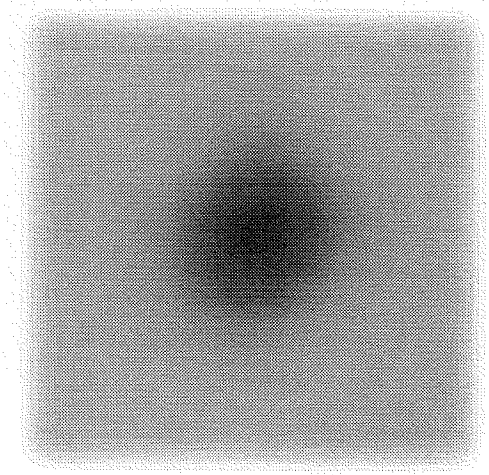

(d) four incident waves with S/N=15dB.

Fig. 4.18 A dielectric cylinder and its microwave images.

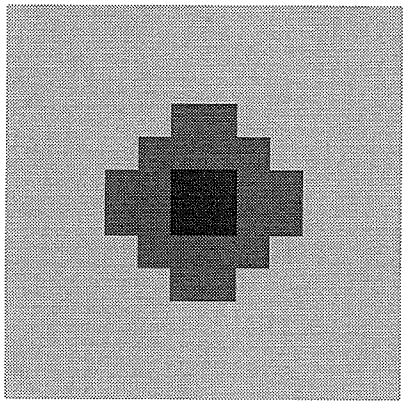

(a) Original permittivity (real part) distributions.

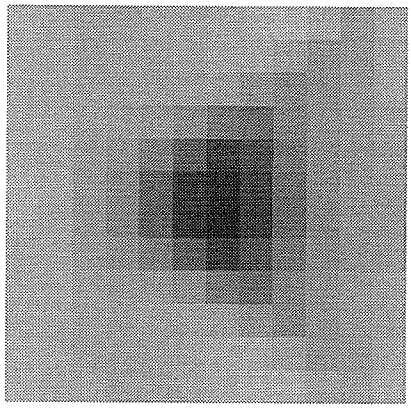

(b) Reconstructed dielectric permittivities (real part) with monoview technique for S/N=40dB.

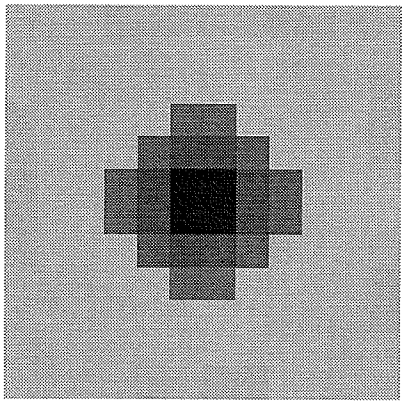

(c) Reconstructed dielectric permittivities (real part) with four–view process for S/N=40dB.

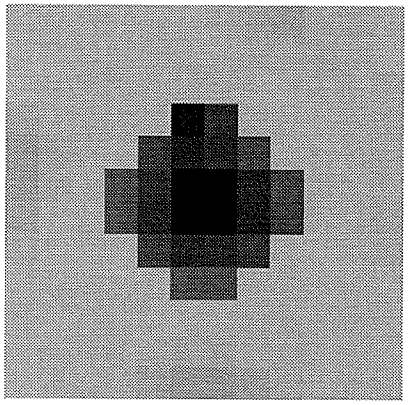

(d) Reconstructed dielectric permittivities (real part) with four–view process for S/N=15dB.

Fig. 4.19 A lossy dielectric cylinder with two layers.

5

SELECTION OF THE REGULARIZATION PARAMETER FOR MICROWAVE IMAGING

5.1 Introduction

As we mentioned before, one of the advantages of linearized inverse methods based on the equivalent current formulation lies in their fast reconstruction algorithms. However, because of the limited space for situating the receivers and the difficulty of combining a jointed system of equations for multi–illuminations, the resulting systems are usually underdetermined. For more complex dielectric bodies, this underdetermined system may not contain enough information to yield an expected result. Although the studies regarding the limitation of each method are still ongoing, we may predict that the equivalent current modelling based methods are more efficient only for the dielectric properties of relatively small problems. For more complex dielectric inverse problems, efforts have been made to solve the two coupled non–linear equations directly [11]–[14]. The general procedure is that a multiview process is usually first employed to construct an overdetermined system of equations. The total fields in the dielectric bodies are then calculated by giving an initial guess to the object function. Substituting the total field into the first equation, the first approximation of the object function is obtained by solving an ill–conditioned linear systems of equations. The process performs iteratively until an acceptable error level is obtained. If the initial object function is assumed to be the same as the background, the method is called the Born iterative meth-

od[11]. The above iterative method can also be modified, such as the distorted Born iterative method[12] and the Newton–type iterative method[14]. Because the problem is ill–conditioned in determining the object function in each iteration, the regularization technique is employed to stabilize the matrix decompositions that are involved in the process of the reconstruction. One of the difficulties in the procedure is the selection of the regularization parameter. If this parameter is too big, too much useful information could be lost. If it is too small, a convergent solution might not be obtained. In the Born iterative method and the distorted Born iterative method, this parameter is selected experimentally. In the Newton type iterative method, it is chosen in terms of the relative mean square error of the reconstructed scattered field and the measured field. This process allows the parameter adjusting its value from iteration to iteration accordingly. However, a new scalar presenting the magnitude of the regularization parameter was introduced and no indication given how to select this new parameter.

In this chapter, we first review the general procedure of solving nonlinear integral equations associated with the microwave imaging in the spatial domain. Then we present three methods for selecting this parameter. The first method is applicable to the situation when the upper bound of the object function variance and the upper bound of the measured data noise variance are known. The second method can be used if only the upper bound of the object function variance is detectable. If this information is not available, the third method can be employed to find the regularization parameter. The efficiency of these methods is illustrated by reconstructing two–dimensional dielectric objects with noiseless measured data and also with data containing noise. In the first example, a dielectric cylinder with continuous dielectric permittivity distribution along cross–section is considered. In the second example, an object with discontinuous dielectric permittivity distribution is investigated. In the third example, we use noisy data to reconstruct the same dielectric profile to the second one to test the robustness of the methods. All the examples show the efficiency and the robustness of

the presented methods.

5.2 Reconstruction procedure

Consider the following two coupled nonlinear matrix equations employed for microwave imaging in spatial domain in the case of one illumination[11]–[14], [22]–[25]

$$\mathbf{E}^s = [G_2][E^t]\mathbf{O} \tag{5.1}$$

$$\mathbf{E}^t = ([I] - [G_1][O])^{-1}\mathbf{E}^i \tag{5.2}$$

where $\mathbf{E}^s$ is a column vector representing the measured scattered electric field of dimension m (m denotes the number of detectors), $\mathbf{E}^t$, $\mathbf{E}^i$ and $\mathbf{O}$ are column vectors of dimension n (n indicates the number of cells in which the investigation region is divided) representing the total field, the incident field and the object function respectively, $[E^t]$ and $[O]$ are diagonal matrices consisting of the elements of $\mathbf{E}^t$ and $\mathbf{O}$ respectively, $[G_1]$ and $[G_2]$ are matrices of dimensions $n \times n$ and $m \times n$ respectively, and $[I]$ is the identity matrix. The general procedure of solving these two equations is that the first approximation of the total field in eqn. (5.1) is taken to be just the incident field. Substituting the object function obtained from eqn. (5.1) in eqn. (5.2) gives the first estimate of the total field $\mathbf{E}^t$. Then this $\mathbf{E}^t$ is used in eqn. (5.1) to obtain the second estimate of the object function and the iterations continue until a stable solution is obtained. In this process, eqn. (5.2) is always well–conditioned. Therefore, once the object function is given, the solution of (5.2) can be obtained directly. However, eqn. (5.1) is, in general, ill–conditioned and, usually, instead of solving (5.1) directly, an attempt is made to regularize it. The solution to the regularized equation may give a reasonable approximation to the solution of the original ill–conditioned equation allowing us to develop a satisfactory image.

Taking into account the global effect of all the illuminations yields for each iteration step

$$\mathbf{E}_T^s = [D]\mathbf{O} \tag{5.3}$$

where $[D]$ is a $vm \times n$ matrix consisting of the submatrices obtained from the product $[G_2][E^t]$ for all the v illuminations *i.e.*

$$[D] = \begin{bmatrix} [G_2]_1\ [E^t]_1 \\ [G_2]_2\ [E^t]_2 \\ [G_2]_3\ [E^t]_3 \\ \vdots \\ [G_2]_v\ [E^t]_v \end{bmatrix} \tag{5.4}$$

and $\mathbf{E}_T^s$ is a column vector of dimension vm consisting of all $\mathbf{E}^s$

$$\mathbf{E}_T^s = [\mathbf{E}_1^s,\ \mathbf{E}_2^s,\ \mathbf{E}_3^s,\ \ldots,\ \mathbf{E}_v^s]^T \tag{5.5}$$

This equation is ill–conditioned in general, with the measured field in $\mathbf{E}_T^s$ containing noise and errors, and $[D]$ containing the errors accumulated in $[E^t]$ in the previous iterations. The regularized solution of eqn. (5.3) is given by

$$\mathbf{O} = ([D]^H[D] + \alpha[I])^{-1}[D]^H\mathbf{E}_T^s \tag{5.6}$$

with H denoting the conjugate transpose of a matrix and α the regularization parameter. In order to obtain an acceptable solution, an appropriate regularization parameter must be chosen. To the best of our knowledge there is no general rule presented in the literature regarding the selection of this parameter for electromagnetic imaging algorithms. In the following, we consider the problem from a stochastic point of view and show the possible ways to estimate this parameter. Taking into account the inaccuracies and the noise in $[D]$ and $\mathbf{E}_T^s$, we rewrite eqn. (5.3) as

$$\mathbf{E}_T^s = [D]\mathbf{O} + \mathbf{N} \tag{5.7}$$

where $\mathbf{N}$ is a vm–dimensional vector indicating the error $\mathbf{E}_T^s - [D]\mathbf{O}$ at the iteration step considered. We treat this error term $\mathbf{N}$ as being a random variable and then the solution $\mathbf{O}$ of eqn.

(5.7) is also a random variable. Under the assumption that these two variables are uncorrelated, the following expression is employed to evaluate **O** from eqn. (5.7) [43]

$$\mathbf{O} = ([D]^H[R_\mathbf{N}]^{-1}[D] + [R_\mathbf{O}]^{-1})^{-1}[D]^H[R_\mathbf{N}]^{-1}\mathbf{E}_T^s \tag{5.8}$$

where $[R_\mathbf{N}]$ and $[R_\mathbf{O}]$ denote the correlation matrices of **N** and **O**. Assuming that **N** and **O** are also isotropic random variables, we have

$$[R_\mathbf{N}] = \sigma_\mathbf{N}^2[I] \tag{5.9}$$

$$[R_\mathbf{O}] = \sigma_\mathbf{O}^2[I] \tag{5.10}$$

with $\sigma_\mathbf{N}^2$ and $\sigma_\mathbf{O}^2$ denoting the variances of the random vectors **N** and **O**. Thus, eqn. (5.8) becomes

$$\mathbf{O} = ([D]^H[D] + \sigma_\mathbf{N}^2/\sigma_\mathbf{O}^2[I])^{-1}[D]^H\mathbf{E}_T^s \tag{5.11}$$

Comparing eqn. (5.11) with eqn. (5.6), we find that the role of the regularization parameter α is played by

$$\alpha = \sigma_\mathbf{N}^2/\sigma_\mathbf{O}^2 \tag{5.12}$$

Although these variances are unknown in most microwave imaging problems, (5.12) still allows us to evaluate α from a practical point of view.

5.3 Methods for Selecting the Regularization Parameter

Equation (5.12) shows us that the regularization parameter can be interpreted in terms of the variances of noise and the object function. Here we consider three cases and present the corresponding expressions for this parameter.

A. Upper bounds of $\sigma_\mathbf{N}^2$ and $\sigma_\mathbf{O}^2$ are known

Suppose the values of $\sigma_\mathbf{N}^2$ and $\sigma_\mathbf{O}^2$ are not known, but their upper bounds can be fixed from our previous knowledge and experience. If we use the notations $C_\mathbf{N}$ and $C_\mathbf{O}$ for these

upper bounds, *i.e.*

$$\sigma_{\mathbf{N}}^2 \leq C_{\mathbf{N}} \tag{5.13}$$

$$\sigma_{\mathbf{O}}^2 \leq C_{\mathbf{O}} \tag{5.14}$$

we employ as the regularization parameter

$$\alpha = C_{\mathbf{N}}/C_{\mathbf{O}} \tag{5.15}$$

Since

$$\| \mathbf{E}_T^s - [D]\mathbf{O} \|^2 = \| \mathbf{N} \|^2 \tag{5.16}$$

and the Maximum likelihood estimate of the noise variance $\sigma_{\mathbf{N}}^2$ is given by eqn. (2.84), *i.e.*

$$(1/vm) \| \mathbf{E}_T^s - [D]\mathbf{O} \|^2 = (1/vm) \| \mathbf{N} \|^2 \tag{5.17}$$

we see that if the measured data is noisier the bigger regularization parameter must be used, and *vice versa*. On the other hand, if the selected regularization parameter is bigger than the desired one, higher reconstruction error can be expected.

B. Upper bound of $\sigma_{\mathbf{O}}^2$ is known

In some applications, only the upper bound of the object function $C_{\mathbf{O}}$ can be fixed. For example, in biomedical applications the range of electric qualities which characterize the tissues in the body under most conditions can be evaluated from previous experience. Using the maximum likelihood estimator of noise variance (eqn. 2.84), the regularization parameter at each iteration step can be expressed as

$$\alpha = \frac{1}{vm} \frac{\| \mathbf{E}_T^s - [D]\mathbf{O} \|^2}{C_{\mathbf{O}}} \tag{5.18}$$

where the matrix $[D]$ and vector $\mathbf{O}$ are those from the preceding iteration. To avoid too small values of α as the iterative process progresses, when at a certain iteration step the reconstruction error

$$\| \mathbf{E}_T^s - [D]\mathbf{O} \|^2 / vm \tag{5.19}$$

becomes less than an imposed value, the value of α corresponding to that step should be used for the next iterations (in the simulations presented in Section 5.4, this value is chosen to be equal 10^{-4} in the case of noiseless data and equal to the order of the variance of the noise in the case of data containing noise). The whole iterative procedure is summarized as follows:

(1) apply Born approximation to eqn. (5.3);

(2) calculate α using eqn. (5.18);

(3) find the object function $\mathbf{O}$ from eqn. (5.6);

(4) calculate $\mathbf{E}^t$ using eqn. (5.2) and then $[D]$ from eqn. (5.4);

(5) check relative error $\| \mathbf{E}_T^s - [D]\mathbf{O} \|^2 / vm$; if less than the imposed value, go to (3) and use the latest α until a stable value of $\mathbf{O}$ is obtained; if not, go to (2).

C. σ_N^2 and σ_O^2 are unknown

In this case, the Levenberg–Marquardt scheme [69],[70] can be applied to the imaging process. The Levenberg–Marquardt scheme was originally developed to solve general non-linear algebraic equations. The main point is that at each iteration the squared Euclidean norm of the the difference between the given data and the recovered data is calculated. If the difference at that iteration is smaller than the previous one, then decrease regularization parameter by a factor, or continuously increase it by a factor until a decrease is obtained. A starting regularization parameter of 0.01 was suggested. However, in our numerical simulations we find that Marquardt's suggestion that the regularization parameter be increased or decreased by factors which are powers of 10 is not applicable in general to the problems of microwave imaging. For some increasing/decreasing factors the error is oscillating and the iteration process does not seem to behave as a convergent process, at least for the first 10 to 20 iterations in the examples considered. Numerical tests performed by the author indicate that an increasing factor of 1.5 coupled with a decreasing factor of 0.5 performs much better

for this type of electromagnetic imaging problems.

In our imaging process, an initial positive value is taken for the regularization parameter to be used in the first iteration, whose selection will be discussed later. At each iteration, the difference between the calculated scattered field and the measured scattered field defined in eqn. (5.19) is estimated. If the difference decreases from one iteration to the next one, the regularization parameter to be used in the succeeding iteration is decreased by a factor which is chosen to be 0.5. If the difference does not decrease, the parameter is increased by a factor of 1.5, until a decreased difference is achieved. This iterative process is ended when the error in the computed scattered field decreases to an acceptable value.

For the initial value of the regularization parameter, we know that the correlation matrix of the object function can be expressed as (see eqn. 2.89)

$$[R_{\mathbf{O}}] = \sigma_{\mathbf{N}}^2 \, ([D]^H[D] + \alpha[I])^{-1} \, ([D]^H[D]) \, ([D]^H[D] + \alpha[I])^{-1} \tag{5.20}$$

whose diagonal elements are the corresponding variances of the object function. Using the total variance (see eqn. 2.91) of the object function and assuming $\alpha = 0$ in eqn. (5.20), yields

$$\sigma_{\mathbf{O}}^2 = n\sigma_{\mathbf{N}}^2[tr([D]^H[D])]^{-1} \tag{5.21}$$

With eqn. (5.12), we find that the initial regularization parameter takes the form

$$\alpha_0 = (1/n)tr([D]^H[D]) \tag{5.22}$$

The reconstruction algorithm is summarized as follows:

(1) determine the initial regularization parameter α and the matrices G_1, G_2, and choose a desired level of accuracy;

(2) calculate the total field $\mathbf{E}^t$ in (5.2) and construct the matrix $[D]$ in (5.3);

(3) find the object function $\mathbf{O}$ from (5.6);

(4) compute the relative error of the scattered field calculated from (5.3) with respect to the measured scattered field, *i.e.* $\| \mathbf{E}_T^s - [D]\mathbf{O} \|^2 / \| vm$; if the error is less than the desired value, the iteration is terminated or go to step 2; otherwise, go to step 5;

(5) after the first iteration, reduce the initial regularization parameter by a factor of 0.5 and go to step 2; in each subsequent iteration, compare the error norm with the one in the preceding iteration; if the error norm decreases, reduce the regularization parameter by a factor of 0.5 and go to step 2; otherwise, increase the parameter 1.5 times for the microwave imaging problem considered and go to step 3.

The iterative process continues until the desired level of accuracy is achieved or until the error norm maintains a practically stable value.

5.4 Numerical Results

To illustrate the methods presented in this chapter, we consider a few two dimensional objects similar to those in[11], [12]. In all examples, the size of the investigation domain is $1.4\lambda_0 \times 1.4\lambda_0$, where λ_0 is the wavelength of the background medium which is now assumed to be free space. To apply the moment method, we divided the investigation domain into 196 subsquare of equal size of $0.1\lambda_0 \times 0.1\lambda_0$. Eight incident waves with unity amplitude and frequency of 100 MHz are used to illuminate the region from eight directions at 45 degrees from each other. For each illumination, 36 receivers uniformly distributed on a measurement loop are used. Figure 5.1 shows the geometry of the investigation region. The scattered fields at the receiver points are calculated by the moment method with pules functions and point matching. The resulting simultaneous linear equations are solved using LU factorization method. The relative mean square error of the reconstructed permittivity defined as

$$\delta_\varepsilon = \left[\frac{\sum_{i=1}^{n} |\varepsilon_i - \tilde{\varepsilon}_i|^2}{\sum_{i=1}^{n} |\varepsilon_i|^2} \right]^{\frac{1}{2}} \tag{5.23}$$

is used to compare the overall accuracy of the reconstructed permittivity, where where ε_i

and $\tilde{\varepsilon}_i$ are the values of the original permittivity in the *i–th* cell and of the reconstructed per-

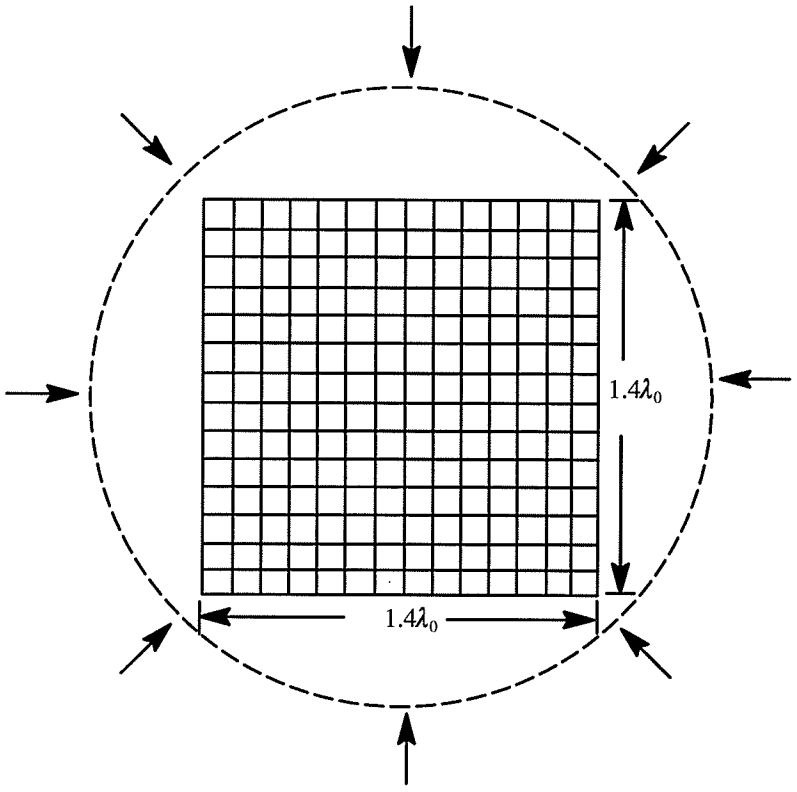

Fig. 5.1 The geometry of a two–dimensional region with 36 detectors uniformly distributed along the broken line and 8 incident waves.

mittivity, respectively, with the summations extended over all the cells in the investigation region. The relative error of the scattered fields defined as

$$\delta^2_{E^s} = \frac{\sum_{j=1}^{v}\sum_{k=1}^{m} |E^s_{jk} - \tilde{E}^s_{jk}|^2}{\sum_{j=1}^{v}\sum_{k=1}^{m} |E^s_{jk}|^2} \tag{5.24}$$

is employed to evaluate the overall accuracy of the reconstructed scattered fields, where E^s_{jk}

and $\tilde{E}^s_{jk}$ are the values of the detected electric field and the reconstructed electric field at the *k–th* receiver for the *j–th* view of the incident field.

A. Continuous Profile

As the first example, we consider a object with a cosinusoidal variation of the permittivity along the cross–sectional Cartesian coordinate axes and their origin at the center of the cross section and oriented normal to the cylinder sides, with a peak value of $1.6\varepsilon_0$. The radius of the measurement circular loop is $1.5\lambda_0$. The profile is shown in Fig. 5.10 (a)

Fig. 5.2 shows the real part and imaginary part of the scattered electric field at the detectors generated by one of the microwave illuminations.

In Fig. 5.3 and Fig. 5.4, the relative errors of the reconstructed scattered electric fields and dielectric permittivity are plotted versus the number of iterations for various values of the regularization parameters. The solid lines indicates the results yielded from the proposed method C. When the same value of the regularization parameter is employed for all iterations, a stronger regularization yields bigger reconstruction errors, while too weak a regularization may not insure the iteration convergence. Applying the method C to this problem, we obtain convergent results with relatively small final reconstruction errors.

Fig. 5.5 and Fig. 5.6 show the relative error of the reconstructed scattered electric fields and the relative error of the reconstructed dielectric permittivity versus the number of iterations for various increasing/decreasing factors. We see that Marquardt's suggestion [70] that the regularization parameter should be increased or decreased by factors which are powers of 10 is not applicable in general to the problems of microwave imaging. For some increasing/decreasing factors the reconstructed results are oscillating and the iteration process does not seem to behave as a convergent process, at least for the first 10 to 20 iterations in the examples considered. These figures indicate that an increasing factor of 1.5 coupled with a decreasing factor of 0.5 performs much better for this type of electromagnetic imaging prob-

lems. The relative error of the reconstructed scattered electric field by the increases/decreases of 1.5/0.5 is less than 10^{-6} after the tenth iteration and keeping decreasing. The relative error of the reconstructed dielectric permittivity is less than 10^{-3} after the tenth iteration.

Fig. 5.7 and Fig. 5.8 give the relative errors of the reconstructed electric fields and the reconstructed dielectric permittivities from the presented three methods. In the method A, we assume the upper bound of the error variance of the reconstructed scattered fields is 10^{-4}. For the upper bound of the variance of the object function, we simply take it to be 0.4, a little bit bigger than the squared peak value of the object function. In the method B, the upper bound value of the object function variance is the same as that in the method A. If computed scattered field error defined in eqn. 5.19 is less than 10^{-4}, the value of the regularization parameter stops updating in order to avoid too weak a regularization. In the method C, the increasing/decreasing factors of 1.5/0.5 are used in the reconstruction process. In these figures, we see that all three methods yield quite small reconstruction errors either for the permittivity or for the scattered fields. The iteration processes in both method A and method B become stable after the eighth iteration the similar reconstruction errors. Method C gives a similar relative error to methods A and B at the first eight iterations, but yields even smaller reconstruction error afterwards.

In Fig. 5.9, the traces of the regularization parameter versus the number of iterations in the three methods are plotted. In method A, the constant regularization parameter performs in all the iterations. In method B, the regularization parameter stops changing after the sixth iteration. It is noteworthy that the stabilized regularization parameter yielded from method B is almost coincidence with the constant regularization parameter used in the method A. In method C, no increased parameter was observed.

Fig. 5.10(a) shows the original distribution of the relative dielectric permittivity with the peak value of 1.6. Figs. 5.10 (b), (c), and (d) are the reconstructed relative dielectric per-

mittivity distributions with the peak values of 1.59304 in (a), 1.59307 in (b) and 1.59279 in (c).

B) Discontinuous Profile

As the second example, we consider an object with discontinuous dielectric permittivity distribution along the cross–section. The diameter of the object is $1.0\lambda_0$ with the peak permittivity $1.6\varepsilon_0$. 36 receivers located on a circular loop of radius $1.2\lambda_0$ around the investigation region are used to detect the scattered electric fields.

The real part and the imaginary part of the detected field detected by the receivers generated by one of the incident waves are plotted in Fig. 5.11.

Fig. 5.12 and 5.13 show the relative error of the reconstructed scattered electric fields and reconstructed dielectric permittivity versus the number of iterations for various regularization parameters. As the results in example A, when constant regularization parameters are used in the algorithm, bigger regularization parameter yields a bigger reconstruction error. A too small regularization parameter may not give a convergent result. The optimum value of the regularization parameter in this simulation seems to be between 10^{-3} and 10^{-4}. When 10^{-4} is selected as the regularization parameter, the algorithm gives smaller errors compared with other constant regularization parameters, but it is going to oscillating. When 10^{-5} is used, the algorithm cannot give convergent results. When applying method C to the problem, convergent results with smaller reconstruction errors are obtained.

The relative errors of the reconstructed scattered electric fields and the reconstructed dielectric permittivity versus the number of iterations are shown in Fig. 5.14 , 5.15, and 5.16 for various increasing/decreasing factors with solid lines indicating the results obtained by method C. Similar to example A, when the increasing /decreasing factors of 10/0.1 and 4/0.25 were used, the algorithm gives oscillating results. Both the increasing/decreasing factors of 1.5/0.5 and 1.75/0.75 yield convergent results. The factor of 1.5 coupled with 0.5

gives smaller reconstruction error. By method C, the relative error of the reconstructed scattered electric fields is less than 2×10^{-8} after the fourteenth iteration and the relative error of the reconstructed dielectric permittivity is less than 7.5% after the fourth iteration. Compared with the results yielded in example A, we also notice that the relative errors are generally higher than those in the first example. This higher reconstruction error is generated by the discontinuous edge of the dielectric profile and the band–limited nature of the algorithm as mentioned in [16]. The regularization parameter plays a smoother role in the reconstruction process, like a spatial domain lowpass filter to smooth the edge of the object causing relatively higher reconstruction errors. This phenomenon can be observed in Fig. 5.19.

Fig. 5.17 and Fig. 5.18 present the results obtained by applying the three methods to the problem. In method A, the upper bound of the reconstruction error variance and the upper bound of the object function variance are assumed to be 10^{-4} and 0.4 respectively. In method B, 0.4 is assumed to be the upper bound of the object function variance and 10^{-4} is used to terminate updating the regularization parameter. In method C, 1.5/0.5 was used for the increasing/decreasing factor. All three methods gave convergent results with tolerable reconstruction errors.

The original relative dielectric permittivity distribution is shown in Fig. 5.19(a), and the reconstructed profiles by the three methods are illustrated in Fig. 5.19 (b)–(d). The peak value of the reconstructed profiles are 1.70079 in (b), 1.70065 in (c) and 1.69706 in (d).

C) Discontinuous Profile with noisy Data

This example allows to test the robustness of the proposed methods by using the data containing noise. We assume the noise has normal distribution with zero mean value. The signal–to–noise ratio defined in eqn. (4.8) is used to evaluate the level of the noise. Fig. 5.20 shows the detected scattered electric field with the signal–to–noise ratio of 20 dB.

Fig. 5.21 and 5.22 show the relative error of the reconstructed scattered electric fields and the relative error of the reconstructed dielectric permittivity with the noisy data of signal–to–noise ratio of 20 dB. Corresponding to the signal–to–noise ratio, the upper bound of the variance of the scattered fields error in method A is assumed to be 10^{-2}, and the upper bound of the object function is assumed to be 0.4 as in the previous examples. In method B, the same upper bound of the object function as in example A is used, and a value of 10^{-2} of the reconstruction error in (5.19) was accepted to stop updating the regularization parameter. In method C, the increasing/decreasing factor of 1.5/0.5 was employed, and 0.01 was chosen for the required reconstruction error. All the three methods yielded convergent results with reasonable reconstruction errors. The relative errors of the reconstructed scattered electric fields is converged to the order of 1.1%, and the relative errors of the reconstructed dielectric permittivity converged to 7.7% after the fourth iteration.

Fig. 5.23 presents the original profile and the reconstructed profiles by using the three proposed methods. The reconstructed peak values of the dielectric permittivities are 1.67216 in (b), 1.64946 in (c) and 1.64967 in (d).

5.5 Conclusion

The general procedure of microwave imaging in spatial domain consists of discretizing the electric field integral equations in the form of two coupled matrix equations by applying the moment method. The associated ill–conditioned systems of algebraic equations are solved iteratively by implementing the regularization technique at each iteration step. One of the difficulties in the procedure is the selection of the regularization parameter. Based on the fact that the Tikhonov regularization parameter can be interpreted in terms of the random noise variance and the object function variance, three methods for selecting this parameter are presented. Their performance is demonstrated by reconstructing two dimensional dielectric objects with both noiseless and noisy computer simulated data. The proposed methods

for the selection of the regularization parameter can also be extended to other iterative methods such as the distorted Born iterative method[12] and the Newton iterative method[14].

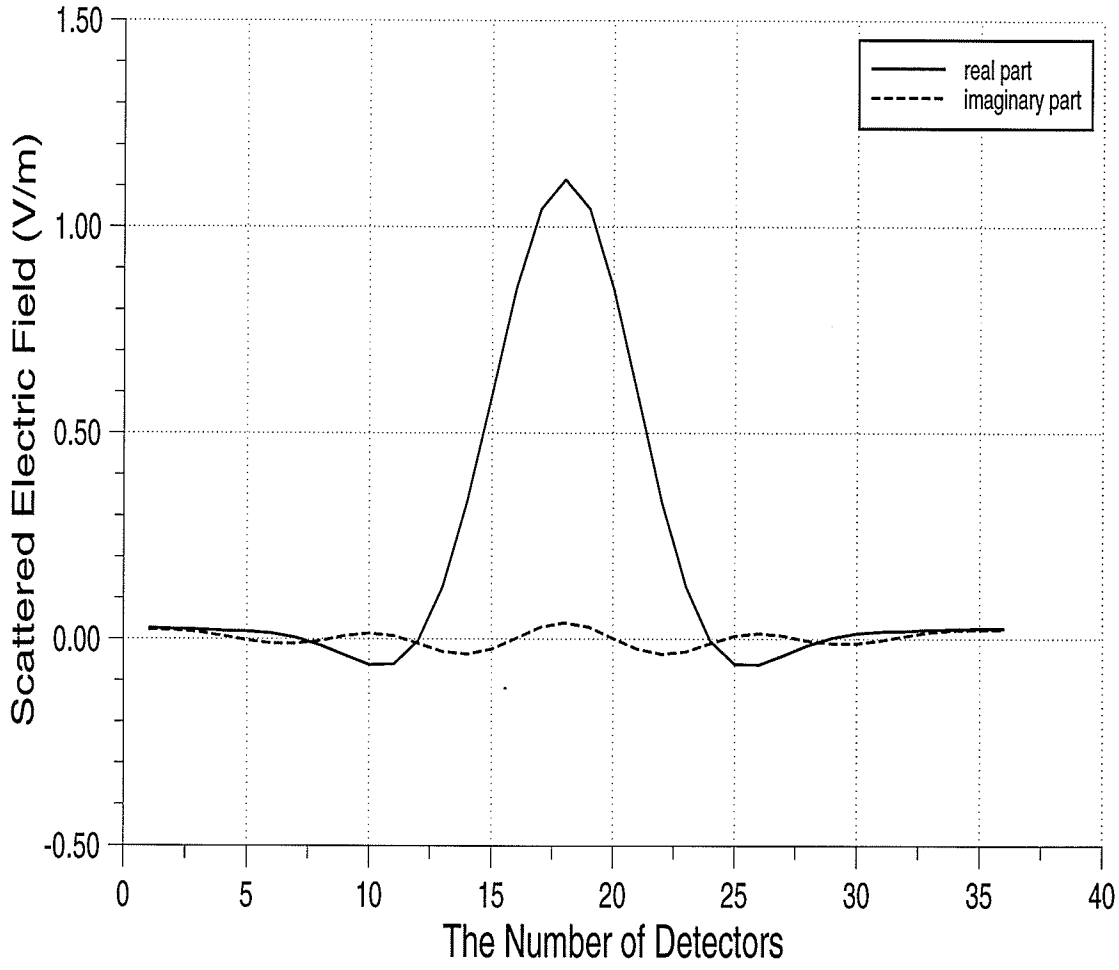

Fig. 5.2 Real part and imaginary part of the scattered field from a dielectric object with consinusoidal permittivity distribution.

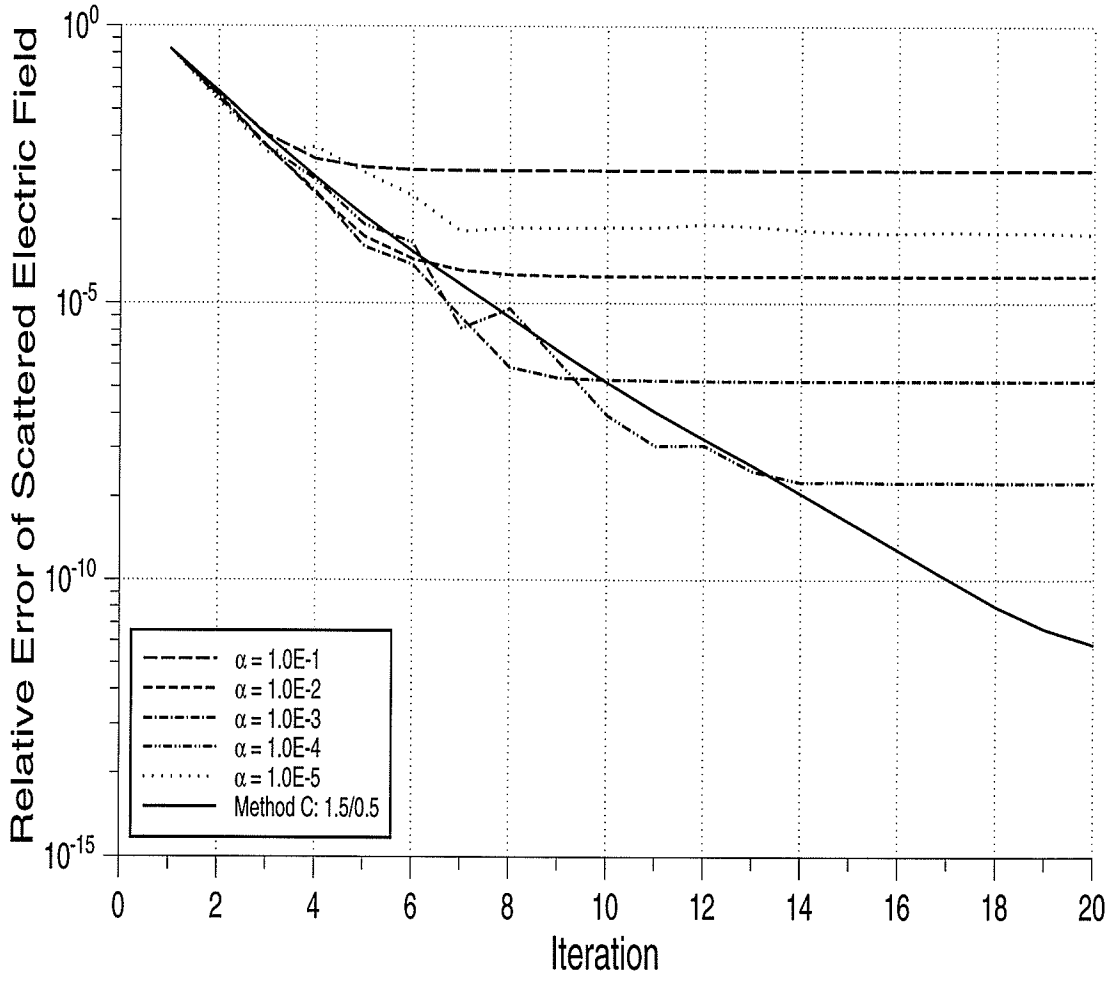

Fig. 5.3 Relative error of the reconstructed scattered electric fields versus the number of iterations for different regularization parameters.

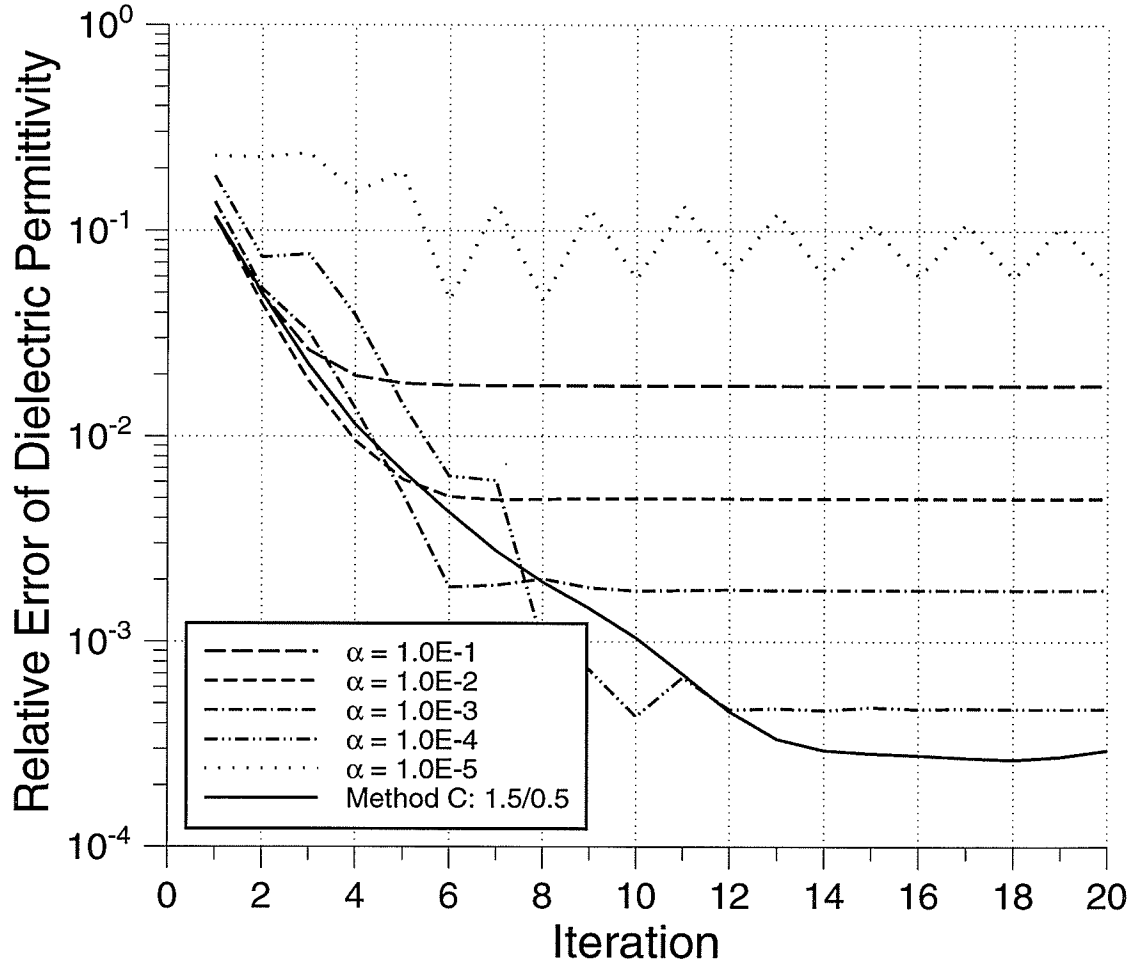

Fig. 5.4 Relative mean square error of the reconstructed dielectric permittivities versus the number of iterations for different regularization parameters.

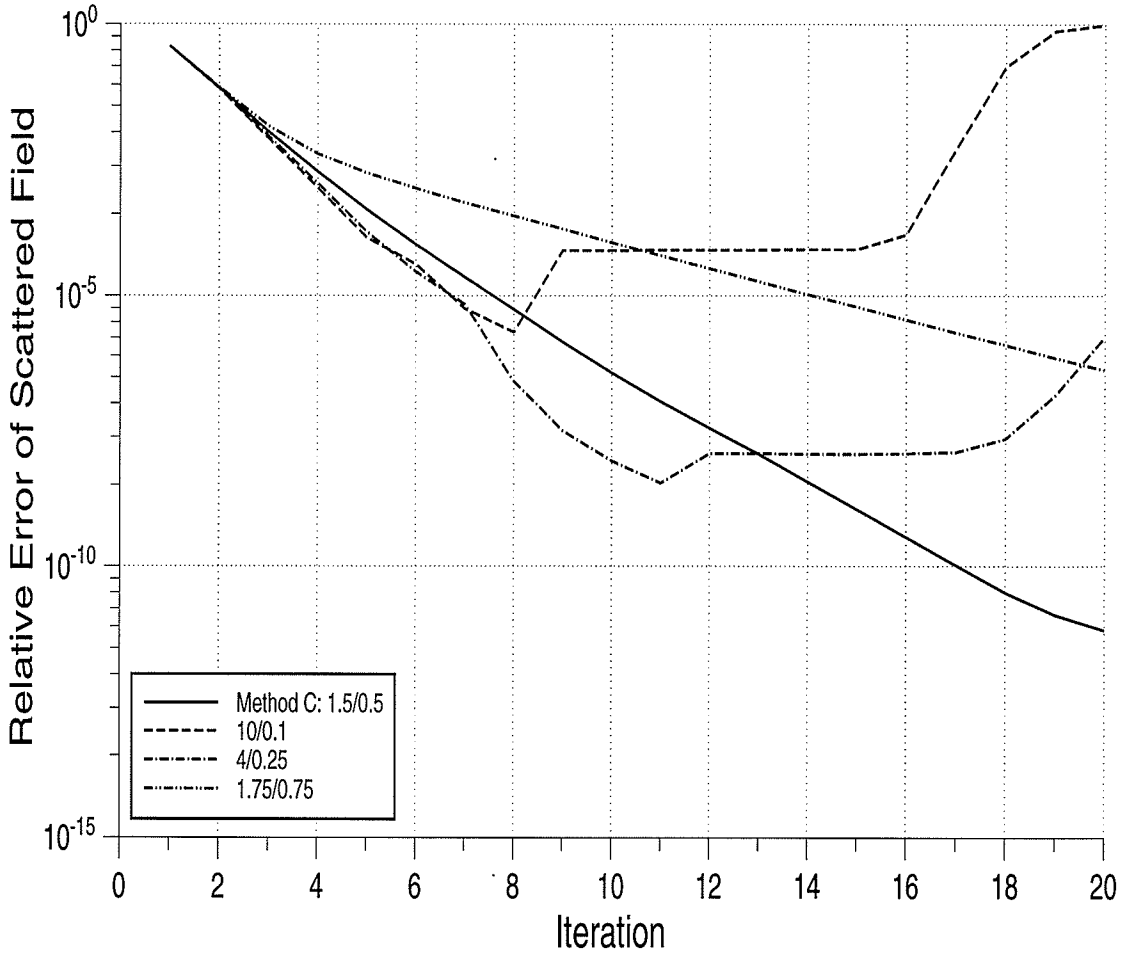

Fig. 5.5 Relative error of the reconstructed scattered fields versus the number of iterations for various increasing/decreasing factors.

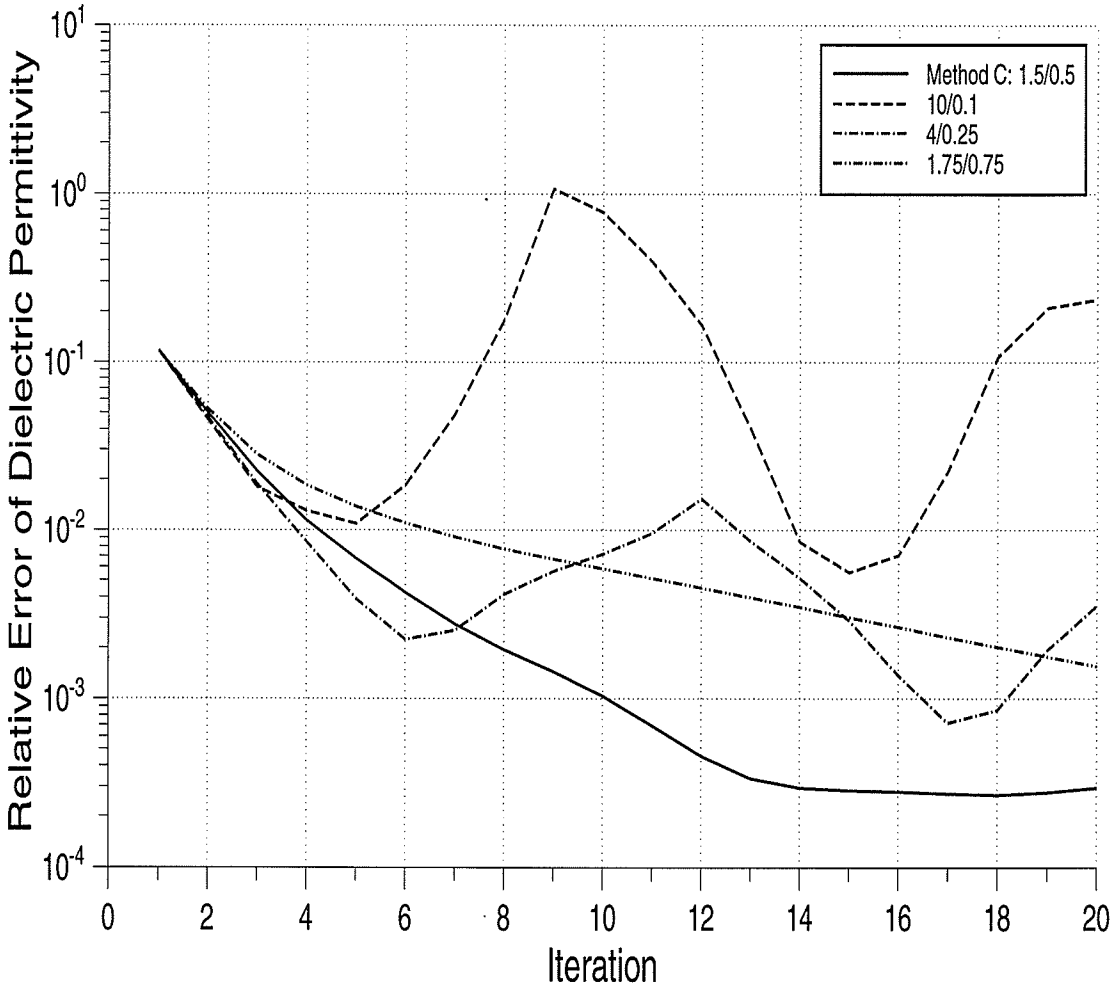

Fig. 5.6 Relative mean square error of the reconstructed dielectric permittivities versus the number of iterations for various increasing/decreasing factors.

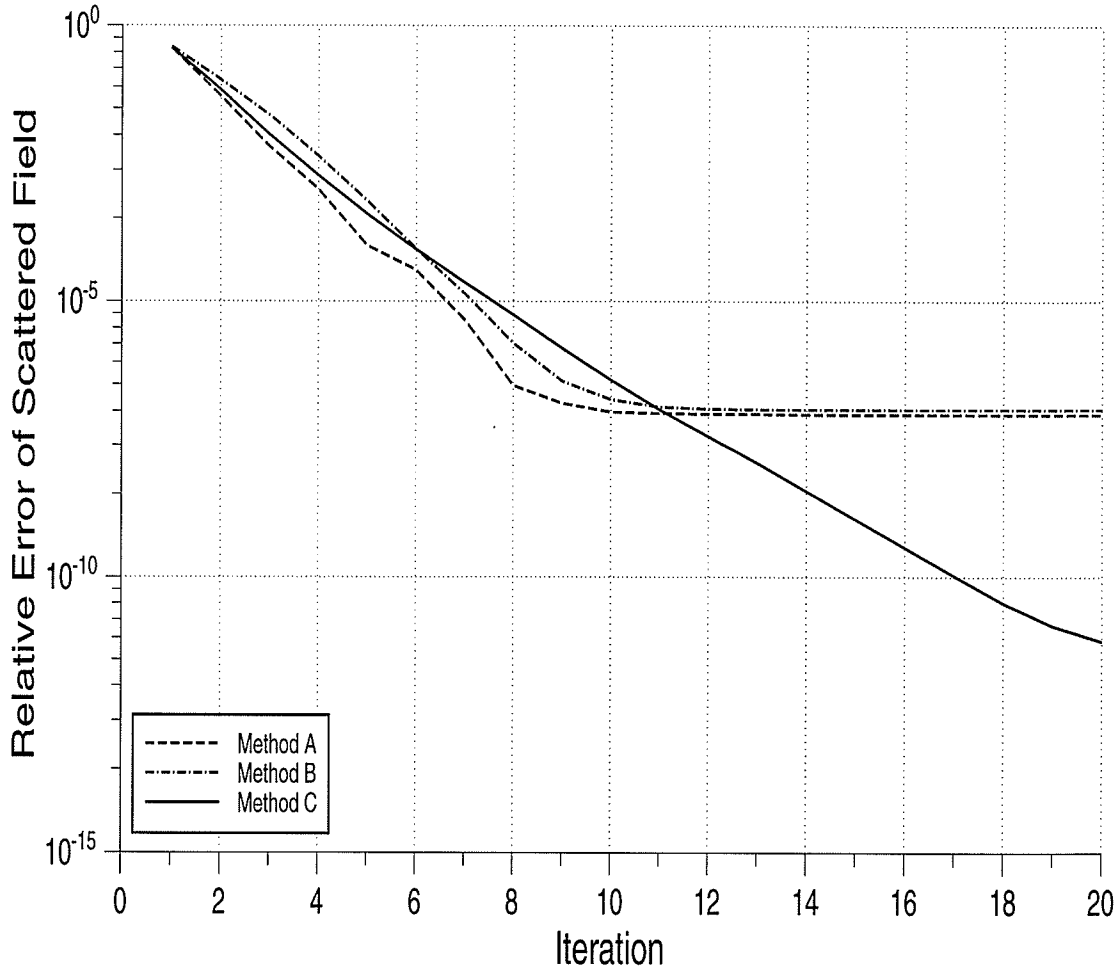

Fig. 5.7 Relative error of the reconstructed scattered electric fields versus the number of iterations by the proposed methods.

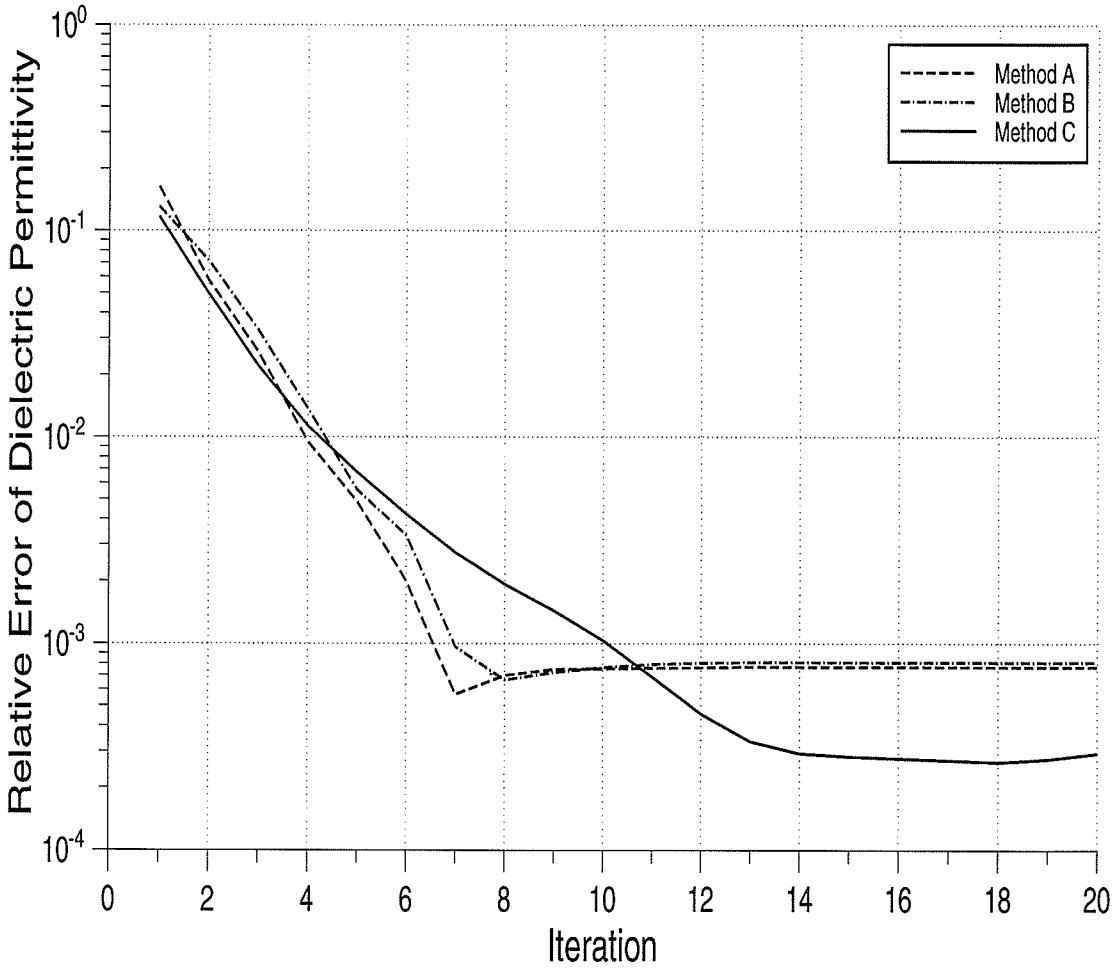

Fig. 5.8 Relative mean square error of the reconstructed dielectric permittivities versus the number of iterations by the proposed methods.

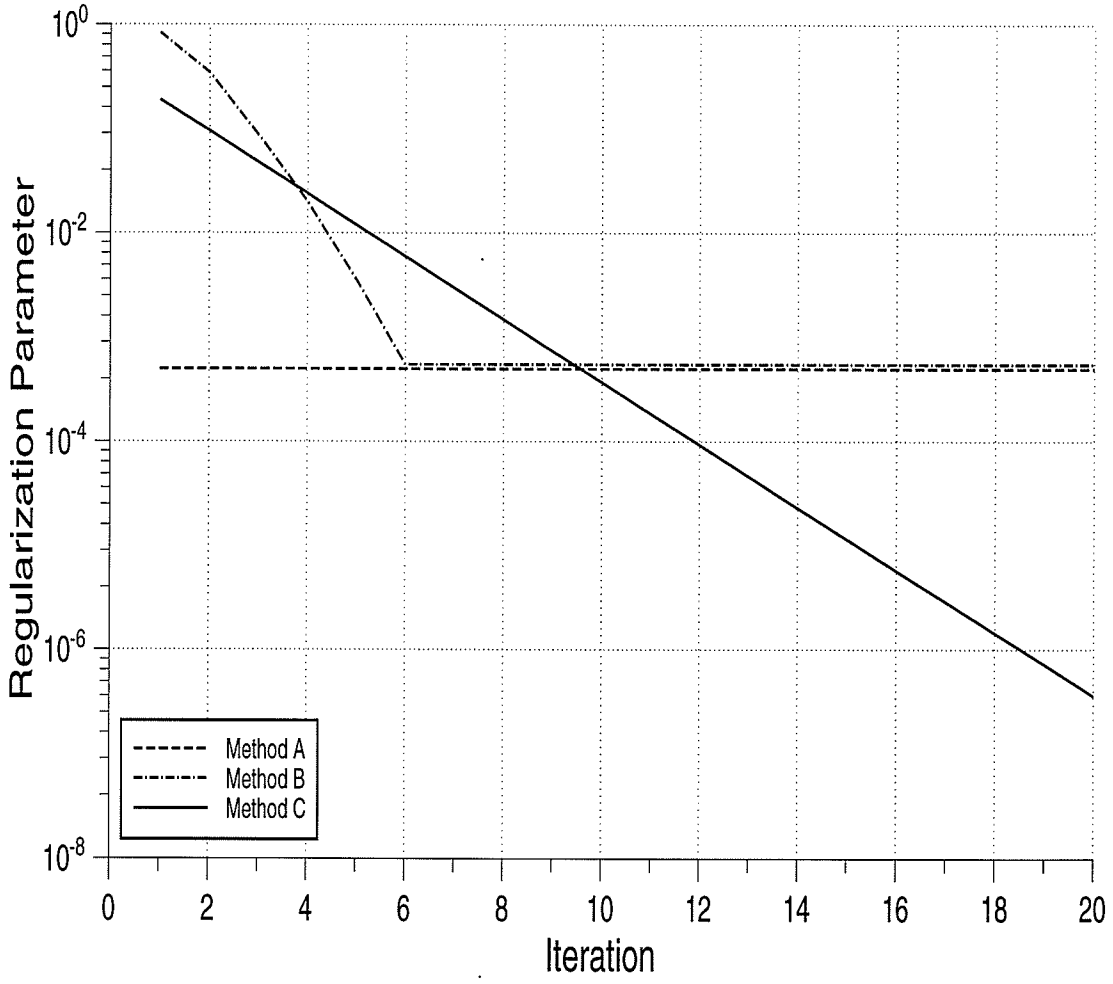

Fig. 5.9 Regularization parameters versus the number of iterations.

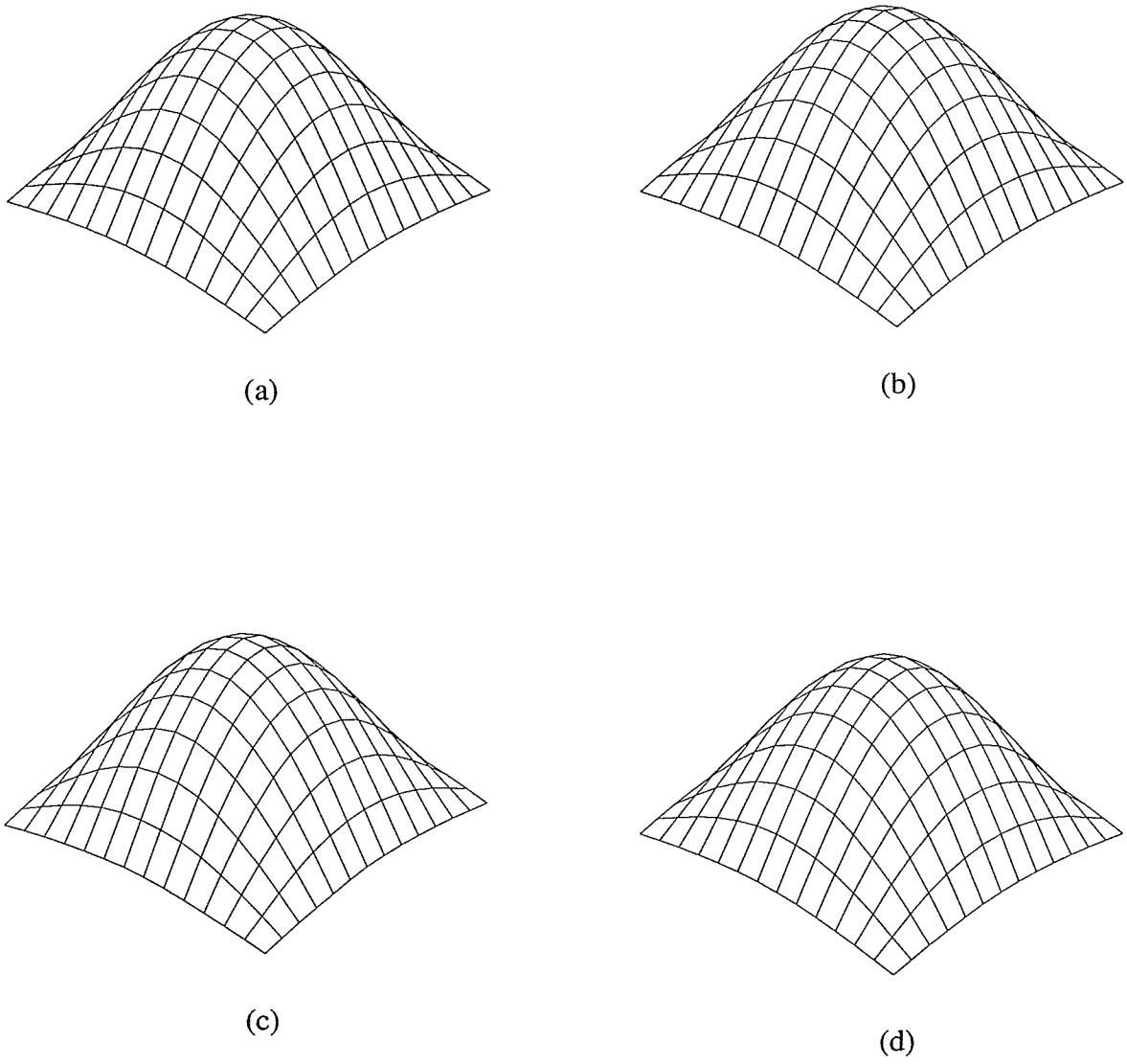

Fig. 5.10 Original and reconstructed cosinusoidal profiles.
(a) original profile; (b) method A; (c) method B;
(d) method C.

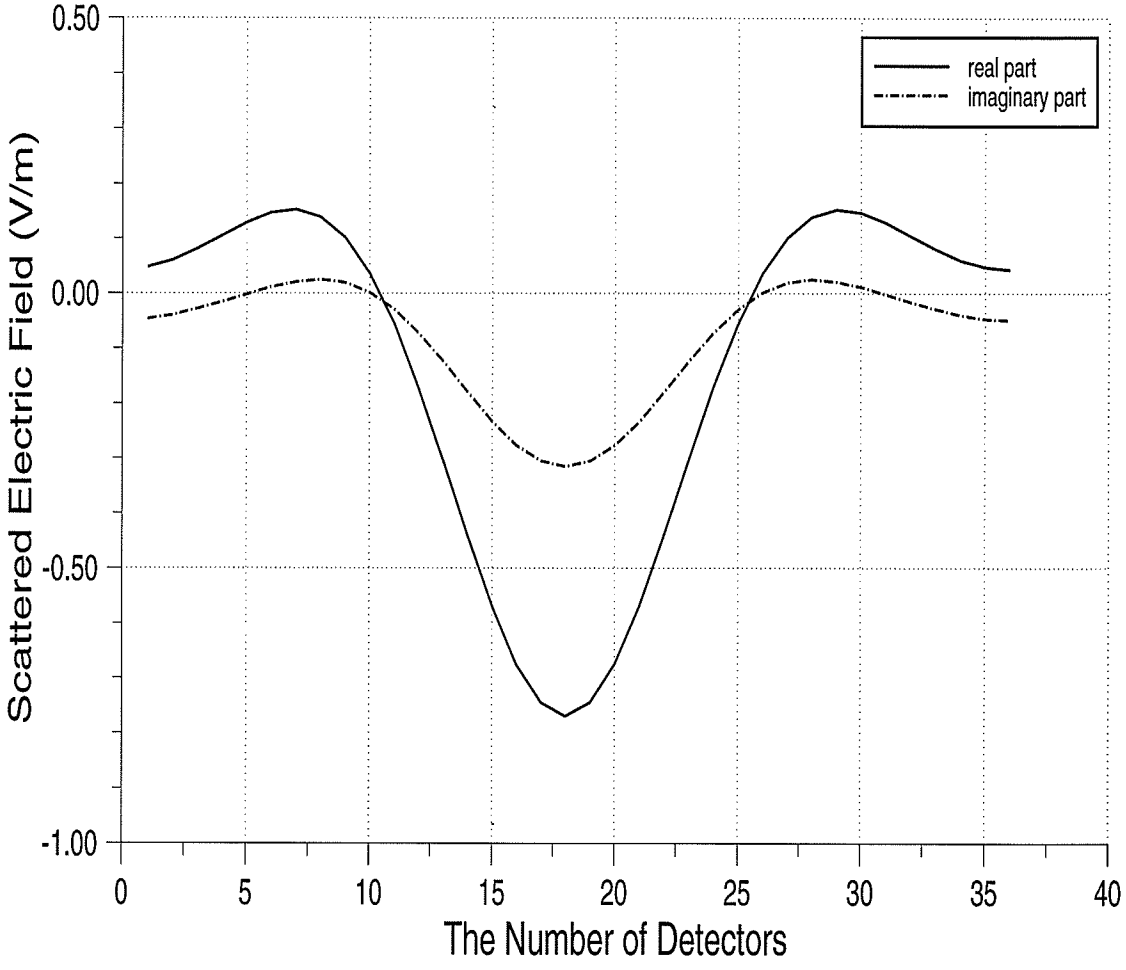

Fig. 5.11 Real part and imaginary part of the scattered field from a dielectric object with discontinuous permittivity distribution.

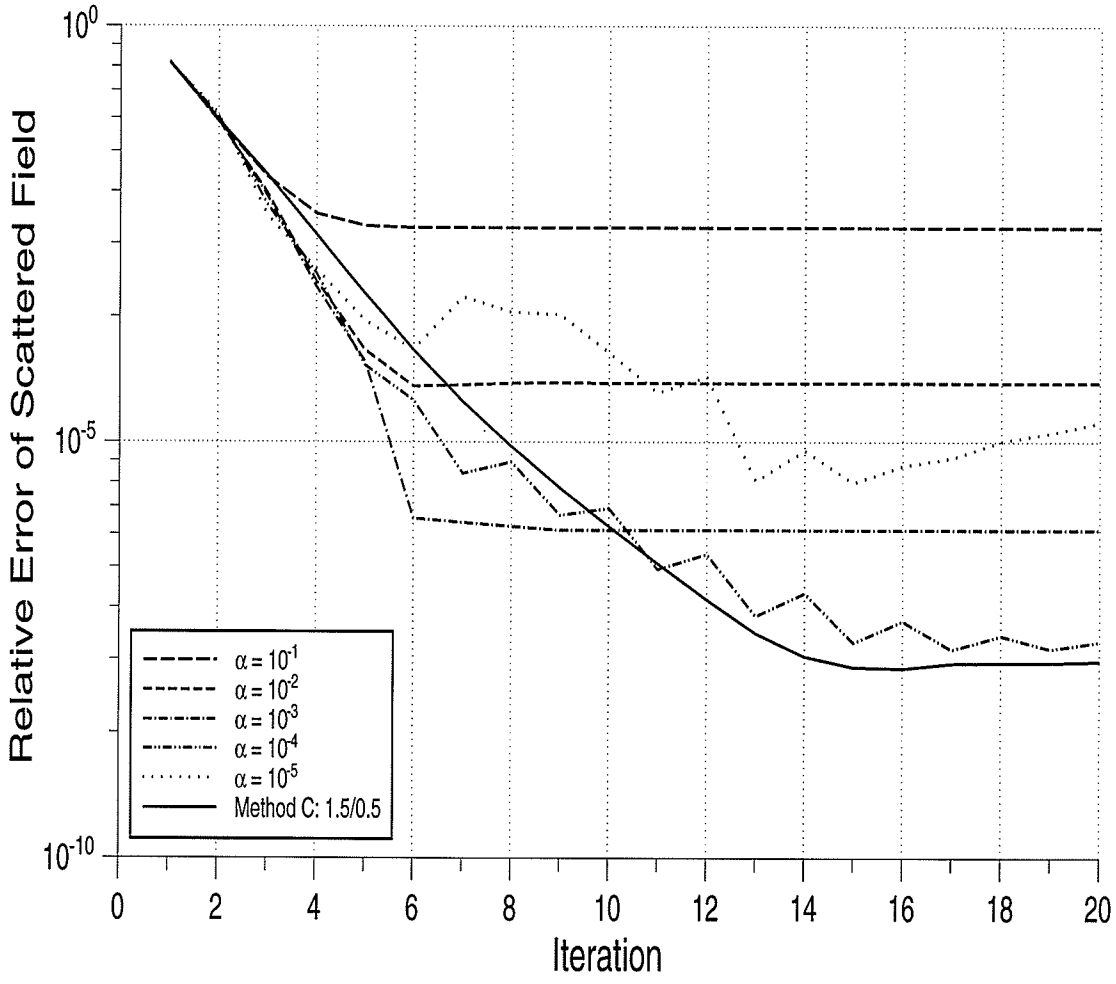

Fig. 5.12 Relative error of the reconstructed scattered fields versus the number of iterations for different regularization parameters.

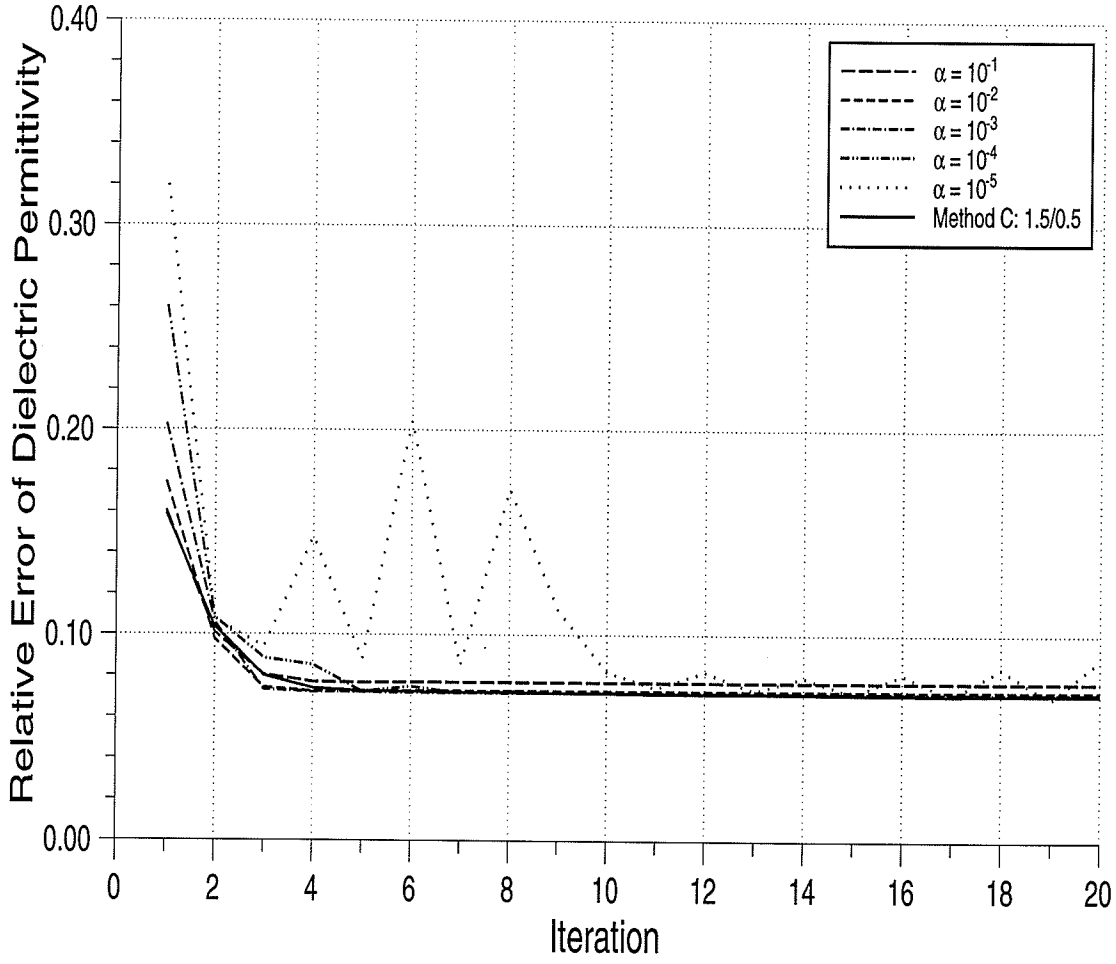

Fig. 5.13 Relative mean square error of the reconstructed dielectric permittivities versus the number of iterations for different regularization parameters.

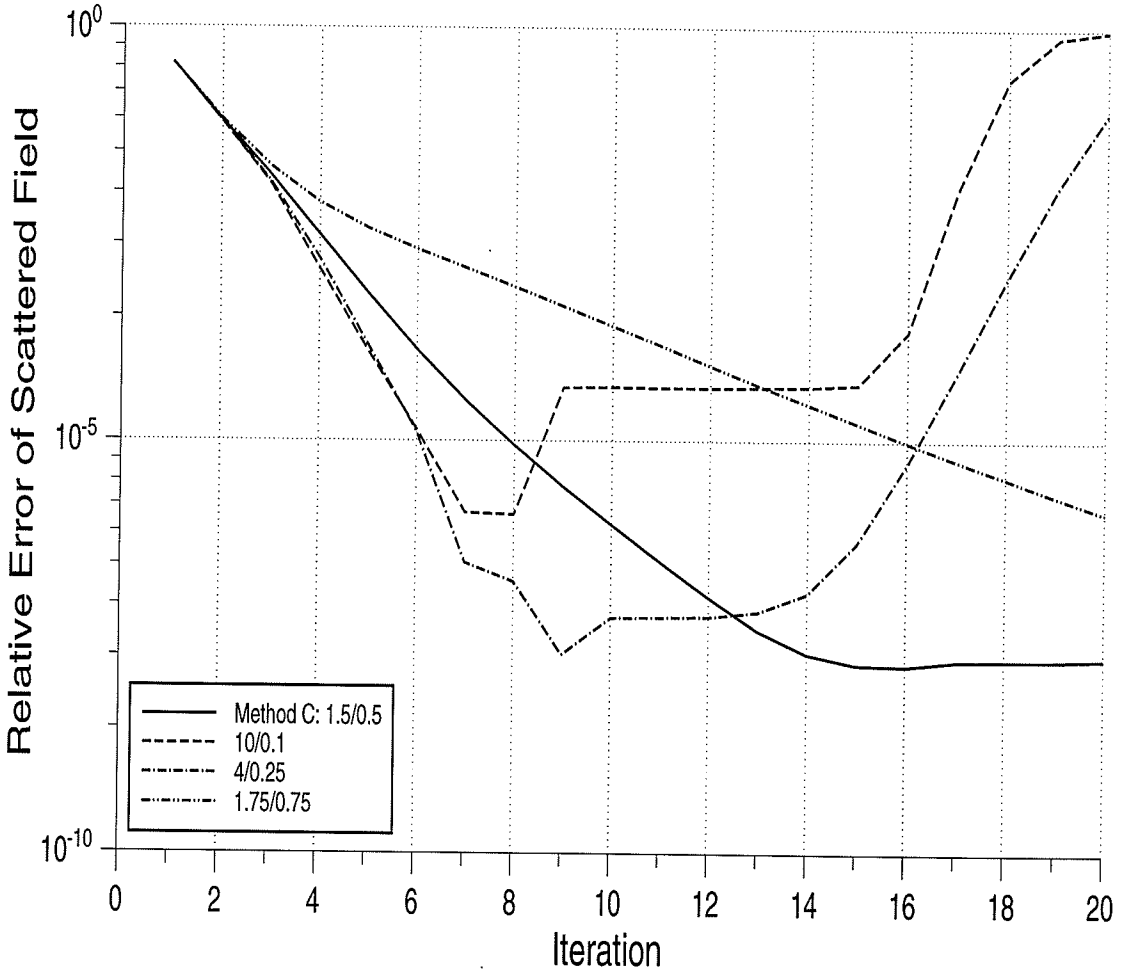

Fig. 5.14 Relative error of the reconstructed scattered fields versus the number of iterations for various increasing/decreasing factors.

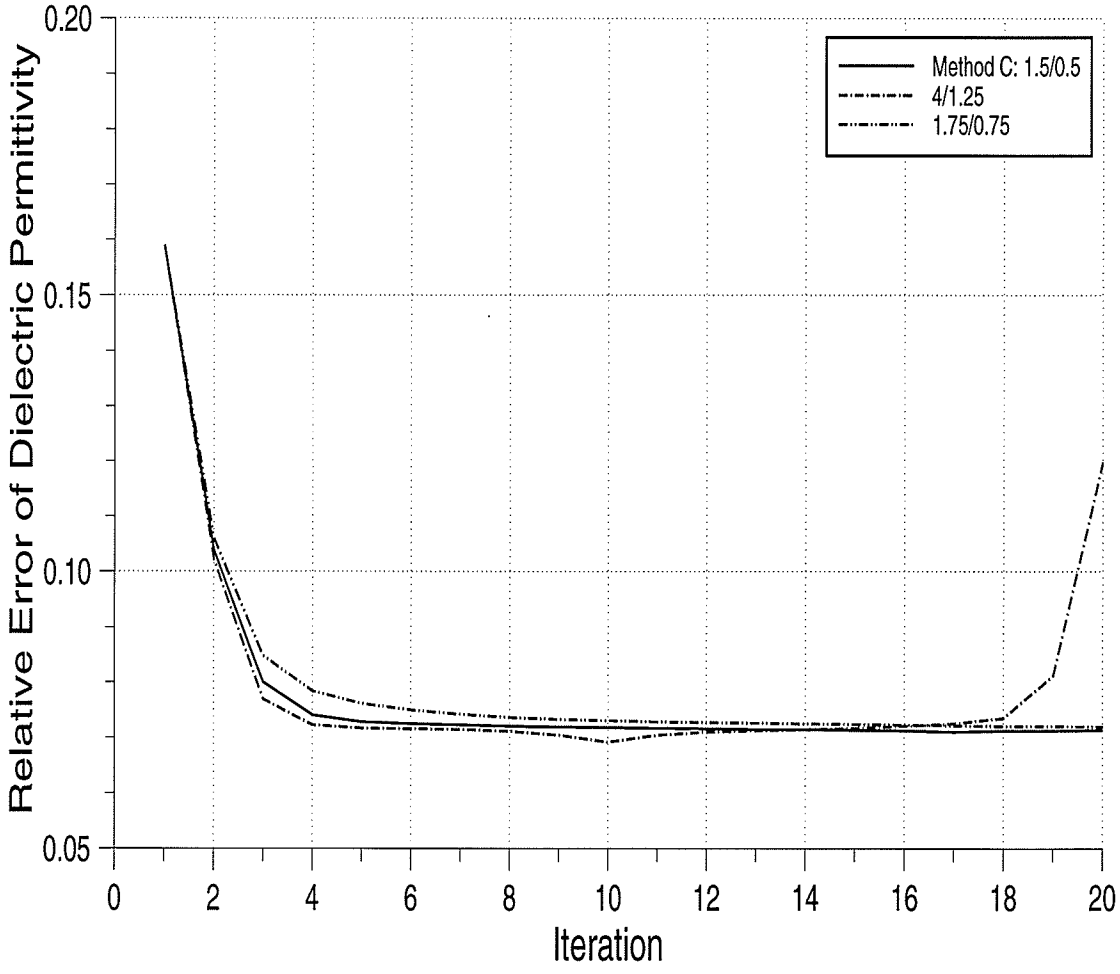

Fig. 5.15 Relative mean square error of the reconstructed dielectric permittivities versus the number of iterations for various increasing/decreasing factors.

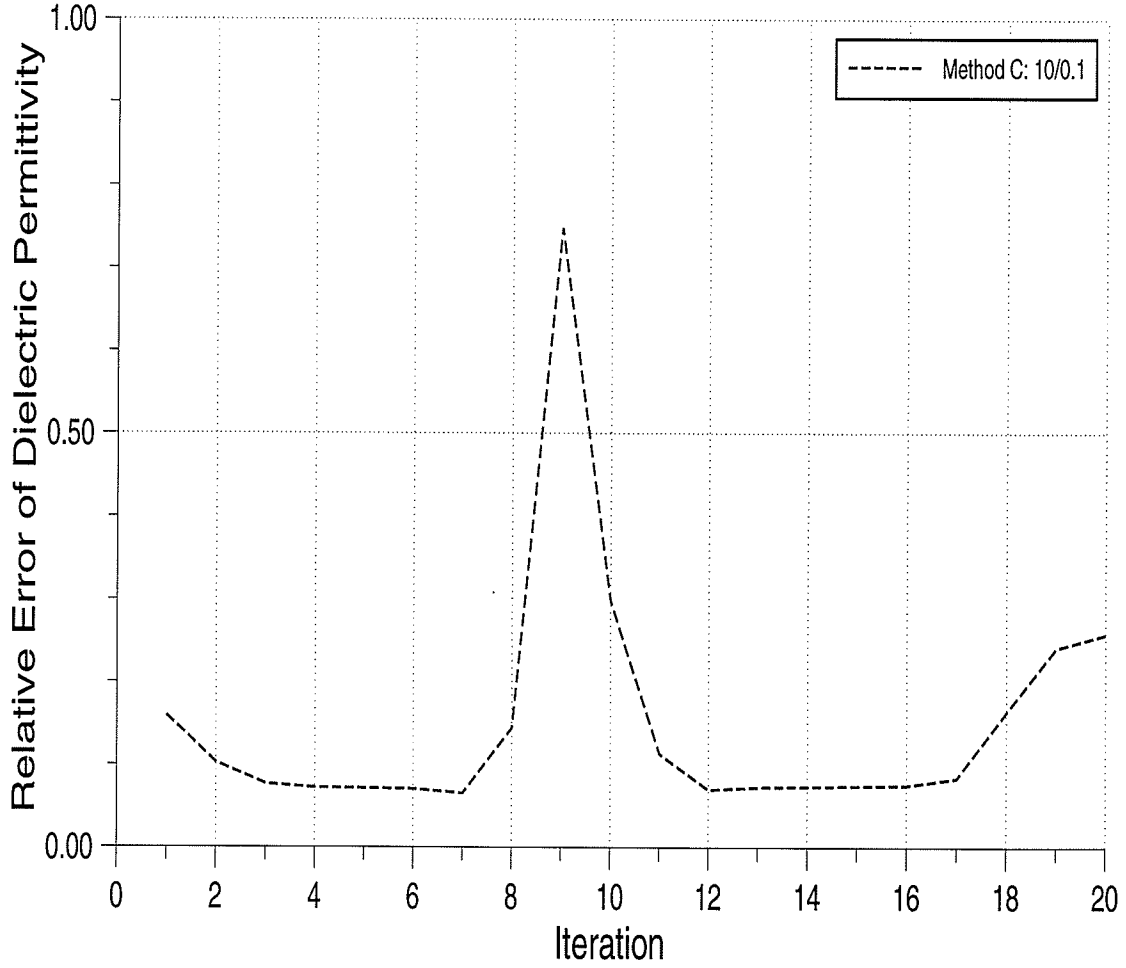

Fig. 5.16 Relative mean square error of the reconstructed dielectric permittivities versus the number of iterations for increasing/decreasing factor of 10/0.1.

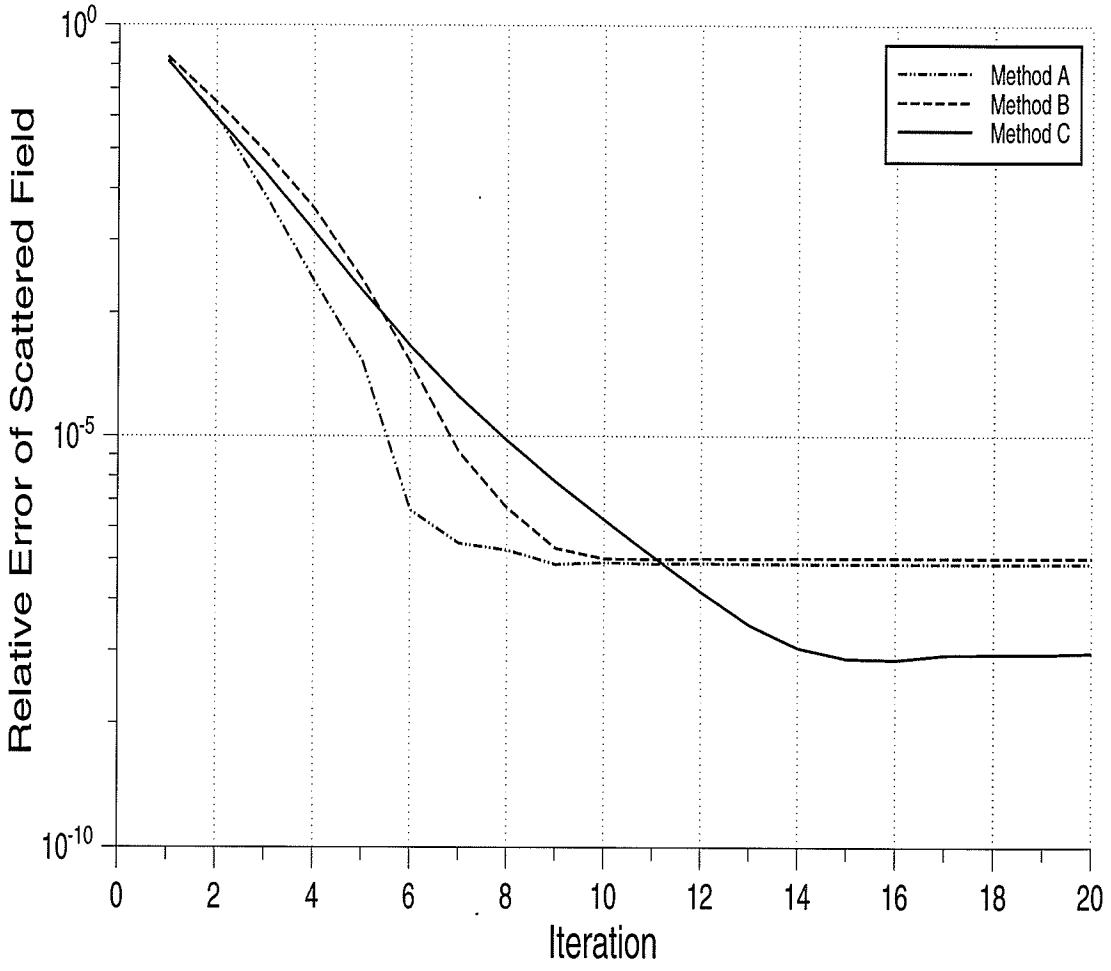

Fig. 5.17 Relative error of the reconstructed scattered electric fields versus the number of iterations by the proposed methods.

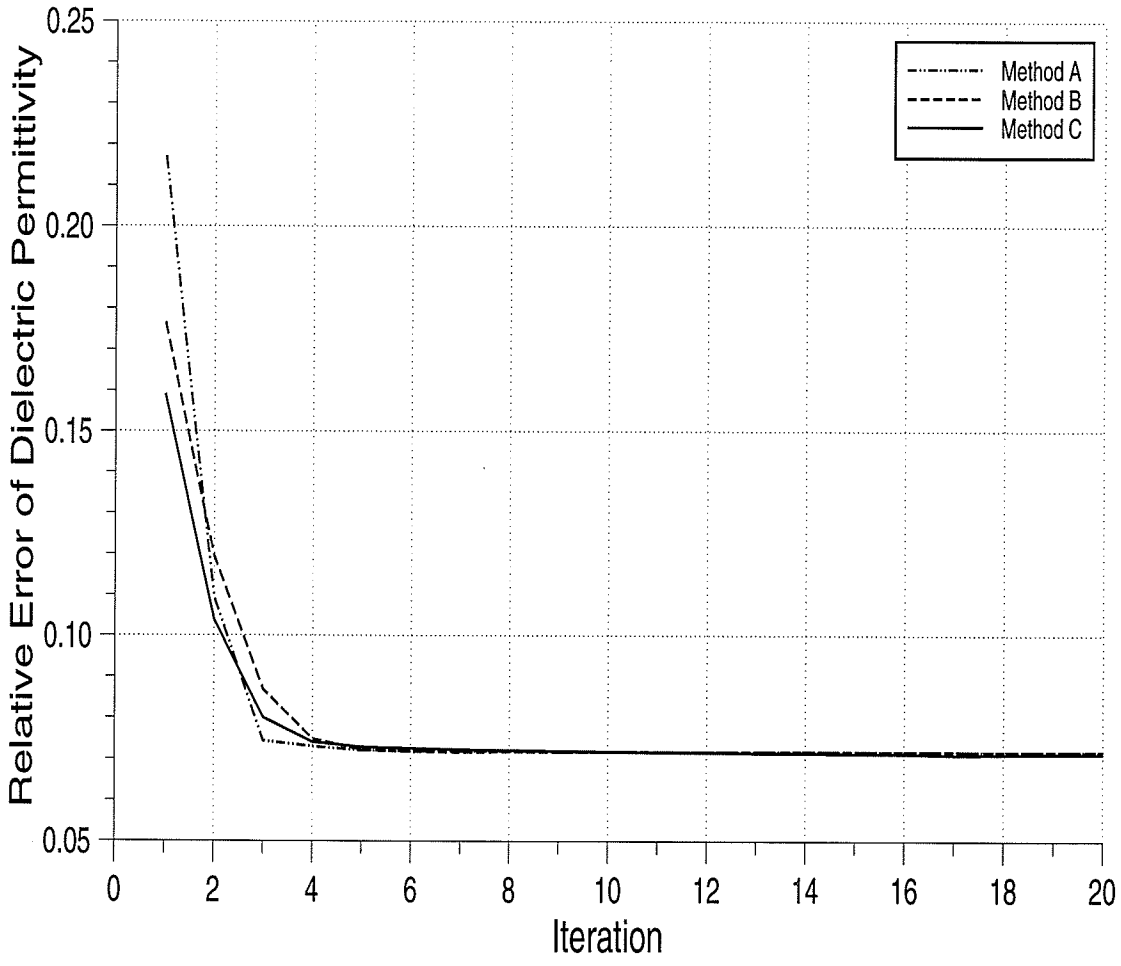

Fig. 5.18 Relative mean square error of the reconstructed dielectric permittivities versus the number of iterations by the proposed methods.

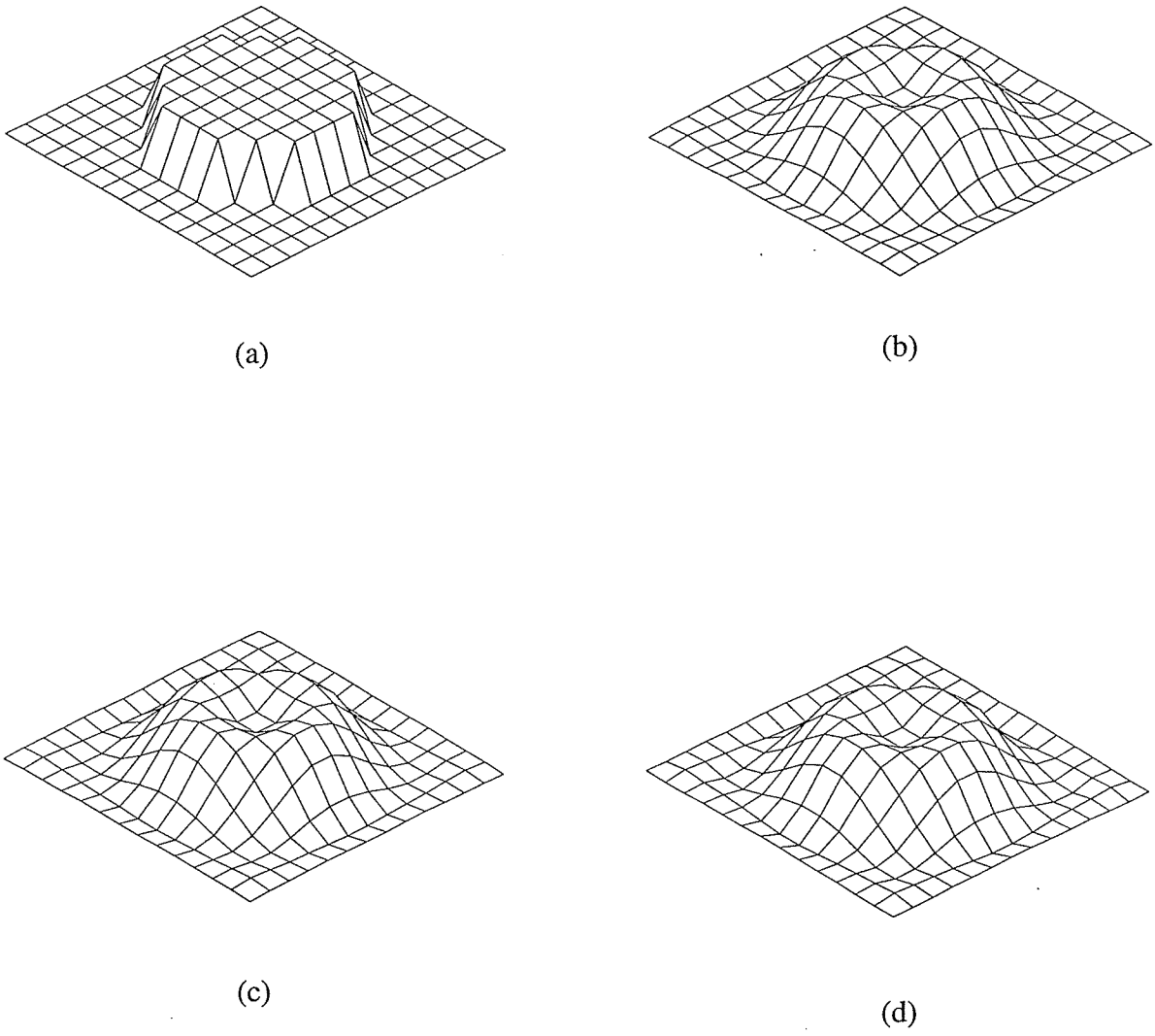

Fig. 5.19 Original and reconstructed dielectric permittivities.
(a) original profile; (b) method A; (c) method B;
(d) method C.

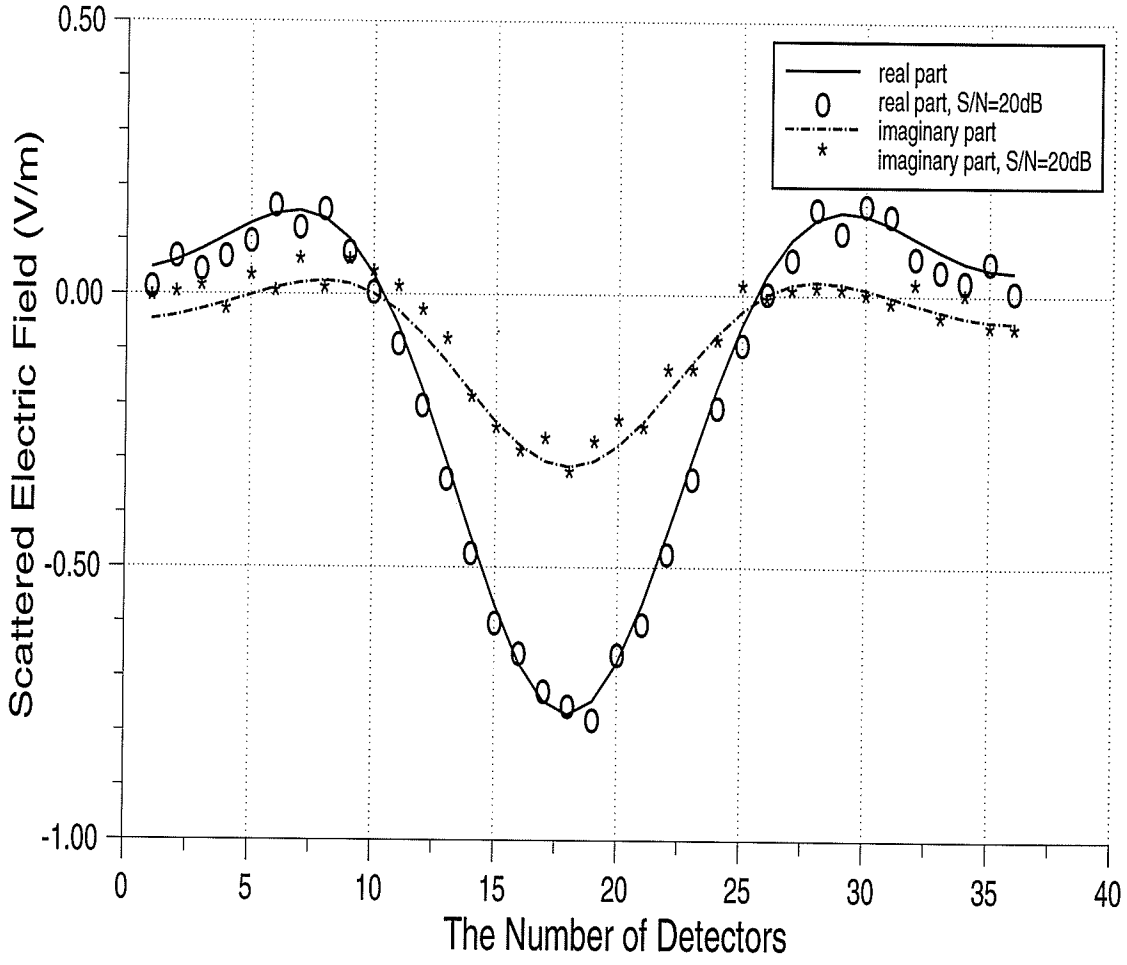

Fig. 5.20 Real part and imaginary part of the scattered field detected by receivers for S/N=20 dB.

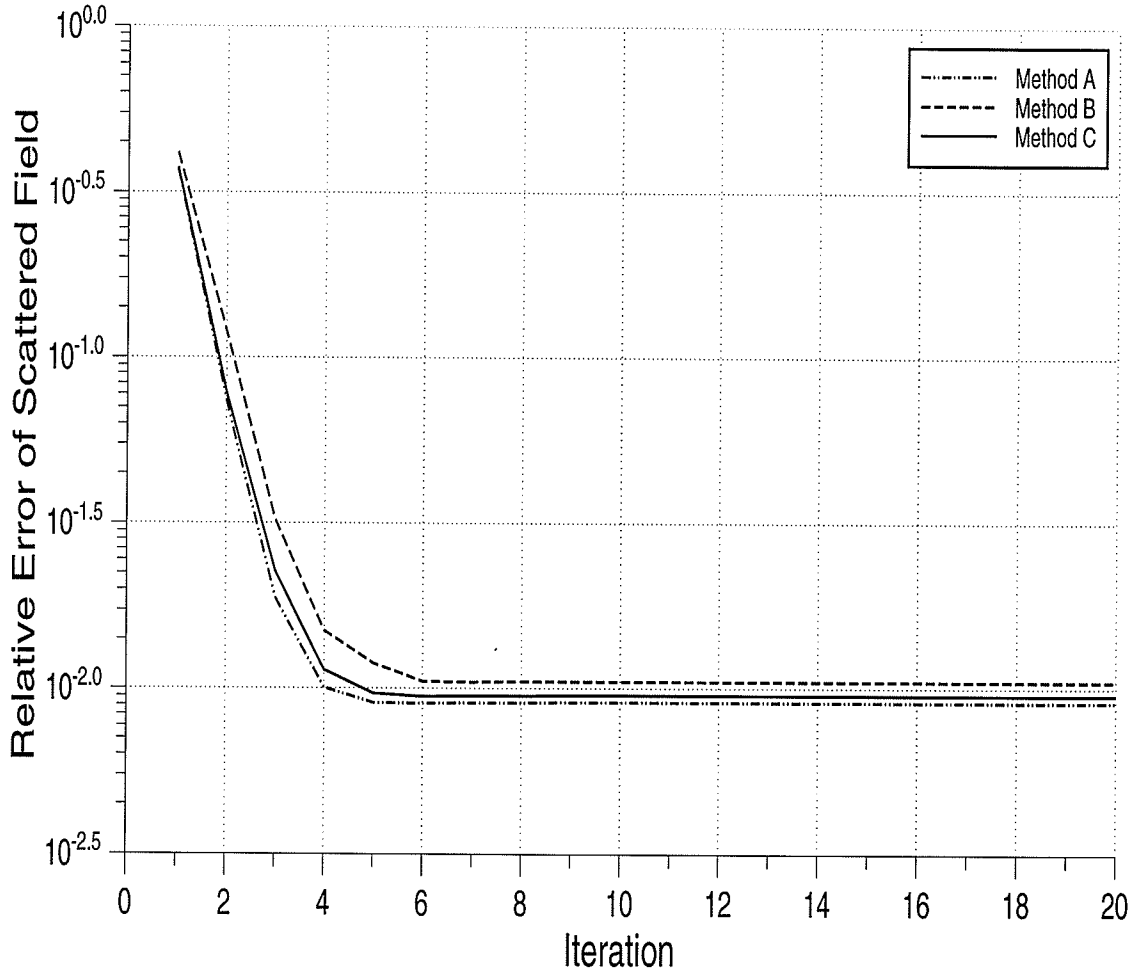

Fig. 5.21 Relative error of the reconstructed scattered electric fields versus the number of iterations by the proposed methods for S/N=20 dB.

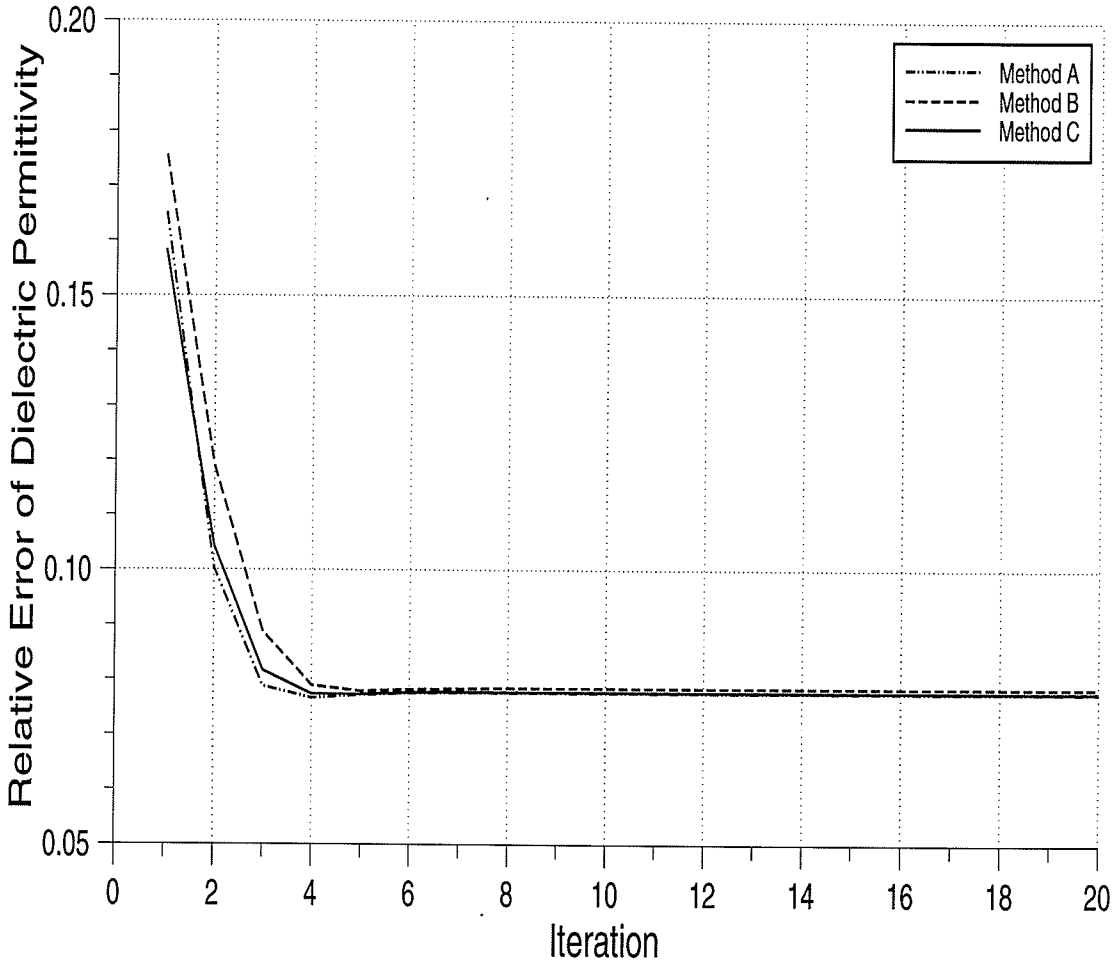

Fig. 5.22 Relative mean square error of the reconstructed dielectric permittivities versus the number of iterations by the proposed methods for S/N=20dB.

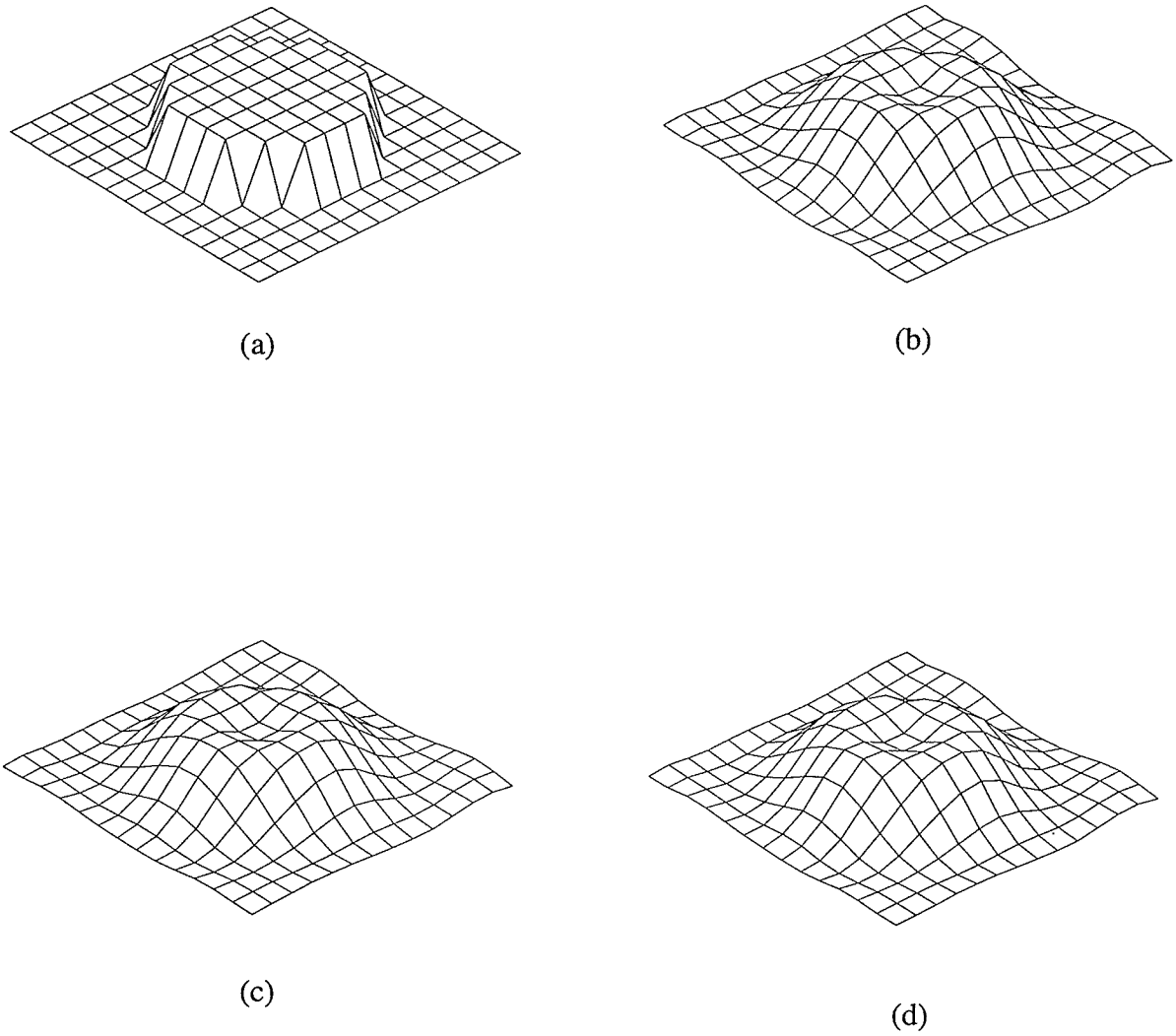

Fig. 5.23 Original and reconstructed dielectric permittivities for the detected data containing 10% noise.
(a) original profile; (b) method A; (c) method B;
(d) method C.

6

CONCLUSION AND FUTURE WORK

6.1 Conclusion

The problem of microwave imaging in spatial domain can be mathematically stated in terms of two coupled electric integral equations or formulated in terms of one linear integral equation by introducing an equivalent current density (equivalent current formulation). The general procedure for solving these integral equations consists of discretizing the integral equations by applying the moment method and the associated ill–conditioned systems of algebraic equations being solved by implementing a regularization technique. Two regularization methods, the Tikhonov regularization and the stochastic inverse scheme, have been considered in this dissertation. The combination of the Tikhonov regularization with the equivalent current modelling has yielded an efficient way of locating the dielectric scatterers. The selection and performance of the Tikhonov regularization parameter in the process of the reconstruction have been demonstrated by computer simulations. It has been observed that the optimum regularization parameter is strongly related to the noise level in the measured fields. The stronger the noise level, the stronger the regularization should be used. This is consistent with the theoretical conclusion that the Tikhonov regularization parameter can be statistically interpreted in terms of the noise variance and the reconstruction variance.

The introduction of the stochastic inverse scheme into the equivalent current reconstruction process has allowed us to develop a new iterative algorithm for reconstructing high

dielectric contrast objects accurately. The stochastic inverse scheme was developed by considering both the measured data and the reconstruction being random processes. Under the assumption that they are uncorrelated and isotropic, the scheme seeks an optimum solution by minimizing the expected value of the error in the reconstructed data. The algorithm consists of three main steps. The nonlinear integral equation used for the reconstruction of the dielectric body is first linearized by introducing an equivalent current density. Secondly, the Tikhonov regularization is employed to obtain a good approximation to the *a priori* data required in the algorithm. Finally, the stochastic inverse is applied to compute the equivalent current distribution within the body. From the reconstructed current density one can simply derive the permittivity distribution which is used directly to develop the object images. Numerical results have shown that this reconstruction procedure is very promising. For relatively simple scatterers, very accurate results can be obtained even by one incident wave illumination and with the measured data containing high level of noise. Multiview techniques can also be used to improve the quality of the images especially for the scatterers with more complex geometrical structures. The low–pass filtering effect which have been noticed in other reconstruction algorithms is not presented in the proposed method. These features have recommended the proposed method for some special applications when a high resolution is required in the presence of noise, especially in defect detecting, remote sensing and material property probing. Compared with other iterative methods presented so far for microwave imaging problems relative to dielectric bodies, the stochastic technique requires less computation time since the number of iterations can be reduced by utilizing *a priori* information which has been supplied in the proposed examples with the application of the Tikhonov regularization; moreover, for each iteration it only needs one matrix inversion, while other iterative techniques require two matrix inversion operations per iteration.

One of the difficulties in the iterative methods for solving the two electric field integral equations directly is the selection of the Tikhonov regularization parameter in each iteration. Based on the fact that the Tikhonov regularization parameter can be interpreted in terms of

the random noise vector variance and the object function variance, this dissertation has presented three methods for selecting this parameter. The first method is applicable to the situation when the upper bound of the object function variance and the upper bound of the measured data noise variance are known. The second method can be used if only the upper bound of the object function variance is detectable. If this information is not available, the third method can be employed to find the regularization parameter. The implementation of these methods is illustrated by reconstructing two dimensional objects with noiseless measured data and with the data containing noise. Simulation results have validated the new methods proposed in this thesis for microwave imaging.

6.2 Future Work

The present work can be used as a starting point for future studies leading to a better understanding of the performance of the stochastic inverse scheme in the procedure of dielectric body reconstruction by microwave imaging. The lack of theoretical basis, such as theories regarding the solution existence, uniqueness, and stability for electromagnetic inverse problems has made it difficult to establish the convergence and stability of iterative reconstruction algorithms proposed so far. More work on the practical implementation of the reconstruction algorithms should be considered. Following is a summary of the recommended future work.

1. It is well known that the moment method yields dense element matrices. For large reconstruction problems, these matrices not only require expensive computation time, but also generate great increased computer round–off errors which are added into the measured data used in the imaging process, thus introducing undesired uncertainties in reconstructions. Techniques which can be utilized to simplify the generated matrices, such as the Wavelet Transformation, are strongly recommended for future studies.

2. Computer simulations for more complex dielectric scatterers are to be performed. The following techniques might be involved: (1) increasing the number of discretization cells, the number of detectors and the number of incident wave illuminations; (2) using time–domain data; (3) employing data processing techniques, such as edge detection and spatial domain filtering [71] to improve the quality of images.

3. Finally, the proposed reconstruction methods are to be extended to three dimensional dielectric scatterers.

LIST OF REFERENCES

[1] E. Wolf, "Three–dimensional structure determination of semitransparent objects from holographic data," *Opt. Commun.*, vol. 1, pp. 153–156, 1969.

[2] K. Iwata, and R. Nagata, "Calculation of refractive index distribution from interferograms using the Born and Rytov's approximations," *J. Appl. Phys.*, vol. 14, pp. 1921–1927, 1975.

[3] R. K. Muller, M. Kaveh, and G. Wade, "Reconstructive tomography and applications to ultrasonics," *Proc. IEEE,* vol. 67, pp. 567–587, 1979.

[4] M. Slaney, A. C. Kak, and L. E. Larsen, "Limitations of imaging with first order diffraction tomography," *IEEE Trans. Microwave Theory Tech.,* vol. 32, pp. 860–873, 1984.

[5] J. V. Candy, and C. Pichot, "Active microwave imaging: a model–based approach," *IEEE Trans. Antennas Propagat.*, vol. 39, pp. 285–290, 1991.

[6] A. Broquetas, J. Romeu, J. M. Rius, A. R. Elias–Fuste, A. C. Cardama, and L. Jofre, "Cylindrical geometry: a further step in active microwave tomography," *IEEE Trans. Microwave Theory Tech.*, vol. 39, pp. 836–844, 1991.

[7] F. C. Lin, and M. A. Fiddy, "Image estimation from scattered field data," *Int. J. Imaging Syst. Technol*, vol. 2, pp. 76–95, 1990.

[8] J. V. Candy and C. Pichot, "Active microwave imaging: a model–based approach," *IEEE Trans. Antennas Propagat.,* vol. 39, pp. 285–290, 1991.

[9] L. Joffre, M. S. Hawley, A. Broquetas, E. Delos Reyes, M. Ferrando, and A. R. Elias–Fuste,"Medical imaging with a microwave tomographic scanner," *IEEE Trans. Biomed. Eng.*, vol. 37, pp. 303–312, 1990.

[10] M. Slaney, M. Azimi, A. C. Kak, and L. E. Larsen, "Microwave imaging with first order diffraction tomography," in *Medical Applications of Microwave Imaging,* L.E.

Larsen, and J. H. Jacobi, Ed., 1986, pp. 184–212.

[11] Y. M. Wang, and W. C. Chew, "An Iterative solution of two–dimensional electromagnetic inverse scattering problem," *Int. J. Imaging Syst. Technol.*, vol. 1, pp. 100–108, 1989

[12] W. C. Chew and Y. M. Wang, "Reconstruction of two–dimensional permittivity distribution using the distorted Born iterative method," *IEEE Trans. Med. Imaging,* vol. 9, pp. 218–225, 1990.

[13] M. Moghaddam and W. C. Chew, "Study of some practical issues in inversion with the Born iterative method using time–domain data," *IEEE Trans. Antennas Propagat.,* vol. 41, pp. 177–184, 1993.

[14] N. Joachimowicz, C. Pichot, and J.–P. Hugonin, "Inverse scattering: an iterative numerical method for electromagnetic imaging," *IEEE Trans. Antennas Propagat.,* vol. 39, pp. 1742–1752, 1991.

[15] W. Wang and S. Zhang, "Unrelated illumination method for electromagnetic inverse scattering of inhomogeneous lossy dielectric bodies," *IEEE Trans. Antennas Propagat.,* vol. 40, pp. 1292–1296, 1992.

[16] M. M. Ney, A. M. Smith, and S. S. Stuchly, "A solution of electromagnetic imaging using pseudo–inverse transformation," *IEEE Trans. Med. Imaging,* vol. 3, pp. 155–162, 1984.

[17] S. Caorsi, G. L. Gragnani, and M. Pastorino, "Two–dimensional microwave imaging by a numerical inverse scattering solution," *IEEE Trans. Microwave Theory Tech.*, vol. 38, pp. 981–989, 1990.

[18] —, "Equivalent current density reconstruction for microwave imaging purpose," *IEEE Trans. Microwave Theory Tech.*, vol. 37, pp. 910–916, 1989.

[19] ——, "An approach to microwave imaging using a multiview moment method solution for a two–dimensional infinite cylinder," *IEEE Trans. Microwave Theory Tech.*, vol. 39, pp. 1062–1067, 1991.

[20] —, "Numerical electromagnetic inverse–scattering solutions for two–dimensional infinite cylinder buried in a lossy half–space," *IEEE Trans. Microwave Theory Tech.*, vol. 41, pp. 352–356, 1993.

[21] M. Hagmann and R. L. Levin, "Procedures for noninvasive electromagnetic property and dosimetry measurements," *IEEE Trans. Antennas Propagat.*, vol. 38, pp. 99–106, 1990.

[22] Y.M. Qin and I.R. Ciric, "Efficient Techniques for Choosing the Regularization Parameter for Microwave Imaging", in *Proc. ANTEM'96*, 1996, (Montréal, Canada).

[23] I.R. Ciric and Y.M. Qin, "Self–adaptive selection of the regularization parameter for electromagnetic imaging," in *Proc. CEFC'96,* 1996, (Okayama, Japan).

[24] Y.M. Qin and I.R. Ciric, "High resolution electromagnetic imaging of lossy objects in the presence of noise," *IEEE Trans. Magn.,* vol. 31, no. 3, May 1995.

[25] ———, "Method of selecting the regularization parameter for microwave imaging," *Electron. Lett.,* vol. 30, no. 24, pp. 2028–2029, Nov. 1994.

[26] ———, "High Resolution Electromagnetic Imaging of Lossy Objects in the Presence of Noise," in *Proc. CEFC'94*, 1994, (Aix–les–Bains, France).

[27] ———, "Dielectric Permittivity Reconstruction in a Highly Noisy Environment, " in *Proc.* PIERS'94, 1994, (Noordwijk, The Netherlands).

[28] ———— , "Stochastic Inversion for Microwave Imaging of Dielectric Bodies in the Presence of Noise," in *Proc. 1994 IEEE Int. Symp. Antennas Propagat.,* 1994, (Seattle, USA).

[29] ———, "Stochastic reconstruction of Dielectric Permittivities with Multiple Illumina–tions", in *Proc. ANTEM'94*, 1994, (Ottawa, Canada).

[30] ———, "Dielectric Body Reconstruction with Current Modelling and Tikhonov Regu–larization," *IEE Electron. Lett.,* vol. 29, pp. 1427–1429, 1993.

[31] ———, "Inverse Scattering Solution with Current Modeling and Tikhonov Regulariza–tion," in *Proc. 1993 IEEE Int. Symp. Antennas Propagat.,* 1993, (Ann Arbor, USA), pp.

492–495.

[32] ———, "Equivalent Current Reconstruction in Electromagnetic Imaging of Dielectric Bodies, in *Proc.* PIERS'93, 1993, (Pasadena, USA).

[33] P. M. Meaney, K. D. Paulsen, A. Hartov, and R. C. Crane, "An Active Microwave Imaging System for Reconstruction of 2–D Electrical Property Distribution", *IEEE Trans. Biomed. Eng.,* vol. 42, no. 10, pp. 1017–1026, October 1995.

[34] P. M. Meaney, K. D. Paulsen, and T. P. Ryan, "Two–Dimensional Hybrid Element Image Reconstruction for TM Illumination", *IEEE Trans. Antennas Propagat.*, vol. 43, no. 3, pp. 239–247, 1995.

[35] J. Larrigan and L. Shafai, "Microwave Imaging of Inhomogenious Dielectric Cylinders", in *Proc. ANTEM'92,* 1992, (Winnipeg, Canada), pp. 696–701.

[36] H. Harada, D. J. N. Wall, T. Takenaka, and M. Tanaka, "Conjugate Gradient Method Applied to Inverse Scattering Problem", *IEEE Trans. Antennas Propagat.*, vol. 43, no. 8. pp. 784–792, August 1995.

[37] R. M. Bevensee, "Solution of underdetermined electromagnetic and seismic problems by the maximum entropy method," *IEEE Trans. Antennas Propagat.*, vol. 29, pp. 271–274, 1981.

[38] X. Chen and W. X. Zhang, " Solution of inverse problems by the general maximum entropy method," in *Proc. 1991 IEEE Int. Symp. Antennas Propagat.*, (London, Canada), 1991, pp. 1308–1311.

[39] L. Garnero, A. Franchois, J.–P. Hugonin, C. Pichot, and N. Joachimowicz, "Microwave imaging–complex permittivity reconstruction by simulated annealing," *IEEE Trans. Microwave Theory Tech.,* vol. 39, pp. 1801–1807, 1991.

[40] S. Caorsi, G. L. Gragnani, S. Medicina, M. Pastorino, and G. Zunino, "Microwave imaging method using a simulated annealing approach," *IEEE Microwave Guided Wave Lett.,* vol. 1, pp. 331–333, 1991.

[41] R. F. Harrington, *Field computation by moment methods,* New York, Macmillan, 1978.

[42] A. N. Tikhonov and V. Y. Arsenin, *Solutions of ill–posed problems*. V.H. Winston & Sons, 1977.

[43] J. N. Franklin, "Well posed stochastic extensions of ill–posed linear problems," *J. Math. Anal. Appl.,* vol. 31, pp. 682–716, 1970.

[44] T. Sarkar, D. D. Weiner, and V. K. Jain, "Some mathematical considerations in dealing with the inverse problems," *IEEE Trans. Antennas Propagat.*, vol. 29, pp.373–379, 1981.

[45] D.C. Sabatier, "Theoretical Considerations for Inverse Scattering," *Radio Science*, vol. 18, no.1, pp.1–18, Jan.–Feb. 1983.

[46] M. Baribaud, F. Dubois, D. EnMéd, R. Floyrac, and S. Wang, "Tomographic Image Reconstruction of Objects from Multi–incidence Microwave exploration," *IEE. Proc.,* vol. 132, Pt. H., no. 5, pp. 286–290, Aug. 1985.

[47] J.M. Gironés, L. Jofre, M. Ferrando, E. de los Reyes, and J. Ch. Bolomey, "Microwave Imaging with Crossed Linear Arrays," *IEE Proc. vol.* 134, Pt. H, no. 3, pp. 249–252, June 1987.

[48] S.–Y. Kim, "Electromagnetic imaging of 2–D inhomogeneous dielectric objects by an improved spectral inverse technique," *IEEE Trans. Magnetics,* vol. 26, no. 2, pp. 634–637, 1990.

[49] S. M. Lee, S. Y. Kim, and J. W. Ra, "Filtering effects on permittivity profiles reconstructed by a spectral inverse scattering technique," *IEE Proceed.–H,* vol. 139, pp. 507–512, 1992.

[50] A. G. Tijhuis, *Electromagnetic inverse profiling*, VNU Science Press BV, 1987.

[51] J. Hadamard, *Sur les problèmes aux dérivées partielles et leur signification physique,* Bull. Princeton Univ., pp. 49–52. 1902.

[52] C.T. Tai, *Dyadic Green's Function in Electromagnetic Theory*, Scranton: International Texbook, 1971.

[53] R.F. Harrington, *Time–Harmonic Electromagnetic Fields,* New York: McGraw–Hill,

1961.

[54] J. H. Richmond, "Scattering by a dielectric cylinder of arbitrary cross section shape," *IEEE Trans. Antennas Propagat.*, vol. 13, pp. 334–341, 1965.

[55] R. Mittra and C. A. Klein, "Stability and convergence of moment method solutions," in *Numerical and Asymptotic Techniques in Electromagnetics*, R. Mittra, Ed., New York: Springer–Verlag, 1975.

[56] N. Bleistein and J. K. Cohen, "Nonuniqueness in the inverse source problem in acoustics and electromagnetics," *J. Math. Phys.*, vol. 18, no.2, pp. 194–201, Feb. 1977.

[57] A. J. Devaney and E. Wolf, "Radiating and nonradiating classical current distributions and the fields they generate," *Physical Review,* vol. 8, no. 4, pp. 1044–1047, Aug. 1973.

[58] A. J. Devaney, " Nonuniqueness in the inverse scattering problem," *J. Math. Phys.,* vol. 19, no. 7, pp. 1526–1531, July 1978.

[59]M. Guarnieri, A. Stella, F. Trevisan, "A Methodological Analysis of Different Formulations for Solving Inverse Electromagnetic Problems", *IEEE Trans. Magnetics,* vol. 26, no. 2, pp.633–625, March 1990.

[60] E. L. Hall, *Computer image processing and recognition.* United Kingdom: Academic Press (London), pp.232–234, 1979.

[61] M. Bertero, C. DeMol, and G. A. Viano, "On the problems of object restoration and image extrapolation in optics", *J. Math. Phys.*, vol. 20, pp. 509–521, 1979.

[62] H. D. Vinod and A. Ullah, *Recent advances in Regression methods*, Marcel Dekker, Inc. New York, 1981.

[63] D.C. Momtgomery, *Introduction to linear regression analysis,* John Willey&Sons, Inc. 1982.

[64] G. A. F. Seber and C. J. Wild, *Nonlinear regression*, John Willey &Sons, Inc. 1989.

[65] J.P. Burg, "Maximum entropy spectral analysis," in *Modern spectral analysis,* D.G. Childers, Ed., New York: IEEE Press, 1978, pp. 34–41.

[66] A. Taflove and K.R. Umashankar, "The FD–TD method for numerical modelling of

electromagnetic wave interaction with arbitrary structures", in *PIER 2, Progress in Electromagnetic Research, Chapter 8,* Editor: M.A. Morgan, 1990, pp. 363–366.

[67] K. Aki and P. G. Richards, *Quantitative seismology theory and methods.* vol. II, Freeman (San Francisco), 1980.

[68] L. M. Delves, G. C. Pryde, and S. P. Luttrell. "A super–resolution algorithm for SAR images," *Inverse Problems*, vol. 4, pp. 681–703, 1988.

[69] K. Levenberg, "A method for the solution of certain non–linear problems in least squares," *Quart. Appl. Math.,* vol. 2, no. 7, pp. 164–168, July 1944.

[70] D.W. Marquardt, "An algorithm for least–squares estimation of non–linear parameters," *SIAM J. Appl. Math.,* vol. 11, no.2, pp. 431–441, June 1963.

[71] M. Frank and C.A. Balanis, "Method for improving the stability of electromagnetic geophysical inversion," *IEEE Trans., Geosci. Remote Sensing*. vol. 27, pp. 339–343, May 1989.

[72] C. N. Dorny, *A vector space approach to methods and optimization,* Huntington, New York: Krieger, 1980.